Initial investigation of the proteomic and immunohistochemical characteristics of the acrosyringium belonging to the human eccrine sweat gland.

Thesis submitted in accordance with the requirements of the University of Liverpool for the degree of Doctor in Philosophy

by

Maximilian Abramo Tobia Harris

March 2023

Abstract

Perspiration is a vital haemostatic function primarily involved in thermoregulation of the human body. The eccrine sweat glands (ESG) are responsible for the generation and secretion of sweat. Much research has been done into the secretory coil and the luminal duct regions of the ESG, whereas comparatively little is known about the acrosyringium. The region of the ESG that transects the epidermis. Due to the size and sparsity of acrosyringia in the epidermis, existing methods for the proteomic analysis of formalin fixed paraffin embed (FFPE) tissue were not feasible. An optimised workflow of extraction and proteomic analysis of FFPE tissue was developed that only required 0.01mm^3 (<500 µg) of FFPE tissue, 25-fold less material than other published methods that use > 0.25 mm^3. The workflow was used with label-free quantitative proteomics to investigate epidermis enriched for acrosyringia, with a view to defining protein components of this structure. Over 1,000 proteins were identified from sub mg levels of FFPE human skin tissue. Of the 1,700 proteins identified across 4 replicate pieces of tissue, 24 were observed to be statistically more prevalent in the acrosyringium enriched epidermis compared with acrosyringium-negative tissue (p-value <0.05). Immunohistochemical (IHC) staining of FFPE skin tissue sections containing acrosyringium was performed using 11 of the 24 proteins identified as more prevalent within the acrosyringium positive samples. 10 of the 11 IHC screen proteins are shown to be expressed in the acrosyringium and the surrounding tissue. Of these proteins, Keratin 6, Annexin A1 (AnxA1) and Calmodulin-like 5 (CALML5) showed the strongest staining of the acrosyringium compared to the surrounding tissue. Following this, experimentation focused on gaining a greater understanding of the roles of AnxA1 whose function is associated to inhibition of inflammation and CALML5 whose function is associated to keratinocyte differentiation, in the context of the acrosyringium by altering the expression of these proteins in an in vitro model. Currently there are no acrosyringium specific cell lines, so testing was performed in the HaCaT cell line (keratinocytes), in which a AnxA1 siRNA knockdown (AsKD) was generated. AsKD and wild-type WT HaCaT cell were stressed with bacterial lipopolysaccharide (LPS) to represent conditions of bacteria within the acrosyringium, and the inflammatory response gauged by the expression of cytokines IL6 and IL8. Results show AsKD expression of IL6 and IL8 was significantly (p >0.001 to >0.05) greater than in the WT controls, in both LPS treated and not treated samples. Demonstrating that AnxA1 plays an active role in maintaining keratinocytes' steady state as well as inhibiting inflammatory factors as part of the stress response. A CALML5 siRNA knockdown was not generated and could not be further investigated.

Table of Contents

Table of Figures

Table of Tables

Abbreviations

ACS - ACROSYRINGIUM

IHC - immunohistochemical

BSA - bovine serum albumin

IL-6 - Interleukin 6

IL-8 - Interleukin 8

NH4OH - Ammonium hydroxide

PTM - Post-Translational Modification

ACS - ACROSYRINGIUM

AmBic - ammonium bicarbonate

AnxA1 - Annexin A1

C - Cysteine

Ca+ - calcium ions

CALML5 - Calmodulin-like 5

CID - collision-induced dissociation

DDA - data-dependent acquisition

DMEM - Dulbecco's Modified Eagle Medium

DMEM - Modified Eagle Medium

DPX - distyrene, plasticizer and xylene

DTT - Dithiothreitol

EDTA - Ethylenediaminetetraacetic acid

ESG - eccrine sweat glands

ESI - electrospray ionisation

FASP - Filter-aided sample preparation

FBS - fetal bovine serum

FDR - false discovery rate

FFPE - formalin fixed paraffin embedded

G - relative centrifuge force

GPCRs - G-protein coupled receptors

HaCaT - High sensitivity of human epidermal keratinocytes

HCGM - High-calcium growth medium

HIAR - heat induced antigen retrieval

HRP - horseradish peroxidase

IAA - iodoacetamide

IHC - Immunohistochemistry

IP3 - triphosphate

KD - knockdown

KRT - keratin

LCGM - Low-Calcium growth medium

LCM - laser capture microscopy

LC-MS-MS - Liquid Chromatography with tandem mass spectrometry

LPS - bacterial lipopolysaccharide

M - Methionine

m/z - mass to charge ratio

MeCN - Acetonitrile

min - minutes

Ms - mass spectrum

MS/MS - Tandem mass spectrometry

N - Asparagine

N/S - Not Specified

Na+ - Sodium ions

NaCl - Sodium chloride

NCE - normalised collision energy

PBS - phosphate buffered saline

PIP2 - phosphatidylinositol 4,5-bisphosphate

PSM - peptide spectral matches

Q - Glutamine

QEXHF - Q Exactive HF Hybrid Quadrupole-Orbitrap Mass Spectrometer

RCF - Relative centrifugal field

RF - radio frequency

RPM - revolutions per minute

RT - Room temperature

SB - Stratum basal

SC - stratum corneum

SCX - Strong cation exchange

SDS - Sodium dodecyl sulphate

SS - Stratum spinosum

STIM1 - stromal interaction molecule 1

STIM2 - stromal interaction molecule 2

TBST - Tris-buffered saline with 0.1% Tween

TEAB - Tetraethylammonium bromide

TEMED- N,N,N',N'-Tetramethylethylenediamine

TFA - Trifluoroacetic acid

TFA - Trifluoroacetic acid

TMT - Tandem Mass Tagging

Tris - tris hydroxymethyl aminomethane

Tris-HCl - Tris(hydroxymethyl)aminomethane hydrochloride

v - Stratum granulosum

Chapter: 1 Introduction

1.1 Sweat secretors in human skin

In humans, there are believed to be four secretory glands that contribute to the sweat found on the surface of the skin(Sato, Leidal, and Sato 1987). They are the eccrine sweat gland (ESG), the Apocrine gland, the Sebaceous gland and the Apoeccrine gland. A comparison of these glands and how they are orientated in the skin is shown in Figure 1.1.

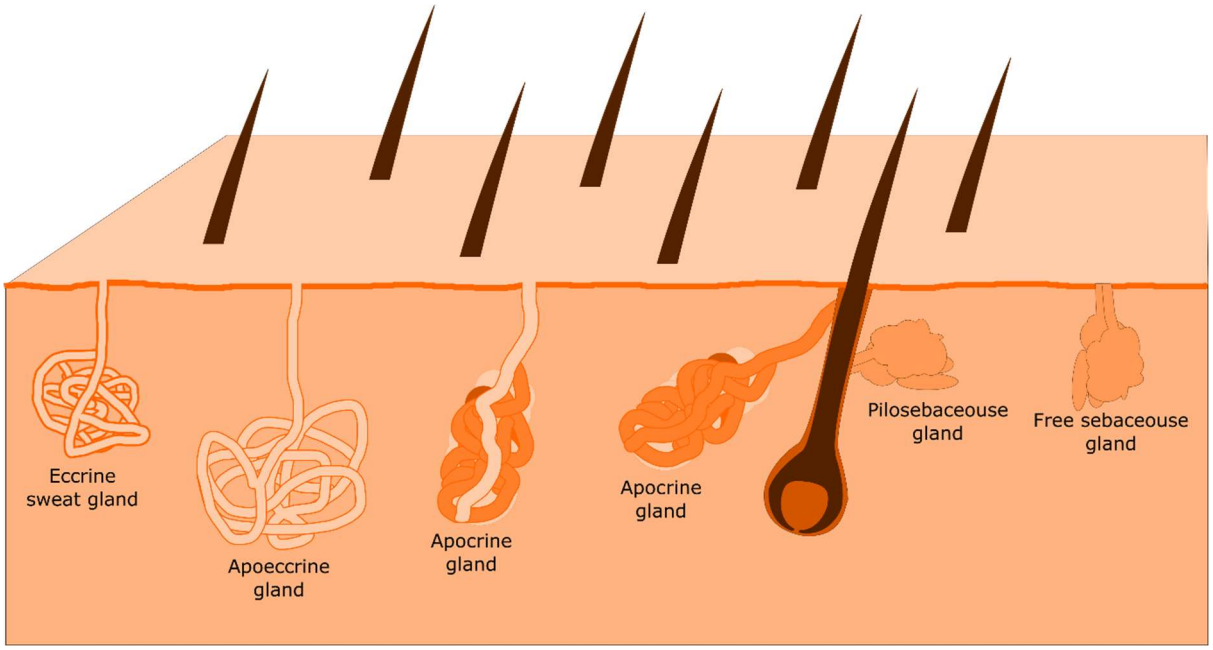

Figure 1.1 Comparison of secretory glands in skin.

Eccrine sweat gland opening on the surface of skin, Apoeccrine gland opening on the surface of skin, Apocrine gland opening on the surface of skin, Apocrine gland opening into a hair follicle and Sebaceous gland.

1.1.1 Apocrine gland

First observed and recoded in 1844 by C. Krause (Montagna W 1974) it was formally named the Apocrine gland in 1922 by Schiefferdecker (Hibbs 1962). The Apocrine gland shares some similar morphological traits with the ESG. Both have two distinct regions, a secretory coil and associated duct, as shown in Figure 1.1. The most notable difference is the average diameter. The diameter of the apocrine gland is approximately 10 times larger than the diameter of the ESG (Steffen et al. 2014; Semkova et al. 2015; Murphrey, Safadi, and Vaidya 2020). In addition, the secretory coil of the Apocrine gland is typical found in the lower region of the dermis or subcontinent fatty tissue, and it is significantly larger than that of

the ESG (Wortsman et al. 2019; Reichel et al. 2017; Hu et al. 2018). Furthermore, in most cases, the luminal duct leads directly from the coil into a pilosebaceous follicle, but also opens directly onto the surface of the skin as shown in Figure 1.1. In either case, Apocrine glands are typically found in close proximity to a hair follicle (Murphrey, Safadi, and Vaidya 2020; Prost-Squarcioni 2006).

Despite being present from birth, the Apocrine gland typically does not begin to secrete products until puberty (Sato, Leidal, and Sato 1987). At this point, the gland begins to secrete a multitude of lipid-based products (e.g. pheromones and steroids) and proteins (Semkova et al. 2015; Murphrey, Safadi, and Vaidya 2020). The secretion is generated in the secretory coil, in which apoptotic caps containing the relevant materials are formed on the luminal surface of the secretory cells. These apoptotic caps undergo decapitations, separating them from the cell, and they are then released into the luminal space, where they migrate though the lumen to either the associated hair follicle or the surface of the skin (Figure 1.1) depending on the gland's location (Hu et al. 2018).

1.1.2 Apoeccrine gland

The Apoeccrine gland is a somewhat controversial topic. That is, it is unclear whether the structures that are referred to as apoeccrine sweat glands should be classified as an independent group of secretory glands, or if in fact they are a variant/subgroup of ESGs. Initially described in 1987 by H. Sato (Sato, Leidal, and Sato 1987), the structure of the proposed apoeccrine gland has morphological traits of both the Apocrine and eccrine glands. Typically manifesting in individuals during and after puberty, apoeccrine glands are believed to develop from existing Eccrine glands in the axilla region (Sato and Sato 1987; Wilke et al. 2007; Sato, Leidal, and Sato 1987) as indicated in Figure 1.2. As with eccrine glands, the luminal structure connects the secretory coil to the surface of the skin (Figure 1.1). However, the secretory coil is located at a similar depth in the dermis as the apocrine gland, this is deeper than ESG. The Apoeccrine secretory coil most closely resembles the ESG. However, the apoeccrine secretory coil is closer in size to that of the apocrine gland. Unsurprisingly, the secretion generated and released from the coil is an isotonic, viscous solution, nearly identical to that of the ESG.

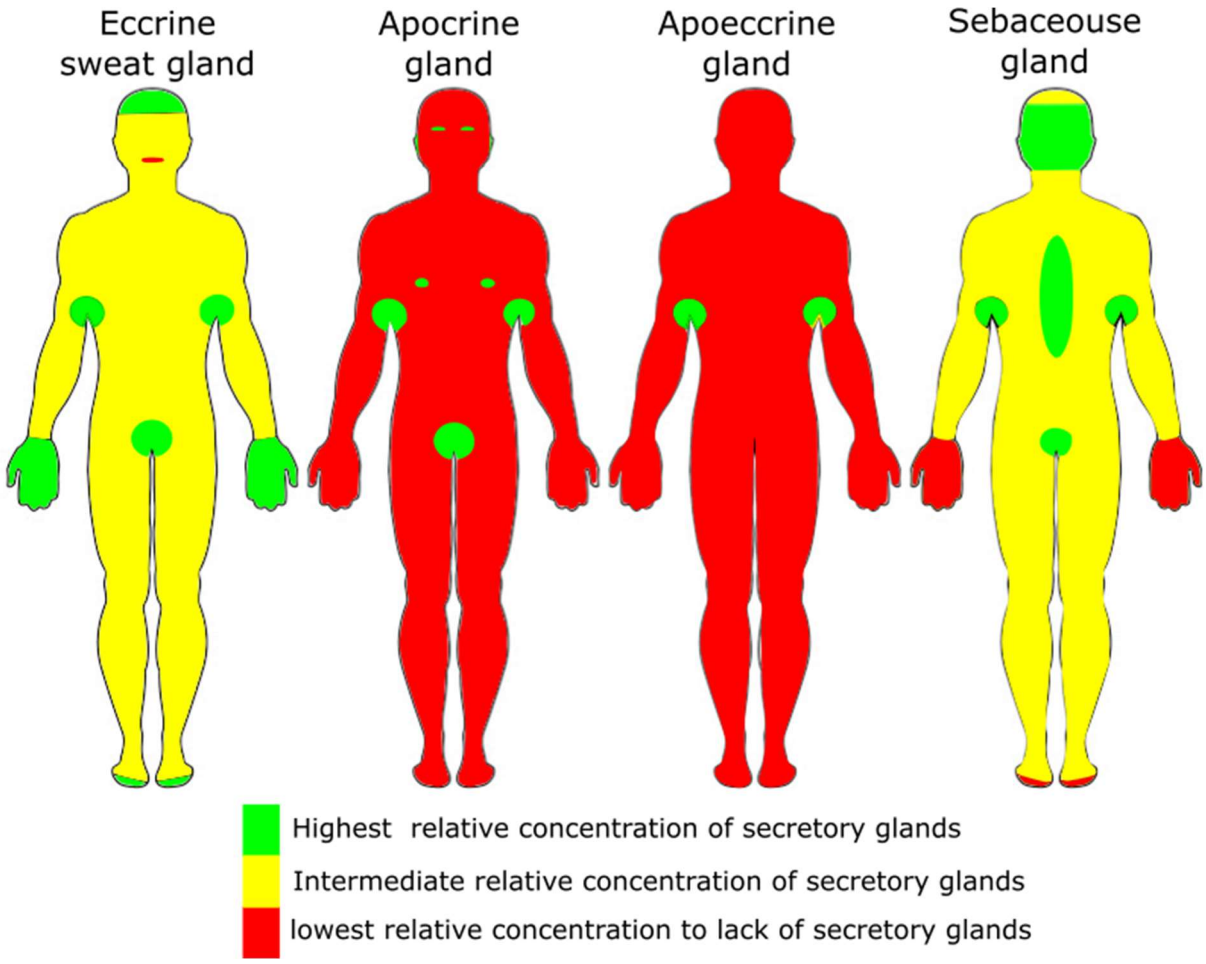

Figure 1.2 Comparison of the distribution of secretory glands in skin.

1.1.3 Sebaceous gland

Sebaceous glands are an additional secretory gland that are typically associated with hair follicles. However, in some in instances such as the eyes, they are independent glands, as shown in Figure 1.2. Originally described in 1826 by Eichorn (Hussain, Mantri, and Cohen 2017), sebaceous glands comprise one or more lobal structures, referred to as acini. These are connected by a number of lumens to a central lumen. The central lumen then connects the main body of the sebaceous gland to either the associated hair follicle or the surface the skin (Hussain, Mantri, and Cohen 2017) (Niedecken et al. 1990) (Strauss 2006). The main function of the sebaceous gland is the secretion of sebum, which is a viscous, lipid-rich secretion generated from sebocytes and keratinocytes undergoing holocrine secretions (Hussain, Mantri, and Cohen 2017; Shi et al. 2015). Because of this, the composition of sebum differs considerably from the secretions generated by all the other secretory glands. Moreover, its exact function is unknown but it is believed to contribute to pheromone

dispersal when it interacts with the skin's microbiome (Hussain, Mantri, and Cohen 2017; Baker 2019; Shi et al. 2015).

1.2 Eccrine sweat gland

The ESG is the component of mammalian skin responsible for generating and secreting sweat onto the outermost surface of the epidermis. Initially observed and reported in 1833 by Purkinje and Wendt and subsequently in 1834 by Breschet Roussel de Vouzzeme (Montagna W 1974), the ESG is a single tubular structure (Cui and Schlessinger 2015; Saga 2001; Sonner et al. 2015; Sato et al. 1989b; Bovell 2015) that starts in a knot-like formation in the dermis, transects the epidermis and opens onto the outermost surface of the skin as shown in Figure 1.3.

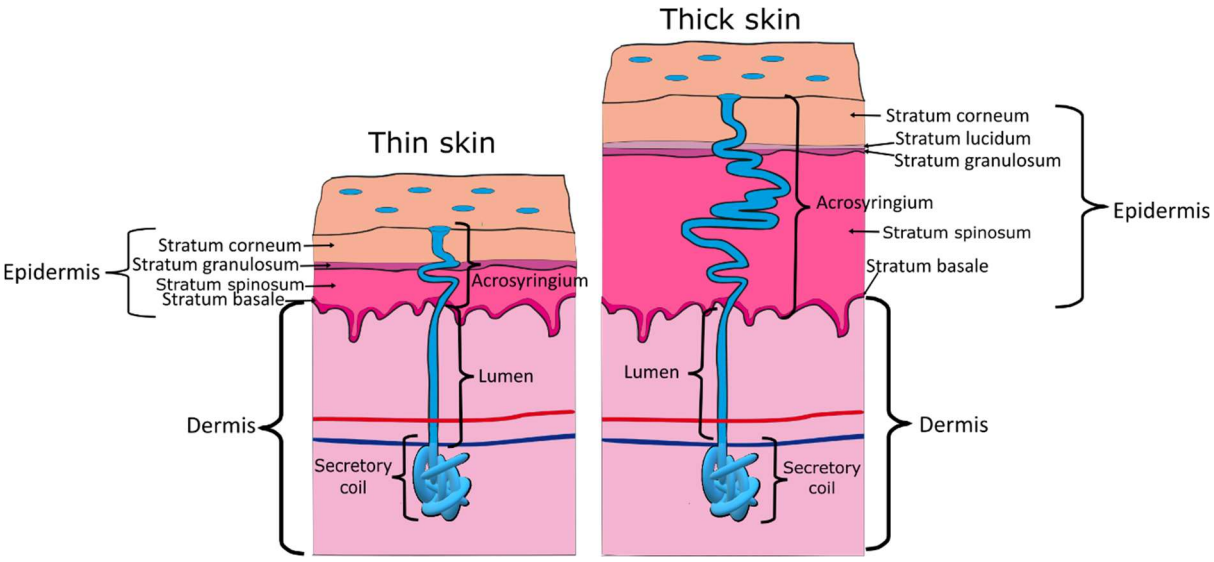

Figure 1.3 Diagrammatic representation of the eccrine sweat gland.

The diagram illustrates the eccrine gland in both thin and thick skin. Furthermore, significant structure/tissue are denoted of the eccrine gland and the surrounding tissue.

1.2.1 ESG structure

The ESG comprises three morphologically and functionally distinct regions: the Acrosyringium, the lumin and the secretory coil (Figures 1.3 & 1.4).

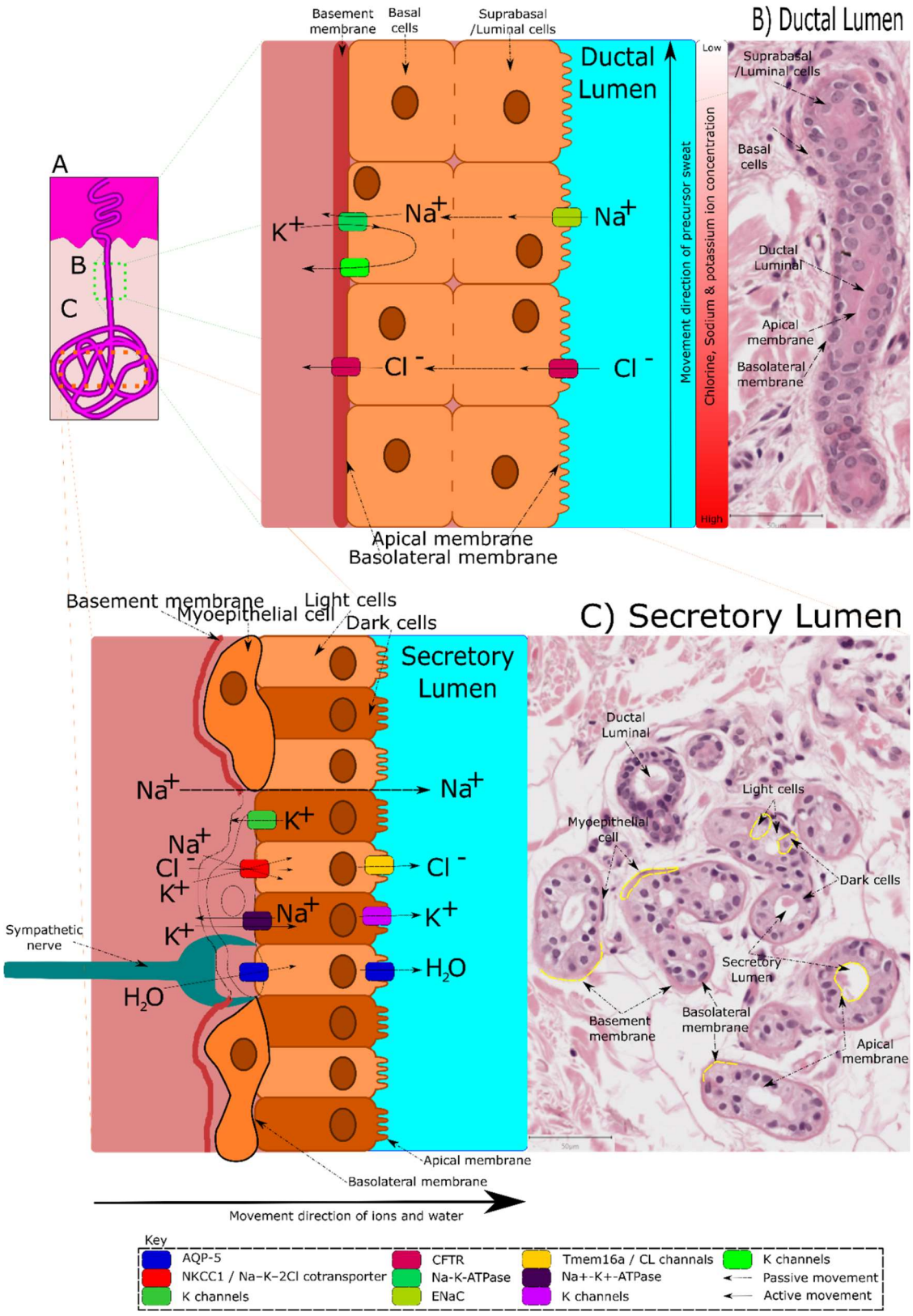

Figure 1.4 summary diagram of sweat generation by the eccrine gland.

A is the simplified representation of the eccrine sweat gland, highlighting the regions that are more closely examined in the rest of the figure. B illustrates the different cells that make up the secretory coil's lumen. The different types and regions are the basal membrane, myofilial cells, light cells, dark cells and apical membrane. These are correlated to a H and E-stained section of a secretory coil. C) illustrates the different cells that make up the Ductal lumen. The basal cells, luminal cells and luminal duct also are identified on an H and E-stained section of the luminal region. Furthermore, the figure illustrates the

reabsorption by the body of ions from preliminary sweat by both active and passive transporters. This in turn generates secretory sweat, which migrates to the ACROSYRINGIUM . Also illustrated are a number of active and passive transporters that are initially used to move ions to generate an osmotic gradient to draw water into the secretory lumen to generate preliminary sweat

1.2.2 ESG secretory coil

As previously mentioned, the Secretory coil (Scoli) has a knot-like morphology, approximately 500–700 µm, typically located 4–8 mm below the surface of the skin. Each of the components has an internal diameter of 30–40 µm and an external diameter of 60–120 µm (Figures 1.3 and 1.4)(Gibbons et al. 2009) (Wilke et al. 2007).There are three main types of cells associated with this region: clear cells, dark cells and myoepithelial cells, as shown in Figure 1.4.

The main function of Scoli is the generation of preliminary sweat, which is initiated by secreting acetylcholine from the post ganglionic neurons associated with the sympathetic nervous system. Acetylcholine binds to muscarinic receptor M3 from the G-protein coupled receptors (GPCRs) family. This, in turn, initiates phospholipase C activity, which causes phosphatidylinositol 4,5-bisphosphate (PIP2) into inositol triphosphate (IP3). IP3 opens IP3Rs, which release endogenous (stored) calcium ions (Ca^{+}) from the endoplasmic reticulum membrane into the cytoplasm. This initiates an influx of endogenous Ca^{+}(Metzler-Wilson and Wilson 2016; Kudlak and Tadi 2021). This release of Ca^{+} activates proteins stromal interaction molecule 1 and 2 (STIM1 and STIM2) causing translocation from the endoplasmic reticulum to the plasma membrane. There they bind with ORAI1, a $Ca2^{+}$ release-activated $Ca2^{+}$ (CRAC) channel. This, in turn, allows for an influx of extracellular Ca^{+} (Prakriya and Lewis 2015; Concepcion et al. 2016; Alzayady et al. 2016; Shaw et al. 2013). It also stimulates a number of ion channels and co-transporters to generate an osmotic gradient between the lumen and surrounding tissue. On the basolateral membrane, the NKCC1 / Na-K-2Cl cotransporter promotes movement of Na^{+}, K^{+} and CL^{-} into the light cell. While ion channels such a Na^{+}-K^{+}-ATPase, NHE1, CFTR and Tmem16a promote the movement of K^{+} and CL^{-} across the apical membrane into the lumen. This is achieved via AQP-5 channels, where water follows this osmotic gradient collecting in the lumen and generating the precursor sweat.(Kahle, Rinehart, and Lifton 2010; Xie et al. 2017; Concepcion et al. 2016; Cui et al. 2016; Toyomoto et al. 1997).

1.2.2.1 ESG lumen / duct

The luminal region of the ESG transects the dermis between the secretory coli & the acrosyringium (Figures 1.3 & 1.4). The lumen region of the ESG comprises a bilayer of cells that form the tubular structure. The innermost surface is a layer of luminal cells followed by a basal cell. Some publications indicate that these two layers of cells act as a syncytium (Bovell 2015; Baker et al. 2019). This therefore allows for free movement of material across the two layers of cells. The key functions of this region is the reabsorption of a portion of ions from preliminary sweat and generating the secreted sweat. Sodium ions (Na^+) reabsorb into the body at this point in a two-stage process (Reddy and Quinton 1994) (Sonner et al. 2015) (Sato 1977). First, passive movement of sodium ions across the luminal surface/apical membrane via epithelial sodium channel (also known as ENaC or amiloride-sensitive epithelial sodium channels) of the luminal cells defuses across the two layers of previously described cells (Sonner et al. 2015) (Clausen, Hilbers, and Poulsen 2017). Second, the sodium ions are then actively transported across the basolateral membrane into the dermis. This active transport is achieved by Na-K-ATPase in an ATP-dependent reaction, in which two potassium ions are exchanged for three sodium ions in the basolateral membrane (Baker 2019; Clausen, Hilbers, and Poulsen 2017; Schwartz et al. 1980; Sato 1977). Reabsorption of chlorine ions (Cl^-) occurs across both the luminal surface/apical membrane and the basolateral membrane via cystic fibrosis membrane channels (CFTR) in a more precise manner (Baker 2019; Clausen, Hilbers, and Poulsen 2017; Sonner et al. 2015) (Sato 1977).

1.2.3 Acrosyringium

The Acrosyringium (ACS) is the region of the ESG that transects the epidermis. It starts in the stratum basal following from the luminal region of the ESG at the interface of the dermis and epithelium (Figures 1.3 to 1.5), and it terminates at the outermost point of the epidermis/stratum corneum (SC). As indicated by Figures 1.3, 1.4 and 1.5, the ACS does not transect the epidermis in a linear and therefore efficient manner. Most illustrations indicate that the ACS is formed in either indirect or helical manner with an approximate diameter of 120–160 µm, and its cadence depends on the thickness and location of the skin in/on the body (Tripathi et al. 2015; Hayut et al. 2014; Feldman et al. 2009; Langbein et al. 2005), as shown in Figure 1.3.

As previously stated, the ACS is a tubular structure that differs from the other regions of the ESG. It comprises a monolayer of cells and a central lumen with an internal diameter of ~20 to 60 μm (Wilke et al. 2007) (Montgomery et al. 1985) (Hibbs 1958). The ACS luminal cells show little to no morphological difference from the surrounding tissue (which are keratinocytes under varying states of differentiation), as shown in Figure 1.5F. The luminal cells and lumen of the ACS remain relatively consistent in the surrounding tissue through the layers of the epidermis, the stratum basal, stratum spinosum and stratum granulosum. Thus, the luminal cells are morphologically indistinguishable from the surrounding tissue in these regions of the ACS, and the diameter of the lumen remains constant. However, in the stratum corneum, the definition of lumen and surrounding cells is replaced with a larger, more irregular lumen/opening to the surface of the skin. Minimal research has been performed on the ACS in comparison to the other regions of the ESG, with most research focusing on IHC staining of the region to identify specific subcellular components. Moreover, there are no specific ACS cell lines available commercially which could contribute to any findings associated with the ACS.

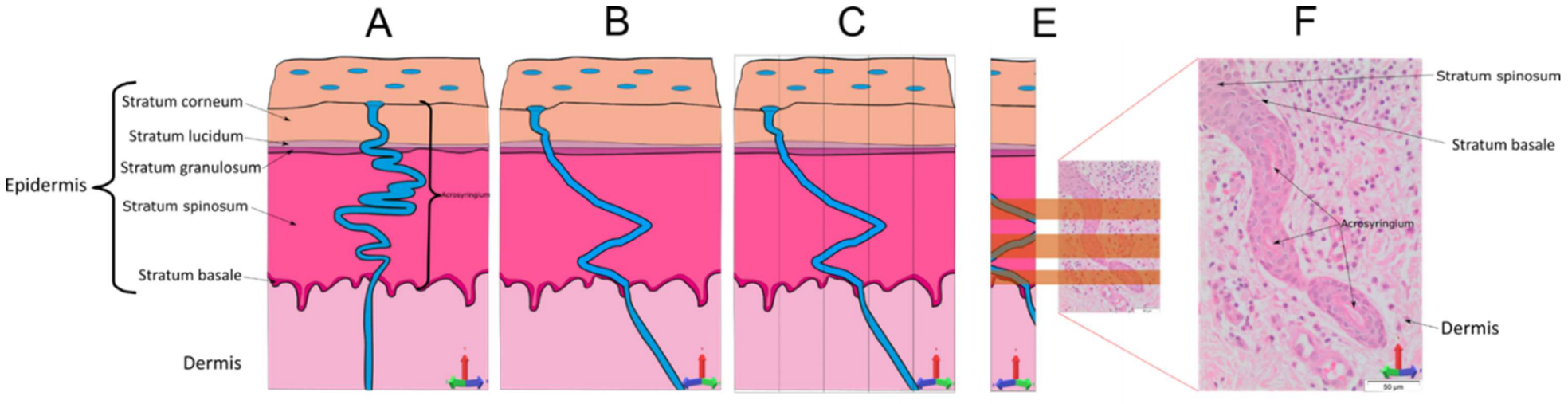

Figure 1.5 Relation of the overall 3-dimensional structure of acrosyringium to individual sections of the acrosyringium.

A) Frontal view of acrosyringium transecting the epidermis. B) Side view of acrosyringium transecting the epidermis. C) Side view of acrosyringium transecting the epidermis, highlighting point of sectioning. D) Comparison to an H and E-stained section of acrosyringium and surrounding epidermis. F) H and E-stained section of acrosyringium with surrounding epidermis and dermis, identifying key structures at 40x magnification.

1.2.4 ESG Function

The primary functions of the ESG are to generate and secrete sweat. Regulated by the central nervous system (Hu et al. 2018), such sweating is mostly associated with thermoregulation and the dissipation of heat from the body by evaporation(Gagnon and Crandall 2018; Verde et al. 1982; Montain, Cheuvront, and Lukaski 2007; Tapper 1990; Sato et al. 1989a). However it is heavily influenced by a number of homeostatic, neurological and physical factors such as hydration, nutrition, health, metal state, drugs, temperature difference with the environment, body mass, age and sex. All these can affect the rate, consistency and location of sweat secreted(Gagnon and Kenny 2012; Kenney 1997; Robinson et al. 1950; Dennis and Noakes 1999; Marino et al. 2000; Best, Caillaud, and Thompson 2012). Furthermore, the sweat secreted by the ESG contains other components that serve other functions. These are lactate, urea, sodium, potassium and amino acids, which act as moisturizing factors to maintain the skin (Watabe et al. 2013). The ESG also has components that contribute to the immune response and defence: antibodies, antimicrobial peptides, proteolytic enzymes and cytokines (Park et al. 2011; Murakami et al. 2002; Horie, Yokozeki, and Sato 1986). The sweat from the eccrine gland been a significant contributor to maintaining and defending the epidermis.

Another function of the ESG contribute to healing epithelial wounds or reepithelialisation of damaged regions, where keratinocytes proliferate from the ESG to promote the healing (Diao et al. 2019; Lu and Fuchs 2014; Rittie et al. 2013; Lu et al. 2012).

1.2.5 ESG Development

The development of eccrine glands occurs prior to birth. With new-borns exhibiting equivalent numbers of ESGs to adults, except that they have a much greater number of ESGs per cm of skin. These are then stretched over a larger region as the individual grows. Furthermore, when a region of the skin is sufficiently traumatised or damaged, resulting in the loss of ECGs (such as from deep burns or loss of skin) no new ESGs form in that region. (Christophers and Plewig 1973; Montagna W 1974; Thomson 1954).

ESGs start developing at approximately week 15–20 of gestation (Montagna W 1974) (Moll and Moll 1992; Ersch and Stallmach 1999; Biedermann et al. 2010). Morphogenesis is initiated by progenitor cells on the epidermal basal layer to invade the hypodermis and form

a sweat gland bud. This bud grows into a column, and once a sufficient depth is reached, the column becomes twisted. The cells in this region then begin to differentiate into myoepithelial cells and luminal cells to form the secretory coli. While this is occurring, a corresponding migration of basal cells progress to the surface of the skin to form an opening to generate the acrosyringium(Li et al. 2012; Lu and Fuchs 2014; Cui and Schlessinger 2015; Christophers and Plewig 1973; Montagna W 1974). Even though it has been formed, ESGs will not become functional and secrete sweat until 3–4 years of age(Montagna W 1974).

1.2.6 Characterisation of acrosyringium

Significant research has been performed on the ESG. This has involved characterising proteomic and immunohistochemical features of the ESG as well as the development of specific cell lines derived from the secretory coli regions. This research focused on the luminal and secretory coli regions of the ESG or the gland as a whole. However, there is information that pertains directly to the acrosyringium.

1.2.6.1 Immunohistochemical Characterisation

Most studies of immunohistochemical staining and profiling of the acrosyringium have focused on its structural components, such as identifying the keratins present. However, other, more generalised studies of the ESG or secretory glands or the skin provided additional insight to the acrosyringium. Theses finding and the publications listed in table 1.1

Table 1.1 summary of published research identifying proteins in the acrosyringium

Pretrain annotation in publication	Pretrain name	Reference
K 1	Keratin 1	(Biedermann et al. 2010; Langbein et al. 2005; Morgan et al. 1999)
K10	Keratin 10	(Biedermann et al. 2010; Langbein et al. 2005; Morgan et al. 1999)
K19	Keratin 19	(Biedermann et al. 2010; Li et al. 2009; Langbein et al. 2005)
K 7	Keratin 7	(Li et al. 2009)
CEA	Carcinoembryonic antigen	(Li et al. 2009)
EMA	epithelial membrane antigen	(Li et al. 2009)
k16	Keratin16	(Langbein et al. 2005)
K17	Keratin 17	(Langbein et al. 2005)
K77	Keratin 77	(Langbein et al. 2005)
K5	Keratin 5	(Morgan et al. 1999)
K11	Keratin 11	(Morgan et al. 1999)
K8	Keratin 8	(Morgan et al. 1999)
K18	Keratin 18	(Morgan et al. 1999)
K4	Keratin 4	(Morgan et al. 1999)
K6	Keratin 6	(Morgan et al. 1999)
Ax-1	Anaxina1	(Bastian et al. 1993)

As previously stated, most of the knowledge base focuses on keratins present in the ACS and how their prevalence changes, depending on the region being focused on. This implies that the Acrosyringium could be undergoing some form of differentiation as it progresses from basal cell to stratum corneum. Congruent to this is the expression of a wide variety of immunological components such as cytokines, inflammatory and S100 proteins.

1.2.6.2 Proteomics Characterisation

To date there is no acrosyringium specific proteomic profile. However, there are three other proteomic profiles from which information can be inferred and compared with once data is obtained. These are proteomic investigations of human skin, which comprise different data sets providing a huge volume of information. These include the Pax DB with over 4000 proteins associated with human skin, and the Manchester skin proteome project, which has shown that healthy skin contains approximately 3000 proteins (Hibbert et al. 2018). The proteomic investigations of the ESG, such as the investigation by Chan Hyun Na of the transcriptomic and proteomic analysis of human ESGs (Na et al. 2019). That study isolated 250 intact ESGs from the abdomen of a single individual, from which 6100 proteins were identified and associated with such functions as secretion, reabsorption (e.g. calcium ion channel) for generating sweat, cell growth, wound healing and a variety of immunological components. Proteomic investigations of human sweat have shown that it contains a myriad of identified proteins that assist with immunological defence, metabolic products, enzymes and waste. With protein identified shown to present is ESG and blood plasma (Raiszadeh et al. 2012; Burat et al. 2021; Na et al. 2019).

1.3 Formalin-fixed paraffin-embedded (FFPE) tissue

Formalin fixation and paraffin embedding (FFPE) of tissue is a form of preservation typically used for clinical samples. It has been in regular use since the mid-1800s(Fox et al. 1985). FFPE is the favoured approach to preservation for several reasons: 1) it prevents the degradation and decay of the tissue and it does not require any specialised storage conditions e.g. temperature, 2) it has a minimal effect on the appearance and morphology of tissue samples, allowing pathologists to make diagnoses, 3) it reinforces and confines the sample to maintain its native structure, allowing for more handling and processing of the tissue sample, such as sectioning and immunohistological staining. The two main aspects of this method of preservation are 1) formaldehyde fixation, which creates a number inter-

and intra-molecular crosslinks in the sample and 2) substitution of water in the sample for paraffin. The process by which samples are treated to generate a FFPE blocks is summarised in Figure 1.5.

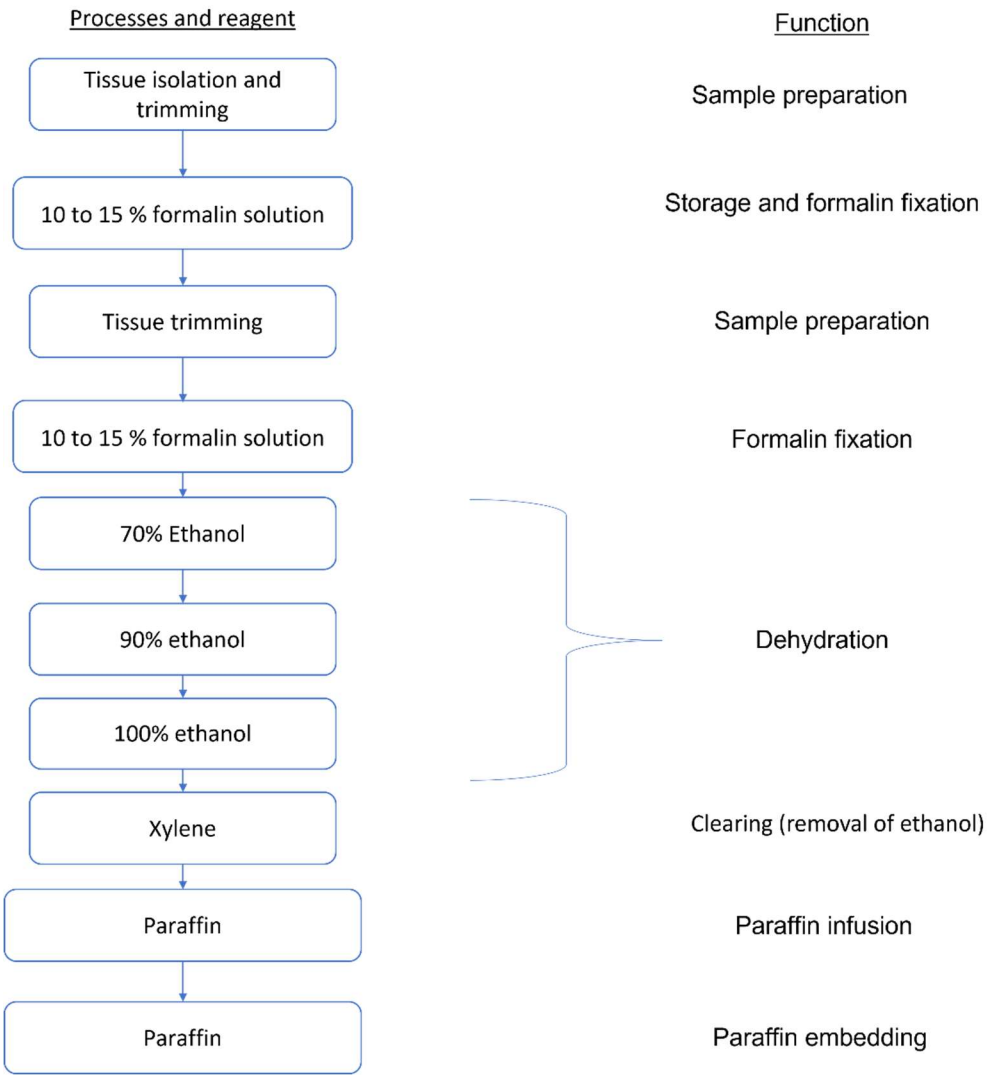

Figure 1.5 Workflow summary of FFPE tissue processing.

1.3.1 Formaldehyde fixation

The formation of methylene bridges by using formaldehyde during fixation is a multiple stage process. Formaldehyde first reacts with the primary amino or thiol group on lysine, arginine, histidine or cysteine residues to form methylol groups. Loss of a water molecule forms the methylol group, resulting in the formation of a Schiff base. Both of these reactions are reversible, however, when the Schiff base reacts with any free residue, i.e. arginine, asparagine, glutamine, histidine, tryptophan or tyrosine. A methylene bridge is formed Schiff base and the free residue locking the amino residues together (O'Rourke and Padula

2016; Giusti and Lucacchini 2013; Fox et al. 1985; Metz et al. 2004; Thavarajah et al. 2012; Puchtler and Meloan 1985)

1.3.2 Method to extract proteomic FFPE tissue peptide

The formation of these inter- and intra-methylene bridges makes FFPE samples more difficult to analyse from a proteomics perspective. This is in part due to traditional lysis or protein purification methods been less effective when isolating proteins and peptides from FFPE samples compared with untreated samples. Secondly if you are able to isolate proteins from as sample it has generally undergone significant PTM (as a result of formalin fixation and storage degradation) that has a number of effects on the analysing the sample :

- Increasing the complexity of the sample as a single unique peptide may now have several variation due to different PTM, or as a results of the aggressive extraction method to isolate the protein. This will also increases the signal : noise threshold.
- Reducing absence of any one peptide due to proportion of it been effect by PTM. Resulting in a reduce likely of been analysed due to grater complexity of sample and low abundance of any one isoform and not reaching the required threshold.(Bantscheff et al. 2012)
- If successfully analysed and a spectrum generated there is a reduced likely hood that it matches with anything in the reference database unless the PTM can be accounted for.

A number of different approach were used to circumvent the limitation caused by methylene bridges when analysing FFPE tissue. These included SDS page extraction, the use of aggressive detergents an buffers and Matrix-assisted laser desorption/ionization (MALDI)(Thompson et al. 2013). These were shown to have limited results. However heat-induced antigen retrieval allowed for the proteomic analysis of FFPE (Bayer et al. 2019; O'Rourke and Padula 2016).

1.3.2.1 Heat-induced antigen retrieval

First described by Shi (Shi, Key, and Kalra 1991), heat-induced antigen retrieval (HIAR) was originally used to enhance immunohistochemical analysis by incubating the samples at ~ 100 ˚C before treatment with antibodies to improve the results of staining. HIAR was then

incorporated into the proteomic analysis of FFPE tissue by Ikeda (Ikeda et al. 1998), who showed that HIAR improved the results of proteomic analysis of FFPE tissue. Subsequent optimisation incorporated HIAR into other proteomic analytical methods, two of the most prevalent in the literature being in-solution digestion and filter-aided sample preparation. However, despite being investigated, the exact mechanisms by which HIAR exposes the components of FFPE tissue for antibody binding or tryptic digestion are unknown. It is hypothesised that adding high-heating steps might denature or break the inter- and intra-molecular methyl bridges formed during fixation(Shi et al. 2006). Otherwise, they would maintain the interconnected structure and prevent the expose of the target sites.

1.3.2.2 In-solution digestion

The first instance of HIAR in conjunction with an in-solution digestion was documented by Shi(Usuda et al. 1996), who treated FFPE tissue with HIAR in a detergent. Then, depending on the detergent used, a buffer changes or clean up may be performed to generate conditions suitable for protein digestion. This sample preparation method showed improved proteomic analysis of FFPE tissue in comparison to its predecessors (Davalieva et al. 2021; Usuda et al. 1996; Shi, Cote, and Taylor 1998). Subsequent optimisations of this method have been published with notable improvement. However, this process continues to be the cornerstone on which subsequent methods have been developed.

1.3.2.3 Filter-aided sample preparation (FASP)

Originally described in 2009(Wisniewski et al. 2009) the FASP method uses multiple protease and fractionation of the sample to maximise the coverage of the sample. Subsequent iterations of this method have been optimised with the use of FFPE (Ostasiewicz and Wisniewski 2017; Ostasiewicz et al. 2010; Wisniewski 2013; Wisniewski, Ostasiewicz, and Mann 2011; Wisniewski et al. 2009), in which FFPE samples were suspended in detergent, heat treated (HIAR) and then lysed. Lysate is then applied to ultrafiltration units where samples are digested and peptides are eluted and then fractionated before LC-MS/MS analysis.

A number of direct comparisons of in-solution digestion and FASP and their derivatives have been performed. These have typically resulted in little difference between them, with the

results in favour of whichever method the paper is focused on (Ostasiewicz and Wisniewski 2017; Davalieva et al. 2021; Foll et al. 2018) (Marchione et al. 2020).

1.3.3 Complications of FFPE vs frozen tissue regarding proteomics

In most studies, the methods of proteomic analysis of FFPE results were compared with fresh/frozen tissue isolated from either the same or a similar piece of tissue. In these comparisons, tissue volumes ranged from 0.1 mm^3 to 5 mm^3. In most instances, peptide and protein identifications showed similar results, with discrepancies of less than 5–20% between the two sample types. Furthermore, the majority of protein identified are present in both samples (approximately 60–80%) (Scicchitano et al. 2009; Ostasiewicz et al. 2010; Nirmalan et al. 2011; Zhang, Muller, et al. 2015; Marchione et al. 2020), confirming that FFPE can be representative of the sample. The differences seen in the peptide and protein profiles between the two groups can certainly be attributed to the additional processing that the fixed samples undergo when they are preserved and then analysed. As seen in Figure 1.5, FFPE tissue is exposed to a number of solvents, such as ethanol, Xylene, paraffin and harsh conditions HIAR could result in the loss or reduce or denaturing of some proteins. Where as the formation of methyl bridges may prevents movement and loss of a proteins and prevent the passive or active degradation of proteins resulting its identification in the FFPE sample. This changes the likelihood that specific peptide ions are selected by the mass spectrometry resulting in a small divergence of identifications.

1.4 Mass spectrometry for proteomics

Proteomics is the study of how proteins function, to which a keep part is understand their structure. This can encapsulate a large number of factors, including how and when it is expressed, how the proteoform may undergo post-translational modifications to be activated, inhibited, translocated, interacting with other proteins or even incorporated into a larger complex (Tyers and Mann 2003; Wilkins et al. 1996). A wide variety of technology and techniques enable us to study proteins. For this study, the focus is on shotgun proteomic/bottom-up proteomics, in conjunction with liquid chromatography-tandem mass spectrometry (LC-MS/MS). The bottom-up approach to proteomics was chosen because it has been shown to be more successful at isolating and identifying proteins from FFPE, compared to a top down approach. It is also more suitable for label-based and label-free quantitative techniques(Gustafsson, Arentz, and Hoffmann 2015).The process of bottom-up

proteome can be separated in to a number of stages Following elution, peptides undergo electrospray ionisation (ESI) to transfer them from a solvent state to a charged gaseous state, that can enter mass spectrometer.

1.4.1 Sample isolation and digestion

Initial isolation of FFPE tissue for proteomic analysis is a multi stage process in which the specificity of isolated material can be veered depending on the target of analysis. The first instance of this is the specificity of tissue initially isolated and preserved using the formalin fixation and paraffin embedded process described in figure 1.5. In the case of this study as surgical bioassays obtained from a biobank were used. Samples contained the acrosyringium (aria of interest) as well as supplementary tissue. Removal of unwanted material/tissue prior to this stage could increase the efficacy of later stages of isolation and analysis as shown in (Zhang, Li, et al. 2015). Following embedding of the fixed tissue black are typical sectioned -using a microtome generating a 5 to 20 µm section. If sufficiently specific these section can be directly possessed for proteomic analysis (Nirmalan et al. 2011; Addis et al. 2009) or can be further micro dissected for a more targeted isolation as was the case in this study. One such method for further micro dissection is laser capture microdissection(LCM) (McGregor et al. 1991). In LCM tissue section cut with the microtome are mounted, to a Poly Ethylene Naphthalate, (PEN) or Poly Ethylene Terephthalate (PET) membrane. PEN and PET being polymers that be cut using a UV laser (249 ŋm). The mounted tissue section are then suspended in a laser capture microscope where the tissue can be imaged and structures of interest identified (e.g. acrosyringium). The UV laser can then be used to micro dissect the regen of interest, causing it to fall way from the rest of the mounted tissue where it can be collected and further prosed for proteomic analysis.

Isolated FFPE samples undergo HIAR in detergent-rich conditions to break methylene bridges and promote the solubility and denaturing of the proteins , (Davalieva et al. 2021; Usuda et al. 1996; Shi, Cote, and Taylor 1998) (Gustafsson, Arentz, and Hoffmann 2015). Samples then undergo reduction and alkylation of cysteine sulfhydryl groups to form S-carboxyamidomethyl-cysteine. This breaks any disulphide bonds and prevents them from reforming later (Suttapitugsakul et al. 2017). Proteolytic digestion is then used to generate peptides. The size, quantity, quality (the fidelity of protases to proteolytic site) and characteristics of the peptides generated are directly related to the protease used. They also dramatically influence the number and confidence of identification by effecting the

complexity of the sample. As a sample with a the greater number of peptides will result in a larger search space increases the likelihood misidentification.

In this instance, Trypsin was used, which cleaved at the C-terminus of Arginine and Lysine residues unless followed by a Proline(Zhang et al. 2013; Quesada-Calvo et al. 2015; Luebker and Koepsell 2016).

1.4.2 Reverse phase high-pressure liquid chromatography

Mass spectrometers have a limited capacity for the isolation and analysis of peptide ions. With less complex samples (e.g., singular proteins) this is inconsequential. However, with complex samples, this is detrimental and results in a more superficial analysis of the sample. To account for this limitation, the rate at which peptide ions are introduced to the mass spectrometer is controlled to prevent or limit the ineffective analysis of peptide ions due to loading. This is achieved by reverse-phase high-pressure liquid chromatography (HPLC) in which peptides are loaded and bound to a C18 column (stationary phase). Then, the peptides are eluted off the column by incrementally increasing the concentration of the organic solvent (mobile phase), such as acetonitrile. The peptides are thuse separated depending on their hydrophobicity, where more hydrophilic peptide ions are eluted first, resulting in a gradient.

1.4.3 Electrospray ionisation

Following elution, peptides undergo electrospray ionisation (ESI) to transfer them from a solvent state to an enter and charged gaseous state to insert into the mass spectrometer. This is a non-destructive form of ionisation (often referred to as soft ionisation) in which the sample in a volatile liquid phase is passed through a strong electric field at high temperature, generating highly charged droplets with an equivalent charge to the capillary tube. The combination of the factors causes the peptides within the droplets to disassociate forming isolates with multiply charges, as gas-phase peptide ions. (Fenn et al. 1989).

Thermo Q Exactive HF hybrid quadrupole-Orbitrap mass spectrometer

In this study, the Thermo Scientific Q Exactive HF hybrid quadrupole-Orbitrap (QEXHF) mass spectrometer was used. The QEXHF is a tandem mass spectrum (Ms/Ms) analyser capable of

higher-energy collisional dissociation (HCD) cell for fragmentation and an Orbitrap mass analyser. A diagrammatic representation of the key components is displayed in Figure 1.6.

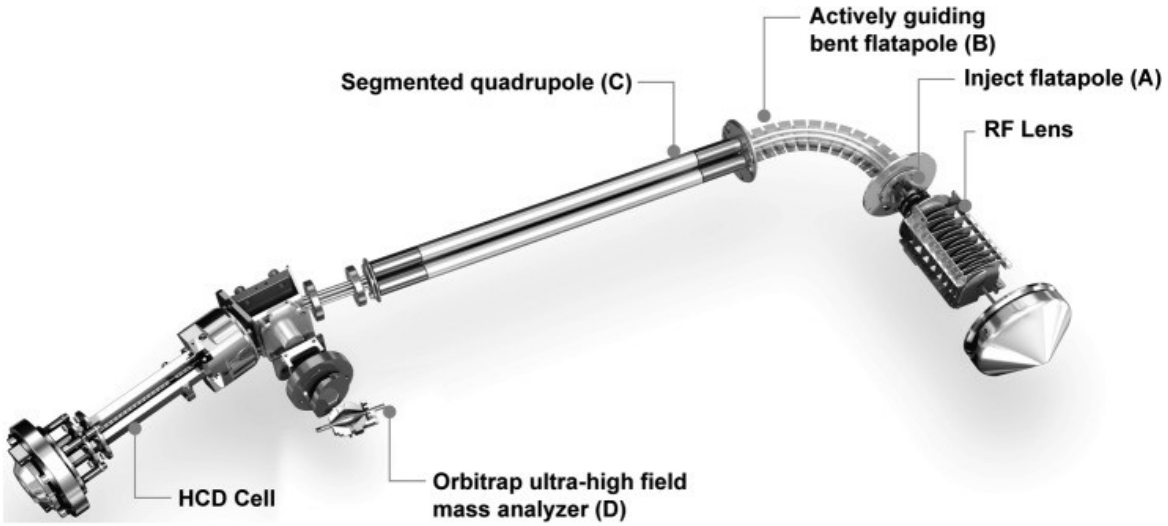

Figure 1.6 Schematic view of the Thermo Scientific Q Exactive HF hybrid quadrupole-Orbitrap mass spectrometer. Taken from Figure 1 of (Scheltema et al. 2014).

Following ESI, the peptide ions are introduced to the QEXHF in which the ions pass through radio frequency (RF) lenses. The ions are focused into an ion beam, preventing unwanted mass separation of the particles of interest. The focused ion beam then passes through an inflection flatapole and bent flatapole, where uncharged neutral species are filtered out. Then, the peptide ion beam enters the quadrupole, where alternating RF potentials are applied to the ions by corresponding poles. This allows for the filtering of the ions by their *m/z* ratio. The filtered peptide ions are then collected in the C trap, where they are arrested by reducing the RF and then introduced to the Orbitrap for identification and generation of the first spectrum providing the intensity and *m/z* of ions present. From the most abundant (a max of the top 16) are identified. The quodrapole is then used to isolate one of the most intense ions which are sent to the C-trap for collection. this packet is then sent to the HCD cell for fragmentation an then to orbitrap to generate the MS2 spectrum. While this is the set of identified ions are collected in preparation for fragmentation and analysis. This is repeated until all 16 targets have been analysed and the process is repeated.

1.4.4 Fragmentation

In the case of the QEXHF, HCD is used to fragment the isolated ions. HCD is a specific form of collision-induced dissociation (CID).CID is performed in a specialised chamber in which packets of ions are excited by increasing the RF voltage, which then collide with a neutral gas (e.g., nitrogen), causing the ions to vibrate to the point it disassociate resulting in fragmentation this typically occurs along the peptide backbone of the ion. This often produces b-ions (N-terminal ion) and y-ions (C-terminal ion), from the precursor ion. However, further fragmentation of these ions can occur, resulting in smaller ions or various species (Olsen et al. 2007). This heterogeneous mixture is then sent to the Orbitrap to generate the MS2 spectrum.

1.4.5 Orbitrap

Originally developed by Makarov in the late 1990s (Makarov 2000), the Orbitrap consists of two key parts, an inner spindle-like electrode and a complementary outer electrode. Ion packets from the C trap are introduced into the cavity between the electrodes at an offset from the electrodes of the central electrode. A voltage is then applied across the inner and outer electrodes, generating an electric field which in turn course the ions to orbit the central electrode and oscillate along its length. The frequency of these oscillations dependent on the mass to charge ratio (*m/z*). The frequency of the repeating oscillation generates a current that can be detected by the out electrode to generate a time-domain signal, which is Fourier transformed and can be used to generate the spectra.

1.4.6 Data analysis

Once collected, the MS1 and MS2 spectra must be processed to determine what proteins were present. This is achieved by processing the data using a search engine, like MASCOT (Perkins et al. 1999) or DB (Zhang et al. 2012), which compares the experimental values with the calculated values of the in silico digests of the proteins from the database (e.g., human proteome) being searched against. This infers the peptide spectral matches (PSM). These are then compered with both the target database and a decoy database, in order to determine the likelihood of a match is legitimate or due to happenstance. The value generated form this is the false discovery rate (FDR) and can be used as selective value to

filter dater depending in the likelihood of it been a random occurrence. For this project a FDR of 1% was used.

1.5 Aims:

The aim of this study was to characterise the proteomic profile of the acrosyringium of the human eccrine sweat gland. To gain further understanding of the components that make up the acrosyringium and from this, derive a better understanding of the overall structure and its functions. Feather expanding into how the acrosyringium and interactions with the local environment, bodily secretions and surrounding tissue. Due to the use of formalin-fixed paraffin-embedded samples for the proteomic analyses. It is necessary to optimise a methodology for protein extraction and analysis, as existing published methods require larger volumes of tissue than could be feasible obtained for this study. Due to the limited amount of tissue samples available and the relatively sparse nature of these glands within the skin. following implement of this optimised method for proteomic analysis of acrosyringium rich tissue, findings are to be validated using immunohistology means to confirm the presence and distribution of spathic proteins in the acrosyringium and surrounding tissue. Following validation it is intended to investigate the effect of altered expression of the significant proteins of interest, in representative keratinocyte model. In order to gain a grater understanding the effects altered expression theses proteins in the context of keratinocytes.

Chapter: 2 Material's & Methods

2.1 Material and solutions

Table 2.1 Buffer composition

Name	**Buffer composition**
ammonium bicarbonate (Ambic) Lysis buffer	0.2% (w/v) RapiGest in 250 mM AMBIC and 1 mM Dithiothreitol (DTT)
Tetraethylammonium bromide (TEAB) lysis buffer	0.5% (w/v) RapiGest in 100 mM TEAB and 1 mM DTT
Zeroing TEAB lysis buffer	0.5% (w/v) RapiGest in 100 mM TEAB and 1 mM DTT
Cell lysis buffer	100 mM tris hydroxymethyl aminomethane (Tris) pH 8.0, 125 mM Sodium chloride (NaCl), 5 mM Ethylenediaminetetraacetic acid (EDTA), 1% (v/v) SDS, 1% (v/v) NP-40, 1% (v/v) sodium deoxycholate, 1X EDTA-free complete protease inhibitor (Roche) and 1X phosSTOP (Roche)
4X Sodium dodecyl sulfate (SDS) -PAGE loading buffer	0.2 M Tris(hydroxymethyl)aminomethane hydrochloride (Tris-HCl) (pH 6.8), 16% (v/v) glycerol, 8% (w/v) SDS, 0.4% (v/v) bromophenol blue, 0.4 M DTT
4X resolving gel buffer	1.5 M Tris-HCl (pH 8.8)
4X stacking gel buffer	0.5 M Tris-HCl (pH 6.8)
Colloidal coomassie stain	0.12% (w/v) Coomassie G250 dye, 10% (w/v) ammonium sulphate, 10% (v/v) phosphoric acid and 20% (v/v) methanol.
SDS running buffer	25 mM Tris, 192 mM Glycine, 0.1% SDS,
Transfer buffer	25 mM Tris, 192 mM Glycine, 0.1% SDS, 20% methanol
Tris-buffered saline with 0.1% Tween (TBST)	20 mM Tris-HCl, 150 mM NaCl, pH 7.4, 0.001 v/v Tween20
Liquid Chromatography with tandem mass spectrometry (LC-MS/MS) Buffer A	0.1% (v/v) Formic acid

LC-MS/MS Buffer B	80% (v/v) Acetonitrile (MeCN) 0.1% (v/v) Formic acid
LC-MS/MS loading buffer	2%(v/v) MeCN, 0.1% (v/v) TFA
LCMS/MS syringe wash	10% (v/v) MeOH
LCMS/MS seal wash	20% (v/v) MeCN, 10% (v/v) isopropanol

2.2 Preparation of fresh and formalin-fixed paraffin-embedded (FFPE) tissue

2.2.1 FFPE sectioning and hematoxylin and eosin staining

FFPE tissue blocks were pre-chilled on ice for 30 min. The tissue blocks were then sectioned using a microtome (Leica microsystems) at a thickness of 4 µm. The sections were subsequently mounted onto plain glass slides and incubated at 40˚C for 1 hour. Following incubation, slides were suspended in fresh xylene three times for 1 min each, followed by immersion in three concentrations of ethanol 100%, 70%, 50% for 1 min each, and washed in water. The slides where then immersed in the following reagents and rinsed in water before being transfer to the next reagent: Haematoxylin for 2 min, 1% acid alcohol for 5 seconds, Scotts's tap water for 30-60 seconds, alcoholic eosin for 2 min and rinsed in water. After the last rinse in water, the slides were sequentially submerged in 50%, 70%, 100% ethanol and xylene for 1 min each, and then stored in fresh xylene. The slides were air dried before applying distyrene, plasticizer and xylene (DPX) and cover slipped as shown in Figure 2.1B.

2.2.2 FFPE Microdissection

FFPE tissue blocks were pre-chilled on ice for 30 min. Membrane slides (Leica 11505151, Leica 11505158) were incubated in a UV crosslinking chamber delivering UV-C at 254 nm, 1 joule of energy for 30 min. The FFPE tissue blocks were then sectioned using a microtome at a thickness of 10 µm, with the sections then being mounted on the prepared slides and incubated at 40˚C for 1 hour. The tissue mounted slides were passed though fresh xylene three times for 2.5 min each, followed by immersion in three concentrations of Ethanol

100%,70%,50% for 1.5 min each and then washed in water and allowed to air dry as shown in Figure 2.1A.

FFPE tissue mounted slides were micro-dissected using a Leica LMD7000 with FFPE tissue settings described in Table 2.2. The microdissected FFPE tissue (isolates) were collected in 0.5 ml Eppendorf tube (0.5 ml ultra high recovery microcentifuge tube E140-2600 , STARLAB (UK)) containing 40 µL of 0.1 M Tetraethylammonium bromide (TEAB) loaded into the gravity feed collection block of the Leica LMD7000. Isolates were centrifuged at 16,500 relative centrifuge force (g) for 2 min, the supernatant disposed of, and re-suspended in 40 µL of fresh 0.1 M TEAB. The centrifugation and buffer change was repeated twice with the isolates being resuspended in 13 µL of 0.1 M TEAB in the final resuspension. These isolates where then 'flash frozen' in liquid nitrogen and stored at -80˚C.

Table 2.2 Leica LMD7000 LCM laser cutting parameters.

Tissue type	Default	FFPE tissue	Frozen tissue
Power w/m2	45	50	22
Aperture f	15	27	10
Speed mm/s	10	4	5
Specimen Balance	15	17	15
Line Spacing For Darw + Scan	12	5	5
Head current	100	100	100
Pulse frequency (Hz)	120	120	120

2.2.3 FFPE immunohistochemistry staining

As above, FFPE tissue blocks were pre-chilled on ice for 30 min. The FFPE tissue blocks when then sectioned using a microtome at a thickness of 4 µm, the FFPE tissue sections were then mounted on X-tra adhesive slides (3800200IHC White) and incubated at 40˚C overnight.

Mounted tissue sections were then transferred to the BOND RXm and processed using the conditions detailed in Table 2.3, depending on the antibody used. After processing the slides, they were submerged in water and sequentially submerged in 70%, 90% and 100% ethanol for 10 second each before transferring to xylene until cover mounting. Any excess xylene was allowed to air dry before applying DPX and coverslip to the tissue section on the slide. The slides were then left to dry.

Table 2.3: Antibody specification obtained form atlas antibodies

Antibody ID	Target	Bond	stain	Incubation	pH	Antibody
HPA000452	KRT17	ER1	Dab	20 min	6	1:500
HPA045697	KRT6a	ER1	Dab	20 min	6	1:500
HPA045934	KRT77	ER1	Dab	20 min	6	1:750
AMAB90558	ANXA1	ER1	Dab	20 min	6	1:250
HPA004135	CPABP2	ER1	Dab	20 min	6	1:200
HPA55992	SERPINB3	ER1	Dab	20 min	6	1:100
HPA036444	ABHD14b	ER1	Dab	20 min	6	1:50
HPA040725	CALML5	ER1	Dab	20 min	6	1:2,000
HPA019869	GSTP1	ER1	Dab	20 min	6	1:1,500
HPA040182	TPSD1	ER1	Dab	20 min	6	1:500
HPA051520	RPN 1	ER1	Dab	20 min	6	1:25
AMAB91136	LAMC1	ER1	Dab	20 min	6	1:50

2.2.4 Frozen tissue microdissection

Leica 11505151 slides were exposed to UV-C at 254 nm, 1 joule of energy for 30 min.

Tissues were sectioned and mounted to slides by LIBL using a cryo microtome at a thickness of 10 µm and stored at -80 ˚C until needed. Before use, the tissue mounted slides were allowed to warm to room temperature (RT) and sequentially submerged into 70%, 90% 100% ethanol for 2 min each, then stored on dry ice until needed.

Frozen tissue mounted slides were microdissected using Leica LMD7000 using frozen tissue settings described in Table 2.2. The microdissected frozen tissue isolates were collected in 0.5 ml Eppendorf tubes containing 40 µL of 0.1 M TEAB loaded into the gravity feed collection block of the Leica LMD7000. Isolates were centrifuged at 16,500 g for 2 min, the supernatant disposed of and resuspended in 40 µL of fresh 0.1 M TEAB. The centrifugation and buffer change was repeated twice with the isolates resuspended in 13 µL of 0.1 M TEAB in the final resuspension. These isolates were then ‘flash frozen’ and stored at -80 ˚C.

Figure 2.1 (A) flow diagram representation of 2.2.1. FFPE sectioning & H&E staining method. (B) flow diagram representation of 2.2.2. FFPE-Microdissection method. (C) flow diagram representation of 2.2.5. Frozen tissue-Microdissection method.

2.3 Heat induced antigen retrieval (HIAR)

Eppendorf ThermoMixer C (5382000031) with a Eppendorf Thermo top (5308000003) (Eppendorf incubator) were preheated to 99 ˚C whilst isolates were thawed to RT and centrifuged at 16,500 g for 2 min. Then, 20.3 µL of TEAB lysis buffer (as described in table 2.1) was added to each isolate then vortexed for 1 min. Isolates were then incubated at 99 ˚C at 825 g for 30 min in an Eppendorf incubator.

Isolates were transferred to an ice bath and incubated for 5 min. Isolates were then vortexed for 1 min and incubated at 80 ˚C at 825 g for 2 hours. Isolates were then transferred to an ice bath for 5 min, and spun down for 10 seconds. Protein content was determined using a Thermo Scientific NanoDrop 2000, set to 280 ηm wavelength

2.4 Fresh tissue lysis

Isolates were thawed to RT, and centrifuged at 16,500 g for 2 min at RT. 100 µL of TEAB lysis buffer (as described in Table 2.1) was added to each isolate and vortexed for 1 min. Isolates were then incubated at 80 ˚C at 825 g for 3 min, transferred to an ice bath for 5 min and spun down for 10 s. Protein content was determined using a Thermo Scientific NanoDrop 2000, set to 280 ηm wavelength.

2.5 Cell Culture and Lysis

2.5.1 Culture media

Low-calcium fetal bovine serum (FBS) – FBS (gibco 10270-106) was treated with 7.6 g/L of Chelex 100 resin (BioRad; catalog number 142-2832) then incubated at 4˚C while being agitated for 1 hour before use.

Low-Calcium growth medium (LCGM) – Dulbecco's Modified Eagle Medium (DMEM) (Gibco 21068-028) media supplemented with 10% (v/v) low calcium FBS, 1% (v/v) 3.0 mM calcium chloride solution , 2% (v/v) 200 mM L-glutamine (Gibco 25030-024) which was then filter sterilised (Millipore; 0.22 µm pore).

High-calcium growth medium (HCGM) - DMEM (Gibco 21068-028) media supplemented with 10% (v/v) low calcium FBS, 1% (v/v) 280 mM calcium chloride solution , 2% (v/v) 200 mM L-glutamine which was then filter sterilised (Millipore; 0.22 μm pore).

2.5.2 Cell passaging and diffraction

2.5.2.1 High sensitivity of human epidermal keratinocytes (HaCaT) bacal Cells

HaCaT bacal cells were cultured in LCGM at 37˚C, 5 % CO_2.

2.5.2.2 HaCaT differentiated Cells

Differentiated HaCaT cells were cultured in HCGM at 37˚C, 5 % CO_2.

2.5.2.3 Cell passage

HaCat cells were grown in the appropriate medium until 70 – 90 % confluence. Growth media was aspirated, and cells were washed twice with Dulbecco's phosphate buffered saline (PBS) (14190094 Gibco) then incubated with Trypsin-EDTA solution (Sigma T3924-100ml) for 20 min at 37˚C, 5 % CO_2. The detached cells were diluted 1 in 6, and re-suspended in the appropriate growth media and re-plated for growth

2.5.2.4 Differentiation of HaCaT bacal cells

HaCaT bacal cells were diluted during passage and resuspended in HCGM instead of LCGM. Evidence of differentiation was observed after 48 hours and differentiation deemed to be complete after 5-7 days.

2.5.3 SIRNA transfection

2.5.3.1 Plate seeding

Twenty four hours prior to siRNA transfection, HaCat cell were plated and grown to 80-90 % confluence. Media was aspirated and cells washed twice with PBS. Cells were then incubated with Trypsin-EDTA solution for 20 min at 37˚C, 5 % CO_2. Cell count was determined using a TC20-Automate cell Counter (BioRad) and each well

of the 12 well plate was seeded with $6.6x10^4$ cells / mL. Well volume was then made up to 1 ml using appropriate growth media (LCGM for HaCaT bacal and HCGM HaCaT differentiated cells) before incubating at 37˚C, 5 % CO_2 for 24 hours.

2.5.3.2 Initial transfection

Transfection was performed in 12-well plates using siRNAs listed in Table 2.4. siRNAs were diluted in 1× siRNA buffer (B-002000-UB-100 Horizon Discovery) to 5 µM, and diluted to 5% (v/v) in Opti-MEM reduced serum medium (Opti-MEM)(31985062 Thermofisher) (100 µl total volume). Transfection reagent (2.5 uL of DharmaFECT 1 Transfection Reagent T-2001-02 horizondiscovery) was mixed with 97.5 µl of Opti-MEM and 100 µl of the siRNA dilution,mixed and incubated at RT for 20 min before adding to 800 µl of LCGM and carefully pipetting onto the plated cells. After 6 hours, the media was replaced with fresh LCGM. After 24 hours, the transfection process was repeated (if necessary).

Table 2.4 siRNA summary table.

Target	Product name	Product code	manufacture
ANXA1	ON-TARGETplus Human ANXA1 (301) siRNA - SMARTpool	L-011161-00-0010	Horizon Discovery Biosciences
CALML5	ON-TARGETplus Human CALML5 (51806) siRNA	L-013401-00-0010	Horizon Discovery Biosciences
GAPD	ON-TARGETplus GAPD Control Pool	D-001830-10-05	Horizon Discovery Biosciences
N/A	ON-TARGETplus Non-targetingPool	D-001810-10-05	Horizon Discovery Biosciences

2.5.4 HaCaT Cell lysis

Cell culture media was aspirated and cells washed with PBS twice. Cells were scraped into 250 µl of cell lysis buffer (as described in table 2.1)and the supernatant collected. Lysis was achieved by sonication (VCX130 Sonics), 10 intervals of 10 sec on 30 sec off at 30% power.

2.6 Cell lysate protein analysis

2.6.1 Cell lysate and protein quantification

Lysate protein quantification was performed using Pierce BCA Protein assay Kit (23225 ThermoFisher) following the manufacturer's recommended protocol, using bovine serum albumin (BSA) standard of 0.0, 0.25, 0.5, 1.0 and mg/mL

2.6.2 SDS PAGE Gel

2.6.2.1 Sample preparation

Cell lysates were diluted as required and mixed with 4X SDS-PAGE loading buffer (as described in table 2.1)in a 1 to 4 ratio before heating at 95ºC for 10 minutes, allowed to cool and prior to loading on to an SDS gel

2.6.2.2 SDS page gel

Samples were run on 10%,15% and 20% (as specified in table 2.5) polyacrylamide gels. Wells in the gel were loaded with either 5 µl of P7719S (new england biolabs Protein Standard 10–250 kDa) protein standard ladder, 35 µl of cell lysate in SDS page loading buffer prepared as described in 2.6.2.1 for samples and lysate controls. Control samples were made up to 0.045 ng/µl of recombinant CALML5 protein in 4X SDS-PAGE loading buffer (as described in table 2.1) and 0.179 ng/ul of recombinant Annexin A1 protein in 4X SDS-PAGE loading buffer (as described in table 2.1) of which 35 µl was loaded into the well as a control sample. Any blank wells in the gel were loaded with 35 µl of 1X SDS-PAGE loading buffer(as described in table 2.1). Separating of proteins was done by electrophoresis at 200V for ~45 min.

Table 2.5 SDS pages gell

SDS Page Acrylamide %	10% resolving gel	15% resolving gel	17% resolving gel	4% stacking gel	Unit
30% acrylamide	3.3	2.5	2.9	1.3	ml
4X resolving gel buffer (as described in table 2.1)	2.5	1.25	1.25	0	ml
4X stacking gel buffer (as described in table 2.1)	0	0	0	2.5	ml
10% SDS	100	0.05	0.05	100	ul
water	4.0	1.15	0.75	6	ml
100 mg/ml ammonium persulfate	100	50	50	100	ul
N,N,N',N'-Tetramethylethylenediamine (TEMED)	10	5	5	10	ul

2.6.3 Coomassie Staining

SDS-PAGE gels were submerged in colloidal coomassie stain and incubated overnight at RT on an orbital shaker, after careful removal of the stacking gel. Gels were destained via repeated washing of the gel with milliQ water while being agitated on an orbital shaker at RT. Washes were repeated until the gel was cleared and could be imaged.

2.6.4 Western blot

Following SDS-PAGE, proteins were transferred either on 0.2 µm nitrocellulose membrane (10600001 amersham protran) or 0.45 µm polyvinylidene difluoride (PVDF) membrane (88518 Thermo scientific) (as specified in the text). Membranes were soaked in methanol before being paired with SDS-page gels. Transfer was performed (as described in table 2.1) at 300 mA for 1.5 hours at 4 °C.

Membranes were blocked in 5% milk in TBST solution (as described in table 2.1) for 1 h on an orbital shaker at RT. Membranes were then incubated with 5 ml of 5% milk in TBST solution with the primary antibody as described in Table 2.6 overnight at 4 °C. Following incubation, the membranes were washed three times for 5 min in TBST, before being incubated in 5 ml of 5% milk in TBST solution with the appropriate secondary antibody (HRP linked antibodies) as described in Tables 2.6 and 2.7, for 1 hour at RT. Following secondary antibody incubation, the membranes were washed five times for 5 min in TBST, followed by incubation with SuperSignal West Pico Chemiluminescent Substrate (Thermo Scientific) according to the manufacturer's protocol. Membranes were imaged using film (Fuji) or CCD camera (Fujifilm LAS-3000).

Table 2.6 Western blot primary antibodies

Target	Product code	Dilution factor	monoclonal or polyclonal	Host species	manufacture
Annexin A1 ANXA1	AMAB90558	1:1,000	Monoclonal	Mouse	atlas antibodies
CALML5 CLSP	HPA040725	1:1,000	Polyclonal	Rabbit	atlas antibodies
CALML5	ab154631	1:500	Polyclonal	Rabbit	abcam
GAPDH	ab8245	1:1,000	monoclonal	Mouse	abcam
keratin 1	200-301-880S	1:1,000	Polyclonal	Rabbit	atlas antibodies
ALPHA-TUBULIN	200-301-880S	1:1,000	monoclonal	Mouse	Rockland

Table 2.7 Western blot secondary antibodies (anti IgG HRP-linked)

Target	Product code	Dilution factor	monoclonal or polyclonal	Host species	manufacture
mouse IgG	7076S	1:1,000	N/S	Horse	Cellsignal
Rabbit IgG	7074S	1:1,000	N/S	Goat	Cellsignal

2.6.5 bacterial lipopolysaccharide (LPS)treatment of HaCat cells

Established cultures of HaCaT cells were seeded into 12-well plates as described in 2.5.3.1, and where necessary, transfected 72 hours after transfection, cell culture media was aspirated and was replaced with the appropriate fresh media containing either 0 mg/ml, 0.10 mg/ml, 1 mg/ml or 10 mg/ml of LPS (SIGMA, L3024). Plates were then incubated at 37˚C, 5 % CO_2 for 24 h. Media was then transferred to Eppendorfs and centrifuged at 2,000 *g* for 10 min. Supernatant was then collected into fresh tubes and stored at -20 °C

2.6.6 Interleukin 6 (IL-6) and & Interleukin 8 (IL-8) ELISAs

IL-6 or IL-8 ELISAs (enzyme-linked immunosorbent assays) were performed using either the Human IL-6 or Human IL-8 ELISA Kits (ab178013 Abcam, ab214030 Abcam) according to the manufacturer's recommended protocol. For the IL-8 ELISAs (but not the IL-6, where the media was not diluted), the media was diluted either 1:10 or 1:100 (for samples treated with 10 mg/mL LPS only) with the provided Sample Diluent NS prior to testing.

2.7 Sample preparation for mass spectrometry analysis.

Dithiothreitol (DTT) was added to the extracted FFPE isolates to a final concentration of 3.06 mM (7.5 µL of 16.7 mM stock made up to 100 mM TEAB added to 33.3 ul of lysate). Samples were vortexed briefly and incubated at 60˚C with shaking (825 g) for 1 hour, then allowed to cool at RT. Iodoacetamide (IAA) was added to 14 mM final concentration (5.1 µL of 125 mM stock in 100 mM TEAB), vortexed briefly and incubated at RT in the dark for 60 min. The reaction was quenched by adding DTT to a final concentration of 7 mM (4.6 µL of 500 mM DTT stock). Trypsin (Promega gold) was added to the sample using a 1:50 trypsin-to-protein ratio. The total final volume was made up to 66.6 µL by adding 0.1 M TEAB. Digests were then incubated at 37˚C, 825 g for 16 hours/overnight. Subsequently, samples were acidified by adding Trifluoroacetic acid (TFA) to a final concentration of 9.59 mM (0.7 µL 1.0 M stock) and incubated at 37˚C, 825 g for 1 hour.

2.8 Tandem Mass Tagging (TMT) labelling

Overnight digests were centrifuged at 17,135 g for 10 min at 4˚C. Resuspended TMT label (in anhydrous MeCN to 10 µg/µL) was then mixed with samples at a ratio of 16 : 1 TMT:protein. After incubation for1 h at RT, 3.4 µL of 5% hydroxylamine was added to each sample and left at RT for 15 min. Samples were dried to completion by vacuum centrifugation. Peptides were resuspended in 66 µL of 100 mM TEAB, 0.1% (v/v) TFA and vortexed for 1 min. Samples were then sonicated for 10 min in a sonicating water bath, and incubated at 37°C for 50 min at 635 g. Samples were subsequently cleaned up, using the C18 method described in section 2.9.2.

2.9 Sample clean up strategies

2.9.1 Direct injection

Peptides for direct injection were resuspended in sample loading buffer (3% (v/v) MeCN and 0.1% (v/v) TFA), vortexed for 1 min and then sonicated in a water bath (US-CU-CA-9L, allendale-ultrasonics, Hertfordshire, UK) at full power (40 KHz) for 10 min. Samples were then centrifuged at 20,308 g for 10 min at 4˚C and the supernatant was transferred to autosampler vials for analysis

2.9.2 C18

Low bind stage tips were loaded with 3 plugs of C18 material (Empore™ Octadecyl C18, 47 mm). These tips were then centrifuged at 5,077 g for 5 min. 200 µL of MeOH was added to each tip, then centrifuged at 5,077 g for 2 min. This process was repeated twice with 200 µL of C18 elution buffer (60% (v/v) MeCN and 1% (v/v)TFA) followed by two washes with C18 wash buffer (1% (v/v) TFA in H2O). The acidified samples were added to the tips and left for 2 min, then centrifuged at 2,539 g for 2 min. This process was repeated before washing the stage tip twice with 200 µL of C18 wash buffer, centrifuging at 2,539 g for 2 min. The tips were then transferred to a fresh Eppendorf tube, where 66.6 µL of the C18 elution buffer was added to the tips and centrifuged at 2,539 g for 2 min. The eluate was passed though the stage tip again and collected before drying to completion by vacuum centrifugation. Desalted dried peptides were resuspended in LC-MS/MS loading

buffer (as described in table 2.1), vortexed for 1 min, then sonicated at full power (40 KHz) for 10 min. Samples were centrifuged at 20,308 g for 10 min at 4˚C and the supernatant transferred to autosampler vials ready for analysis.

2.9.3 Strong cation exchange (SCX)

Overnight digests were acidified by adding 0.7 µL 1.0 M TFA. Samples were vortexed and then incubated at 37˚C, 825 g for 1 h. The supernatant was then transferred to a fresh tube. Each low bind stage tip was loaded with 3 plugs of the SCX material (Empore™ Supelco 47 mm Cation Exchange disc 2251). These tips were then centrifuged at 5,077 g for 5 min. Samples were loaded on to the tip and centrifuged at 3,800 g for 3 min. The flow though was then reloaded onto the tip which was centrifuged at 3,800 g for 3 min. 50 µL of Ethyl acetate and 50 µL of 0.2% (v/v) TFA were added to each tip which was then centrifuged at 3,800 g for 3 min and the flow-through discarded. This was repeated twice. 100uL of 0.2 % (v/v) TFA was then added to the tip which was centrifuged at 3,800 g for 3 min, and flow though discarded. This was repeated an additional two times. The tips were then transferred to fresh collection tubes. Peptides were eluted by adding 60 µL (2.5% (v/v) Ammonium hydroxide (NH4OH), 97.5% (v/v) MeCN) to the tip and centrifuged for 3 min at 3,800 RCF. The elution was then dried to completion by vacuum centrifugation and resuspended in sample loading buffer, vortexed for 1 min and then sonicated (40KHz) for 10 min. Sample were then centrifuged at 20,308 g for 10 min at 4˚C, with the supernatant transferred to autosampler vials for analysis.

2.10 Liquid Chromatography with tandem mass spectrometry (LC-MS/MS)

Peptides for analysis were separated by reversed-phase capillary HPLC before tandem mass spectrometry, using a UltiMate 3000 nano system (Dionex) coupled to a Q Exactive HF™ (QExHF) mass spectrometer (Thermo Scientific, Bremen, Germany) operating in positive electrospray ionisation (ESI) mode. Digested peptides were loaded via a partial loop onto a C18 trap column (PepMap100, C18,

300 µm x 5 mm) with 2% (v/v) MeCN, 0.1% (v/v) TFA at a flow rate of 9 µL/min for seven minutes. Peptides were resolved on an analytical column (Easy-Spray C18 75 µm x 500 mm, 2 µm bead diameter column) at a flow rate of 0.3 µL/min over a 90 min gradient. This comprised of 3.8% LC-MS/MS Buffer B (as described in table 2.1) to 50% B over 90 min followed by washing and re-equilibration of the column.

MS1 spectra were acquired from *m/z* 350 to 2,000, using a resolution of 60 k at *m/z* 200. Automatic gain control (AGC) of $3E^6$ ions was set with a maximum fill time of 100 ms.

Using a data-dependent acquisition (DDA) strategy, MS2 spectra were acquired from the top 16 most abundant ions with a charge state for +2 to +5 with a minimum intensity of $2.2e^5$. These ions were fragmented using collision-induced dissociation (CID) with a normalised collision energy (NCE) of 30, acquiring product ions over. *m/z* 200 to 2,000 at a resolution of 30 k. An AGC of $1E^4$ ions was set with a max fill time of 45 ms. To avoid repeat selection of ions a 20 sec exclusion window was used.

When required, exclusion lists were incorporated into the method above as described in section 2.9.1.

2.10.1 Exclusion lists

Each sample was analysed three times using the same DDA method as described in 2.10 The second and third repeats used an exclusion list generated following searching of the previous LC-MS/MS analyses (see section Table 2.8 for data searching) to improve overall protein coverage.

2.10.2 Primer exclusion list

The raw data (.raw files) from the QExHF first analytical run of the sample were processed using Thermo Proteome Discoverer (V1.4.1.1.4) in conjunction with

Matrix Science Mascot (V2.6). The searches were performed against UniProt UniHumanReviewed_20180425 database using the parameters listed inTable 2.8.

Table 2.8 LC-MS/MS data searching parameters

Parameter	Setting used
Enzyme	Trypsin
Maximum missed cleavage:	2
Instrument:	ESI-QUAD-TOF
Precursor mass tolerance	10 ppm
Fragment mass tolerance:	0.01 Da
Dynamic modification:	Met Oxidation, Asn Deamidation, Gln Deamidation
Static/fixed modification	Cys Carbamidomethyl

Search results were filtered to a peptide false discovery rate (FDR) of 1% (high peptide confidence) and saved as .MSF files.

Exclusion lists were then generated using the Q Exactive exclusion list function with the following parameters:

- Terms to be exported: include all Post-Translational Modification (PTM) passing the set filters Export *m/z* values.
- Retention time window width 1 min.
- Lower retention time limit 8 min
- Upper retention time limit 107 min.
- Mass precision (decimals) 3
- Max concurrent entries:500.

The resulting .TXT file was then imported and incorporated into the QExHF LC-MS/MS method used to perform the first analytical run. The sample was re-analysed (second analytical run) using the LC-MS/MS method including the exclusion list.

2.10.3 Secondary exclusion list

The raw data files form the second analytical run were processed using the same method as the first analytical run (Primer exclusion list).

Exported search results (.MSF files) from first and second analytical run's were analysed together. The results were then filtered to a FDR of 1% and an exclusion list generated and incorporated into original QEXHF LC-MS/MS method as described above, for the third analytical run of the sample.

2.11 Data analysis

2.11.1 Proteome Discoverer

Raw data files from the QExHF analytical runs were processed using Thermo Proteome Discoverer (V1.4.1.1.4) using the Mascot (v2.6) search algorithm (Matrix Science). Data were searched against UniProt UniHumanReviewed_20180425 database using the parameters listed in Table 2.8.

Search results were then saved as MSF output. Search results were filtered to a FDR of 1% (high peptide confidence).

2.11.2 ProgenesisQI

Label-free protein quantification was performed using ProgenesisQI V2.4 (Waters Corporation, Milford). Raw data files from each experiment were imported into ProgenesisQI. Spectra from each individual analytical run were then aligned against the mix reference samples (an equimolar mix of all samples in the experiment) and filtered to remove any ions with a charge state greater or less then +2 to +5 and less than two isotopes. Sample were grouped based on profile *i.e.* acrosyringium $^{+ve}$ and acrosyringium $^{-ve}$. The summary peaks list was then searched as described above and exported as a .XML file.

The search results file was imported into ProgenesisQI and processed. For high confidence in identified proteins, lists were filtered to only those containing at least one unique peptide and a p-value of less than 0.05.

2.12 Bioinformatics

2.12.1 String

UniProt accession numbers for differentially expressed proteins were uploaded and processed in String-db (version 11, https://string-db.org) using the Multiple Proteins by Names / Identifiers. These searches were performed against the homo sapiens database. The resulting network was then further filtered so that only interactions that are based on experimental evidence or database evidence with a high confidence (greater than 0.7) were denoted. Resulting network (string interaction) was then transferred as a .tsv file to Cytoscape (V3.8.0).

Cytoscape was used to customise the network based on quantification data and clustered groups

2.12.2 DAVID Bioinformatics Resources

Functional annotation of proteins of interest was performed using the database for annotation, visualization and Integrated discovery (DAVID) (version 6.8, https://david.ncifcrf.gov/).UniProt accessions numbers from protein's identified from ProgenesisQI analysis of samples were uploaded and searched using Unipot_Accession as selected identifier and gene list as the list type. Resulting functional annotation chart were downloaded as .TXT files. Data was then filtered using a benjamini-hochberg value of >0.05 and similar terms grouped.

Chapter: 3 Optimisation of the Proteomic Analysis of FFPE.

3.1 Introduction

As indicated in Chapter 1.3.2 proteomic analysis of formalin-fixed, paraffin-embedded (FFPE) tissue has been performed and documented on tissue volumes of 0.25 mm^3 or higher (Nirmalan et al. 2011; Yamashita and Katsumata 2017; Giusti and Lucacchini 2013; Bayer et al. 2019). Due to the size of the acrosyringium and sparsity of the eccrine sweat gland (ESG), isolation of these volumes of acrosyringium-specific tissue (~12,000 (0.12x0.12x0.01 mm =$8.5^{-5}mm^3$) acrosyringium sections) per analytical run was not feasible. Investigation of the effect of reducing FFPE tissue volumes in proteomic analysis was required to develop a method that would allow for analysis to be performed on a smaller volume of starting material.

Heat-induced antigen retrieval (HIAR) is a consistent component of a considerable number of published methods analysing FFPE tissue. First described by Shi (Shi, Key, and Kalra 1991), this technique was originally used to enhance immunohistochemical analysis by heating samples before treatment with antibodies to improve staining results. The mechanisms underlying HIAR have not yet been fully understood or characterised. However, it is suggested that the additional intense heating steps could denature or break the inter- and intramolecular methyl bridges/crosslinks formed during fixation, exposing targets for antibody binding. This technique has been refined further by adjusting timings, temperatures, pH and various other parameters (Greenwell, Foley, and Maronpot 1991; Shi et al. 1992; Shi et al. 2013; Shi et al. 1995; Usuda et al. 1996; Shi, Cote, and Taylor 1997, 1998). The incorporation of HIAR into the proteomic analysis of FFPE tissue was first documented by Ikeda (Ikeda et al. 1998), revealing the increased recovery of protein from FFPE tissue treated with HIAR. The technique was expanded upon by Shi (Shi et al. 2006), who combined HIAR with bottom-up proteomics analysis. Following this, a large variety of methods that incorporated the

HIAR technique for the proteomic analysis of FFPE tissue were published, often comparing protein identification between using FFPE tissue and frozen tissue. Example of these methods include high-yield protein extraction and recovery by direct solubilization (HYPERsol) (Marchione et al. 2020), filter-aided sample preparation (FASP) (Wisniewski et al. 2009; Wisniewski, Ostasiewicz, and Mann 2011; Wisniewski 2013), matrix-assisted laser desorption/ionization imaging mass spectrometry (MALDI IMS)(Judd et al. 2019) and direct triptych digestion (Nirmalan et al. 2011).

As starting material/tissue volume was a limiting factor, the focus was on methods that cut down processing/sample transfer and buffer exchange to minimise the loss of material before LC-MS/MS analysis. For example, methods such as FASP and HYPERsol utilised sodium dodecyl sulfate (SDS) as a detergent, which requires additional clean-up steps before protein digestion as SDS is known to interfere with the tryptic digestion of protein to generate peptides. Many publications used alternative detergents (anionic surfactants) such as Rapigest (Addis et al. 2009; Azimi et al. 2016; Alkhas et al. 2011; Longuespee et al. 2016), which allows for the solubilization of proteins and tryptic digestion without additional clean-up steps, reducing the chance of sample loss. The methods published by Shi and Nirmalan (Shi et al. 2006; Nirmalan et al. 2011) formed the starting point for the method that was developed. These methods were feasible with the materials and facilities available, but also had the potential to be optimised with regards to reducing of initial FFPE tissue and minimising the loss of material during sample preparation. For example HIAR and other chemical reactions such as tryptic digest being performed in a single Eppendorf tube. Which would avoiding filtration, protein precipitation or buffer exchange, which could lead to the loss of material for analysis and interned identifications.

3.2 Aims:

To develop and optimise a reproducible method for the isolation, processing and analysis of FFPE tissue by LC-MS/MS

3.3 Chapter 3 experimental overview

In this chapter experimentation focused on optimisation of existing published methods discussed in section 1.3.2.2 on the isolation and proteomic analysis of FFPE tissue. initial proteomic extraction and analysis was performed on liver FFPE tissue sample due to limited availability of appropriate FFPE skin tissue samples. But following initial testing experimentation moved over to analysis FFPE skin tissue samples . Following successful proteomic extraction and analysis from FFPE tissue subsequent experiment parameters were tested to optimise for uses of a smaller initial FFPE tissue volume. These parameters included: sample preparation, initial tissue volume, in solution digest volume, LC-MS/MS analysis methods and data analysis. The resulting optimised methods, significantly reduced the required volume a FFPE tissue starting volume.

3.4 Results and Discussion

The extraction and identification of proteins from FFPE microdissected tissue were first performed on an FFPE tissue block of human liver tissue. The FFPE liver tissue was used to determine the relationship between FFPE tissue volume and protein identification in order to confirm that a smaller volume of FFPE tissue than indicated by published methods could be used to generate a proteomic profile. In turn, this would allow access to additional tissue samples that are more congruent with the research topic from the Liverpool Bio-Innovation Hub (LBIH) Biobank.

3.4.1 Initial extraction

3.4.1.1 Isolation

Using the settings described in Table 2.1, the Leica LMD 7000 was used for the execution/microdissection of FFPE tissue from the sectioned slides as described in section 1.4.1 and illustrated in Figure 3.1 A-C. Some regions where the tissue was denser or more cartilage-like required multiple passes with the laser for isolation, leading to rougher or more chard and rougher cuts. Furthermore, it was not possible to cut through the tissue in some regions due to the presence of fibrous or sinew structures such as connective tissue. These areas did not burn through completely, preventing the collection of the sample, as seen in Figure 3.1 B (panel labelled 'failed extraction' (FE)).

One factor that impeded the capture of the microdissected tissue sections was the presence of static across the slide surface (this was more prevalent on the Leica 11505158 slides). The static caused the excised region to stick to the surface of the slide approximately 0.5–5 mm from the original cut site. To confirm that the excised region had not stuck to another part of the slide, the areas around the cut sites were inspected for shadows and inconsistencies in tissue morphology after the cut was complete. This inspection was performed at a lower magnification than the extraction so that a larger region could be checked efficiently. Excised sections that had stuck to the surface of the slide were shot a couple of times with the laser to dislodge them. If this approach was unsuccessful, the excised section was corralled to an empty part of the slide (with no FFPE tissue present) using short bursts of the laser (<1 sec), and a large region of the membrane was then cut out and collected in

an Eppendorf tube so the excised tissue would have nothing to adhere to when corralled into the hole created in the membrane.

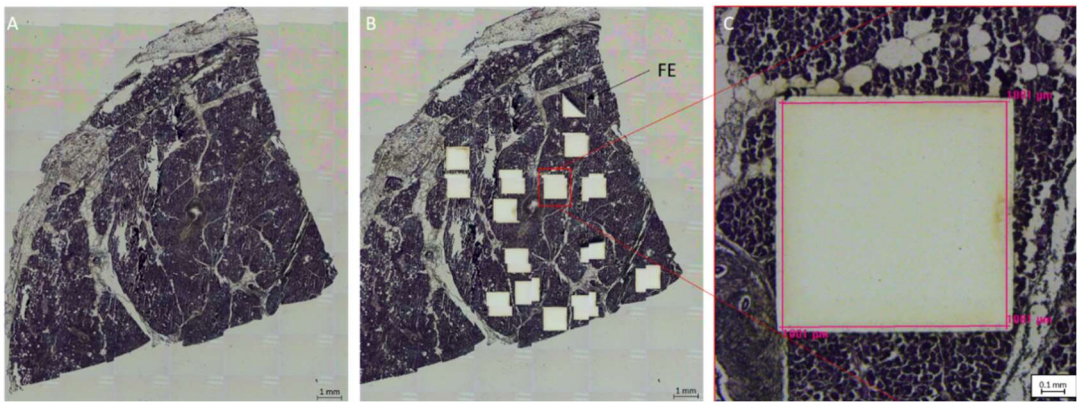

Figure 3.1 Pre and post microdissection images of H&E stained FFPE liver tissue sections.

A) FFPE liver tissue section pre microdissection. B) FFPE liver tissue section post microdissection using a Leica LMD 7000 laser capture microscope. 'FE' indicates a failed extraction. C) Enlarged section of B) highlighting a 1 mm^2 region of excised tissue.

As shown in Figure 3.1, 1 mm^2 sections (with volumes of 0.01mm^3) were extracted from the FFPE liver tissue section. Fifteen of these isolates were combined into a single sample, generating a total volume of 0.15 mm^3 of FFPE tissue per sample replicate. Following HIAR, reduction and deamination of the calculated samples were analysed using nanodrop at 280ηm to determine the protein concentration was estimated to be ~1.1 to 1.6 µg/µl.

3.4.1.2 Preliminary digestion and analysis of FFPE tissue

Protein from three biological replicates of FFPE liver tissue was extracted using the HIAR protocol (Nirmalan et al. 2011) followed by in-solution digestion using trypsin before analysis via LC-MS/MS. Each spectrum of the liver sections was processed using Proteome Discoverer. The spectra were searched against a reviewed Uniprot human proteome database with oxidation of methionine set as a dynamic modification. Results were filtered using a 1% false discovery rate (FDR); then, peptides and proteins were compared (Figure 3.2). Across the three biological replicates, a total of 1,790 proteins were identified, with 54% (968) being present in all three replicates and an additional 21% (376 proteins) being observed in at least two biological replicates. These results confirmed that protein identification from

FFPE tissue was possible using a smaller tissue volume (0.15 mm^3) than that used in previously published methods (0.25 mm^3 or greater) (Nirmalan et al. 2011; Yamashita and Katsumata 2017; Giusti and Lucacchini 2013; Bayer et al. 2019).

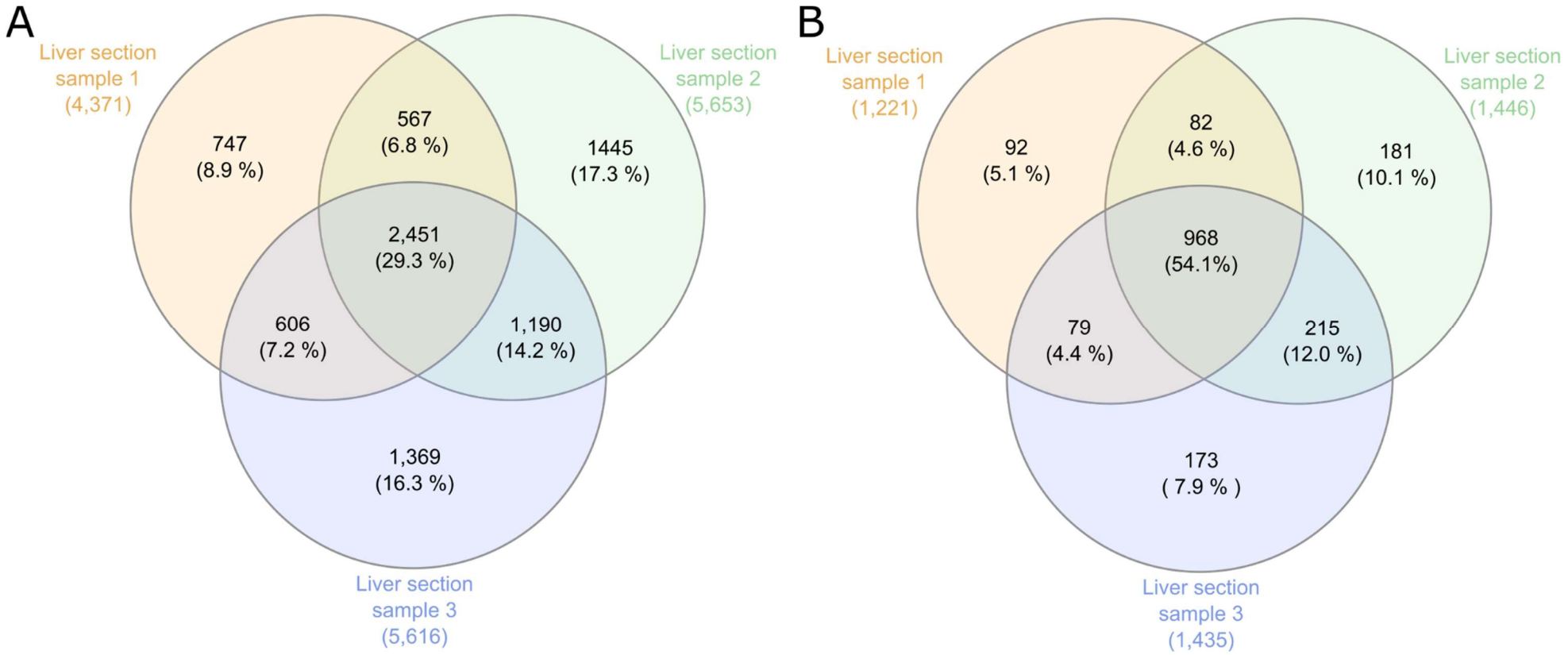

Figure 3.2 Biological replicate comparison of peptides and proteins identified from human liver FFPE microdissections using LC-MS/MS.

Comparison of the A) peptide or B) protein sequences identified across three biological replicates, highlighting the common and unique features identified for each independent biological replicate.

3.4.2 Sample clean-up

While optimising the FFPE tissue extraction method, a number of contaminants were identified, the most prominent being a singly charged ion with a mass of 376 Da eluted at the end of the liquid chromatography (LC) gradient highlighted in Figure 3.3 A-C at ~104 min of the base peak chromatograms (BPC). In some cases, this contaminant was the prominent peak affecting the sample volume that could be loaded onto the LC for each analytical run. To remove the contaminant, both C18 and strong cation exchange (SCX) clean-up methods were evaluated. A digested sample was split in three and treated, and equivalent samples were loaded and analysed by LC-MS/MS. Comparison of the C18 BPC (Figure 3.3 B) and SCX BPC (Figure 3.3 C) revealed a similar profile to the untreated BPC (Figure 3.3 A). Notably, a reduction in the presence of the 376-Da contaminant at ~104 min was visible. Comparison of the clean-up methods regarding the identified proteins (Figure 3.3 D) and peptides (Figure 3.3 E) showed minimal differences in the number and variety of identifications with the majority being present in all three of the samples from the clean-up methods. Figure 3.3 D and E show a small drop in the number of identified proteins and peptides in the cleaned samples compared to the untreated sample. This is unsurprising as these samples underwent additional processing stages involving the binding, washing and elution of the peptides, which could result in the loss of some material. This loss was more significant in the case of SCX. The difference between these clean-up groups could be attributed partially to the stochastic nature of LC-MS/MS analysis, with the observed variation falling within the expected variability among technical replicates. Analysis of pre-and post-blank sample runs surrounded the digested samples showed no presence of

the contaminant, indicating that the contaminant did not bind to the column to be leached in subsequent analytical runs.

As the contaminations were not detrimental to the analysis of the sample and could be removed by washing the samples before HIAR and tryptic digestion, it was decided to proceed without additional clean-up steps such as using C18 and SCX to minimise the chance of sample loss through additional handling.

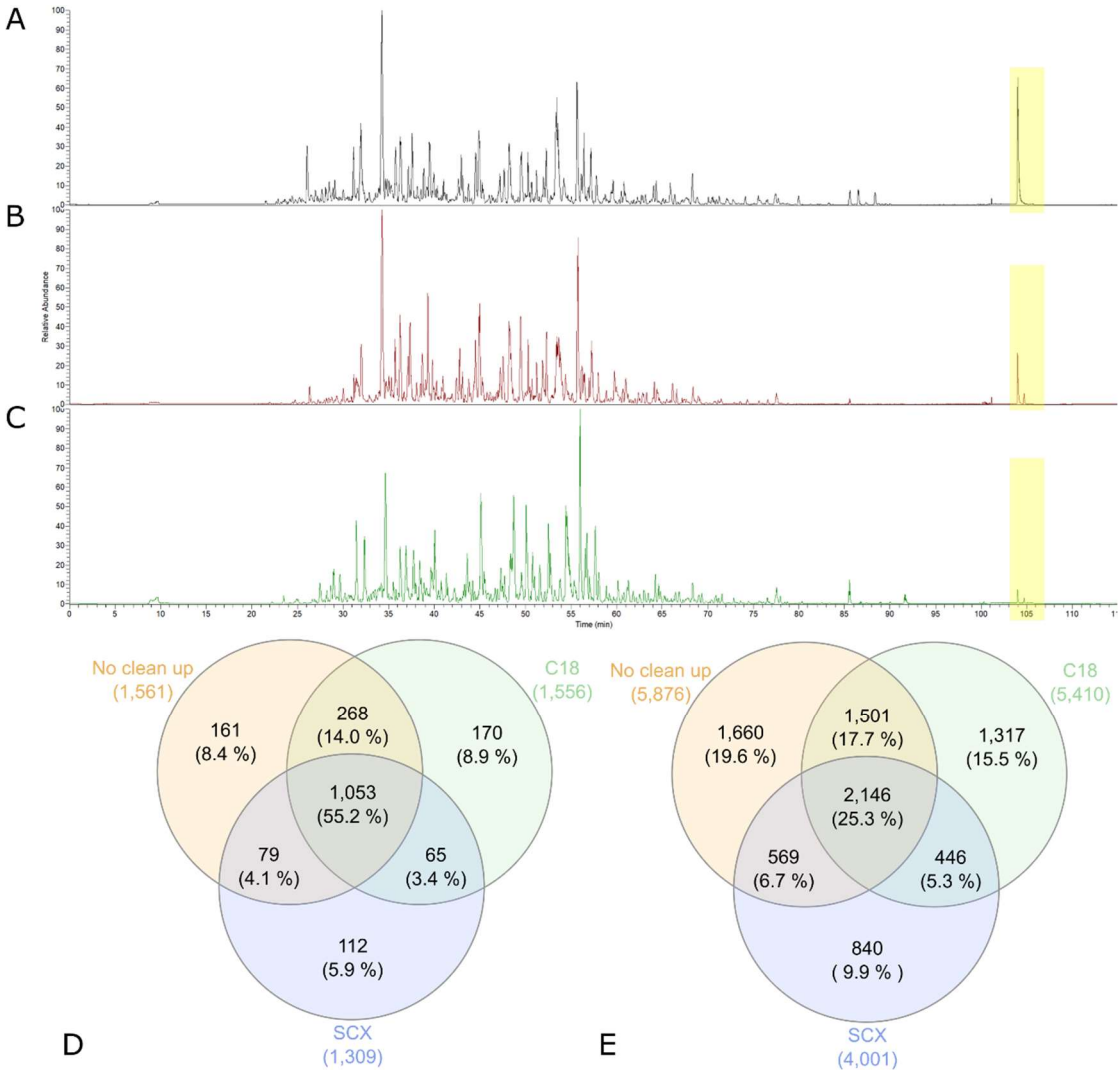

Figure 3.3 Sample clean-up comparison.

A) BPC of untreated digest highlighting the contaminant peak. B) BPC of C18-treated digest highlighting the contaminant peak. C) BPC of SCX-treated digest highlighting the region of the contaminant peak. D) Venn diagram showing the overlap of identified proteins at a 1% FDR between the three different clean-up methods. E) Venn diagram showing the overlap of identified peptides at a 1% FDR between the three different clean-up methods.

3.4.3 Scaling down optimisation

Until this point, FFPE tissue extraction and analysis were performed on 0.15 mm^3 of liver tissue. Based on the previous results, skin FFPE tissue samples were made available, and subsequent development and testing were performed using these skin tissue samples. Following this, various volumes of FFPE tissue were processed and analysed to determine the relationship between tissue volume and protein and peptide identification. The results of the correlation analysis are summarised in Figure 3.4. Unsurprisingly, the smaller the volume of tissue used, the fewer the peptides and proteins identified. An FFPE tissue volume of 0.1 mm^3 appeared to be the smallest volume that could be practically used before the results obtained became unprofitable/unproductive; this volume is equivalent to ~120 (0.12x0.12x0.01 mm =$8.5^{-5}mm^3$) acrosyringium sections. From this point forward, 0.1 mm^3 of skin tissue was used for each replicate.

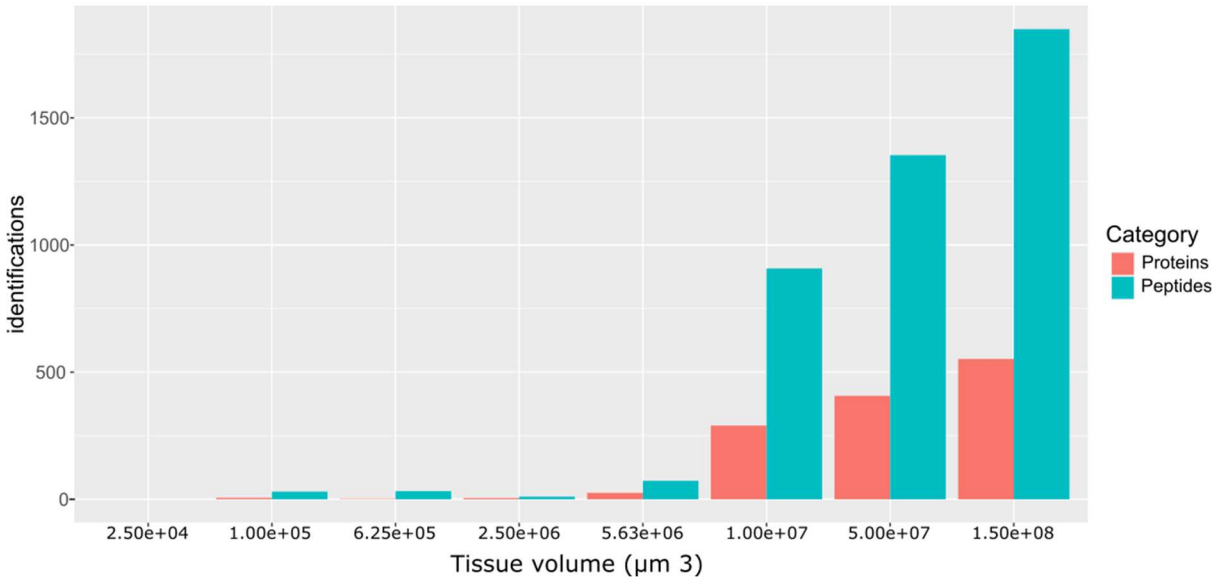

Figure 3.4 Comparison of protein and peptide identification across tissue volumes.

Comparison of the number of peptides and proteins identified from increasing volumes of processed and analysed tissue. Identification was filtered to a 1% FDR at the peptide level.

3.4.4 Reduction of reaction volume

A significant limiting factor of low-concentration peptide samples when performing bottom-up LC-MS/MS is the sample injection volume, which was a maximum of 15 µl. The originally proposed method describes the HIAR reaction being performed in a total volume of 100 µL, with an in-solution digest being performed in a total volume of 200 µL. This is feasible with a larger (e.g., 1 mm^3) volume of starting tissue; however, with a reduced volume of tissue, this results in a sub-optimal concentration due to a lack of peptide ions being analysed and identified. The sample could be concentrated during the sample clean-up steps; however, as these steps were removed from the method, an alternative method of concentration was required, focusing on reducing sample reaction volumes for each stage of HIAR and in-solution digest to minimise sample loss and excessive dilution. Reagent concentrations and volumes were adjusted to maintain the concentration of each reagent at each stage of processing, leading to an overall reduction in reaction volumes from 200 µL to 66 µL (~67 %). Figure 3.5 shows the reduction in reagent volume and increase in the number of proteins and peptides identified. Subsequent extractions and analyses were performed with this reduced reagent volume.

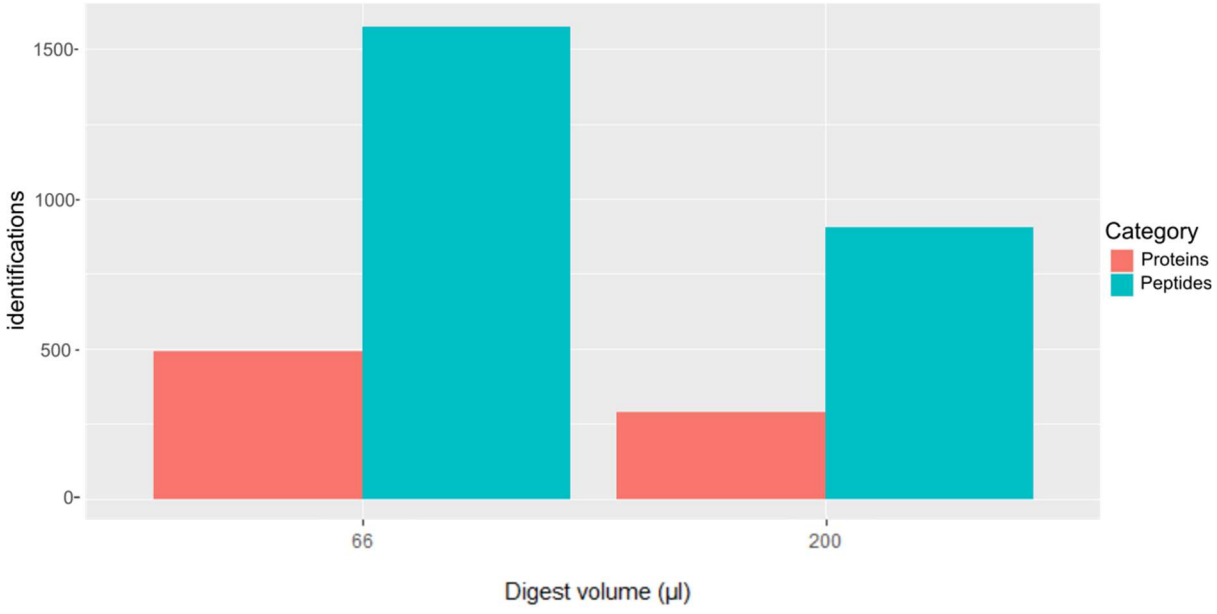

Figure 3.5 Comparison of protein and peptide identification by digest volume.

Comparison of the number of peptides and proteins identified from various digest volumes. Identification was filtered to a 1% FDR at the peptide level.

3.4.5 Exclusion lists

Multiple injection and analysis of a single sample (technical replicates) can enable insights into the sample by increasing the number and confidence of the peptide ions identified. In part this is partly due to the stochastic nature in which peptide ions are selected for analysis and fragmentation, which is influenced by a number of factors such as the abundance of peptide ions, peptide size, number of post-translational modifications (PTM) and isoforms, sample complexity, peptide solubility, overall molecular charge and features such as does the peptide ion fly well. Such factors lead to a more consistent selection of preferred peptide ions and a more varied identification of peptide ions that are less conducive to LC-MS/MS analysis. In other words, when performing technical replicates of complex samples, approximately 60% to 70% of the proteins can be expected to be identified across the replicates, whereas the remaining 30% to 40% can vary. Dynamic exclusion influences the selection of peptide ions for analysis and fragmentation by preventing repeated analysis of already identified ions for a period of time, allowing for the analysis of alternative ions. This feature of LC-MS/MS analysis can be expanded by using exclusion lists generated from previous technical replicates/runs that identify specific ions by their *M/Z* value and when they are likely to be analysed and prevent this from occurring. This, in turn, increases the likelihood of other peptide ions meeting the required thresholds for fragmentation and analysis, and subsequently, peptide and protein identification (Hodge et al. 2013).

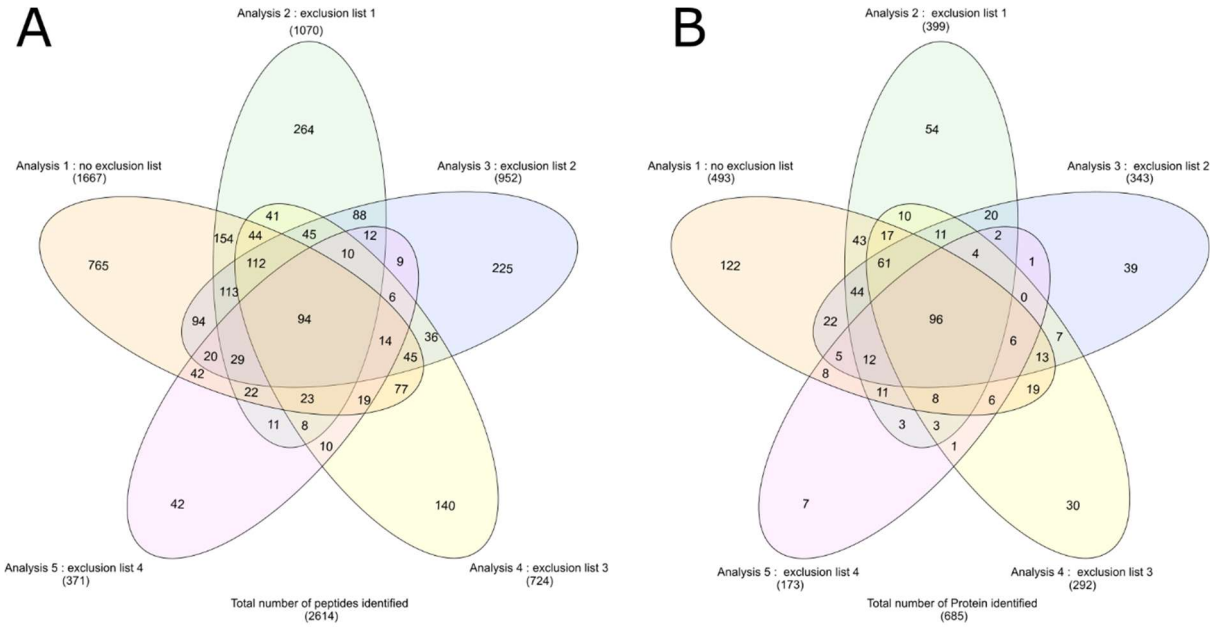

C

Analytical run	total proteins identified	unique proteins not yet identification
1st no exclusion list	493	
2st exclusion list	399	107
3rd exclusion list	343	47
4th exclusion list	292	31
5th exclusion list	173	7

Figure 3.6Comparison of peptide and protein identification with the implementation of exclusions between analytical runs.

A) Comparison of the peptide sequences identified in five technical replicates, highlighting the common and unique elements of each replicate. B) Comparison of the proteins identified in five technical replicates, highlighting the common and unique elements of each replicate. C) Comparison of the proteins identified in five technical replicates analysed in a cumulative manner, highlighting the common and unique elements of each replicate using the previous exclusion list.

All the data presented in Figure 3.6 are from a single experiment, comprising five analytical runs of a single sample (five technical replicates). At the end of each run, a new exclusion list was generated and incorporated into the method for the subsequent analytical runs. Figure 3.6 A and B show that with each analytical run, previously unidentified peptides and proteins are identified, expanding the profile generated. Additionally, the results show a degree of overlap between each run, indicating that the exclusion lists may have a limited effect but a net positive result. Figure 3.6 C compare the proteins identified in a run

compiled with identifications from a previous run. This was done to better understand how much additional information is obtained from each subsequent run. In the case of Figure 3.6 C, approximately 73% of the total protein identifications were from the initial run. Each subsequent run provided an additional number of previously unidentified proteins: the second run provided an additional 14% of the total proteins identified, the third an additional 6%, the fourth an additional 4% and the fifth an additional 0.75%. In Figure 3.6 C, diminishing returns were observed with each consecutive analysis, indicating the need for additional methodological modifications, such as fractionation, alternation in liquid chromatography gradient and adjustment of ACG target and max IT, to gain additional information. With each additional run, the number of additional novel peptide ions and potential identifications inevitably decreases, meaning that the value of each additional run decreases, as shown in Figure 3.6 A-C, where the final 2/5 runs count for < 10% of the total number of identifications. Additionally, other limiting factors also need to be considered, including limited starting material, excessive dilution of the sample to ensure sufficient volumes for analysis, and access to equipment, i.e. duration and cost of each LC-MS/MS analysis. Based on the above results, it was decided to proceed with a total of three analytical runs, which provided the best balance between identifiable information and present limitations.

3.4.6 Open PTM searches

Once synthesised via the translation of mRNA, a proteoform protein will undergo any number of PTMs. These modifications can involve a wide variety of additions and subtractions of different components, affecting the structure and properties of the protein. PTMs are caused by functional processes, enzymatic activity, interactions with the environment and the method of analysis. Proteomics analysis using LC-MS/MS is predicated on the association of the mass of a peptide ion and its fragments to known values. Changes in the mass-to-charge ratio of a peptide ion due to a PTM, e.g. phosphorylation of a cysteine, can lead to a lack of identification or misidentification of the peptide sequence, intern affecting the proportions, confidence and relevance of peptides and subsequently proteins identified from a sample. Thus, compensating for PTMs by including them in the search parameters can increase the number and confidence of the peptides identified. Inversely, compensating for too many PTMs (especially when analysing a complex sample) will have a detrimental effect on identification as each PTM composited for increases the search space, which will increase the potential for misidentification of a peptide ion and reduce the confidence in the identification made. This means that fewer peptides and proteins will meet the thresholds required for successful identification. So, a balance in compensating for a variety of potentially significant PTMs is required for greater confidence in the peptides and proteins identified.

In the initial stages of method development, the PTMs shown in Table 2.8 were used when searching experimental datasets to identify peptides. These PTMs were initially utilised as they were used in the methodology (Shi et al. 2006; Shi, Liu, and Taylor 2007) that formed the basis for the method under development. Furthermore, they were a reasonable set of PTMs to use as carbamidomethylation of cysteine (C) is caused by the use of iodoacetamide (IAA) as part of the in-solution protein digest reacting with sulfhydryl groups to form S-carboxyamidomethyl-cysteine to prevent the formation of disulfide bonds (Suttapitugsakul et al. 2017). Deamidation of asparagine (N) and glutamine (Q), as well as oxidation of methionine (M), are commonplace modifications (regularly naturally occurring PTMs) that are widely used. However, to confirm that the most relevant set of PTMs was being selected as part of the search criteria for this method, an open PTM search utilising PEAKS was performed. PEAKS was used in conjunction with the Unhuman reviewed database to

perform an 'open PTM search' of an FFPE skin sample dataset, with the initial search (closed search) performed using the static modification carbamidomethylation of C and the variable modifications of oxidation of M and deamidation of N and Q. The secondary search (open PTM search) identified other PTMs present on the proteins identified during the first search. The results were filtered to a peptide FDR of 1%.

The PEAKS open PTM search identified over 50 different PTMs with various prevalences associated with skin sample data sets. The top 10 most prevalent PTMs are shown in Table 3.1. Unsurprisingly, the three most significant PTMs were the three used in the initial search on which the open PTM search was based. Of the remaining identified PTMs, methylation of Lysine (K) and arginine (R) and dihydroxylation of phenylalanine (F), K, proline (P), R, tryptophan (W) and tyrosine (Y) were the most prevalent and could potentially be beneficial if incorporated into the search parameters. The remaining identified PTMs occur much more sparsely, and if incorporated into the search parameters used, would likely have a detrimental effect on the confidence of the proteins identified.

Investigation of the PTM methylation of K and R revealed that it is a prevalent modification associated with FFPE tissue samples (Zhang, Muller, et al. 2015). Methylation occurs when proteins are treated with formaldehyde as described in Chapter 1, Section 1.3. The PTM methylation of K and R was incorporated into the search parameters used. The proteins identified were compared with the other searches using different PTM profiles based on the open PTM search; the results are shown in Figure 3.7. When comparing the search results of the original search parameters (Figure 3.7, Search 1) and the search including methylation of K and R (Figure 3.7, Search 2), the majority of proteins identified 1,803 (93.3%) were present in both groups. 94 (4.8%) proteins were identified as unique to the original search parameters and 18 (0.9%) proteins were identified as unique to the adjusted search parameters comprising putative proteins, keratins, ion channels, as well as a variety of other proteins. Of the two search parameters, the original search parameters (Search 1) seem more beneficial due to the higher number of peptide and protein identifications that meet the confidence criteria.

Investigation into the peptides and proteins identified by the open PTM search regarding the dihydroxylation of F, K, P, R, W and Y showed that the majority were associated with

members of the collagen family. Of the ~360 peptides identified with the dihydroxy PTM, 299 peptides were associated with one of seven collagen alpha chains. Each of the individual protein were identified with at least one unique peptide but also displayed, homologous regions/peptides between the different members of the group. As the collagen family is large and encompasses a variety of proteins with diverse functions, it is unsurprising that they adopt a large number of PTMs. As the collagen family is large and encompasses a variety of proteins with diverse functions, it is unsurprising that they adopt a large number of PTMs. Coupled with the fact that collagen is a significant component of skin, it is unsurprising that dihydroxylation was a prevalent PTM in the open PTM search. However, this is not necessarily beneficial to the searches performed as this modification is strongly associated with one particular family of proteins that have already been confidently identified, due to diversity and prevalence within the sample. This is shown in Figure 3.7, Search 3, where dihydroxylation of F, K, P, R, W and Y was incorporated into the search. In comparison with the original search parameters (Search 1), the results of Search 3 are inferior due to a reduction in peptide spectrum matches (PSM) and peptide and protein identifications. A decrease of 3.8% (74) protein identifications was seen when dihydroxylation of F, K, P, R, W and Y was incorporated into the search parameters. Inversely, incorporation of these PTMs did identify an additional 15 (0.8%) proteins, including collagens, keratins and ephrin type-A receptor.

Table 3.1 Open PTM sample analysis, illustrating the top ten most prevalent PTMs identified.

Name	ΔMass (Da)	Position	#PSM
Deamidation	0.98	NQ	3,603
Carbamidomethylation	57.02	C	2,704
Oxidation	15.99	M	1,661
Methylation	14.02	KR	1,265
Dihydroxylation	31.99	FKPRWY	992
Pyro-glu from Q	-17.03	N-term	838
Oxidation	15.99	DKNPRY	600
Acetylation	42.01	Protein N-term	555
Formylation	27.99	K, N-term	503
Phosphorylation	79.97	STY	249

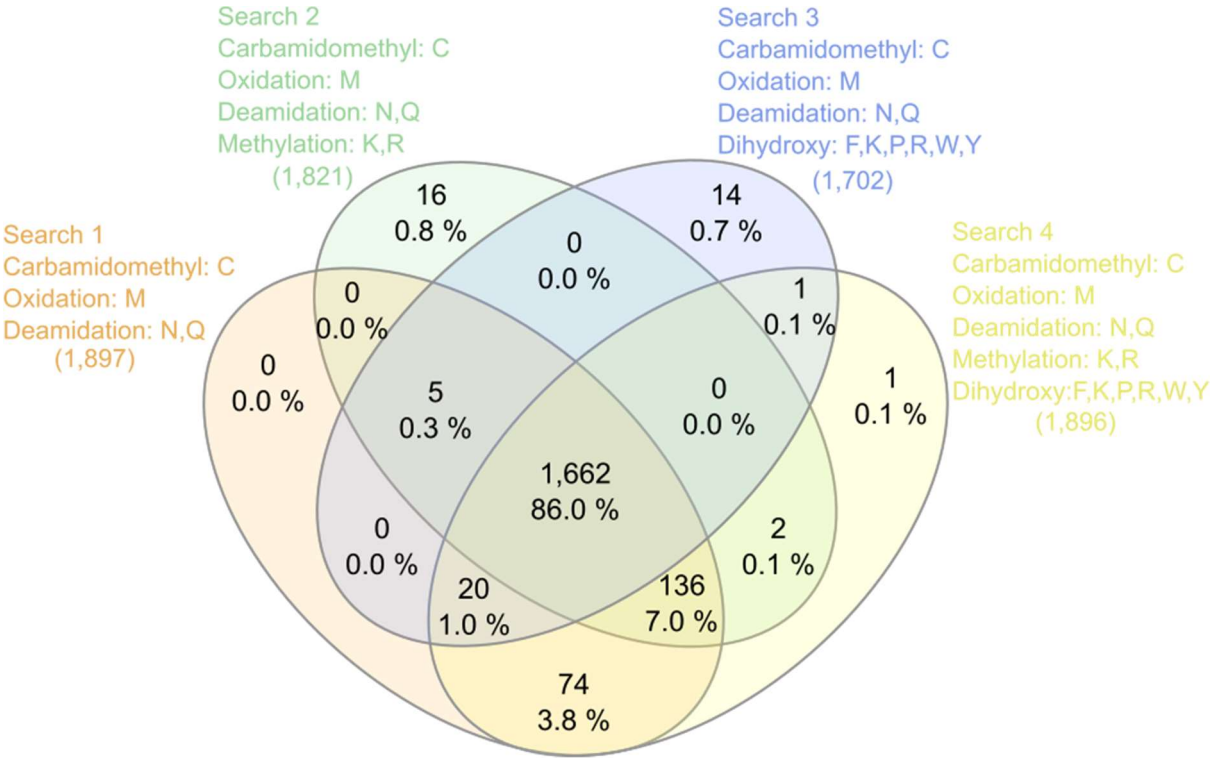

Figure 3.7 Overlap comparison of protein identified with proposed PTMs accounted for.

Each search was performed on the same dataset obtained from LC-MS/MS analysis of axilla skin tissues. The dataset was then analysed using Proteome Discover V1.4 in conjunction with Mascot referencing the uni_human reviewed database downloaded on . Results were then filtered to 1% FDR at the peptide level. These searches being performed are "closes PTM searches" representative of what will be used in the later stages of the project based on the results of the "open PTM search" performed in Peaks.. Search 1 used the originally proposed PTM parameters cysteine (C), deamidation of N and Q and oxidation M. Search 2 used the originally proposed PTM parameters in addition to methylation of K and R. Search 3 used the originally proposed PTM parameters in addition

to dihydroxylation of F, K, P, R, W and Y. Search 4 used the originally proposed PTM parameters in addition to the additional PTMs used in Searches 2 and 3. The comparison shows that a minority of proteins (86%) were identified in all four examples. Introduction of methylation of K and R and dihydroxylation of F, K, P, R, W and Y individually showed a decrease of between 4% and 11% in the number of identifications, with only 31 proteins identified as unique to the searches with the additional PTMs. However, Searches 1 and 4 showed a greater overlap at 98% of the identified proteins.

A combination of all the prospective PTMs with the original search parameters (Search 4 in Figure 3.7) showed the most results when compared with the original search parameter results (Figure 3.7, Search 1), with the majority of proteins identified 1,892 (97.8 %) present in both groups. Five (0.3%) proteins were identified as unique to the original search parameters and consisted of several keratins and a beta-enolase. Four (0.4%) proteins were identified as unique to the adjusted search parameters and comprised of putative proteins, keratins and collagen. The difference between the two search parameters appeared negligible (0.6%). Due to the larger number of identifications and a difference of <1% the incorporation of fewer PTMs into the search parameters was selected to proceed with. Furthermore subsequent stages of analysis include protein quantification, in which accounting for additional PTMs could be detrimental.

3.5 Discussion

Proteomic analysis of FFPE tissue is a researched and documented process requiring fixed tissue volumes of 0.25 mm^3 or higher (Nirmalan et al. 2011; Yamashita and Katsumata 2017; Giusti and Lucacchini 2013; Bayer et al. 2019) summarised in table 3.2 . As such volumes of material were not accessible, I developed an optimised method requiring lower volumes of tissue. A number of aspects were adapted from published methods to generate a working method that utilises 0.01mm^3 of FFPE tissue and can identify ~1,900 proteins with an FDR 1%, allowing a reduction in waste and loss of limited resources when analysing FFPE tissue. Furthermore, when used in combination with material isolated via LCM will allow for a highly targeted proteomic analysis, such as the analysis of specific tissue structures. Despite the

reduction in starting FFPE tissue volume, isolation and analysis of acrosyringium-specific tissue are still not feasible with the developed method as ~480 (0.12x0.12x0.01 mm =$8.5^{-5}$$mm^3$) acrosyringium sections would be required. Thus, an alternative approach to the proteomic analysis of the acrosyringium is required. This will be expanded upon in the next chapter, in which quantitative comparisons are performed between FFPE skin tissue samples without and with acrosyringium.

Table 3.2:Published examples of FFPE tissue proteomic analysis results.

Proteins identified	Tissue volume	Tissue volume	Reference
250-500	0.25mm^3	~5X5X0.01 mm	(Nirmalan et al. 2011)
66	0.8mm^3	~8X10X0.01 mm	(Addis et al. 2009)
192	1.6mm^3	~8X10X0.01 mm	(Azimzadeh et al. 2010)
1,771	0.5mm^3	50x1X1X0.01mm	(Zhang, Li, et al. 2015)

Proteomic analysis of FFPE tissue is well documented and has enormous research potential due to the number, duration of collection, variability and stability of FFPE tissue samples. However, confident peptide identification is only associated with peptides that are not modified by the fixation process as the variety and number of PTMs caused by fixation can differ dramatically between samples. Thus, even though the developed method works for the tissue samples used, it may not be optimal for other FFPE tissue samples. Variations in the fixation process such as tissue type, formalin concentration, time of fixation, and storage time and condition will directly impact the number of crosslinks/methyl bridges that are generated within the sample, thus affecting the quality and quantity of proteins that can be retrieved from these types of samples. When performing proteomic analysis on FFPE tissue, an open PTM search would be advisable with regards to each sample (especially when comparing samples that were isolated and preserved using different methods) to provide greater confidence in the identification and subsequent observations and conclusions made.

As indicated in Figures 3.2-3.4, the number of peptide and protein identifications dramatically dropped when switching from liver tissue to skin tissue samples. This was expected as the liver is a significantly more diverse and metabolically active organ in comparison to the skin, leading to a significant difference in the number and variety of proteins present. The difference between these two tissue types has been reported in other studies; Chinese Human Liver Proteome Profiling (Chinese Human Liver Proteome Profiling 2010) identified 6,788 proteins from healthy liver tissue, whereas the Manchester Skin Proteome (Hibbert et al. 2018) states that healthy human skin contains closer to 2,948 proteins, supporting the expectation of a difference in the number of proteins in the two sample types.

Chapter: 4 Comparison of Acrosyringium-positive and Acrosyringium-negative FFPE Tissue

4.1 Introduction

This chapter focuses on the use of the optimised method described in Chapter 3 to identify the proteins present in acrosyringium-enriched formalin-fixed, paraffin-embedded (FFPE) skin tissue.

4.2 Chapter Aims

The aim of this chapter was to utilise the optimised method described in Chapter 3 to identify proteins enriched in acrosyringium-dense tissue compared with acrosyringium-negative tissue. Having performed this relative quantification study, the expression of proteins determined to be significantly upregulated in acrosyringia was then validated using immunohistochemical staining.

4.3 Chapter 4 experimental overview

In this chapter experimentation focused on implementation of the optimised methods developed in chapter 3 and validation of findings. As the optimised method required a larger then feasible volume of tissue to perform proteomic analysis solely on acrosyringium. A comparison of acrosyringium containing tissue (acrosyringium positive) to tissue absent of acrosyringium (acrosyringium negative) was performed. This comparison was performed repeatedly over several tissue sample isolated from ether the sola of the foot or the Axilla regions. Proteins identified as significantly more prevalent in the acrosyringium positive sample, in three or more of the experiments were then further investigated. Investigation included, investigation into properties, function and pathways associated to these proteins of interest. Furthermore immunohistochemical staining was used to validate proteomic finding and provide addition context of the expression of these proteins of interest in the acrosyringium and surrounding tissue.

4.4 Acrosyringium-positive vs Acrosyringium-negative Tissue

As indicated in Chapter 3, Section 3.1, isolation of individual acrosyringia was possible but not necessarily feasible due to the limited number of samples and sparsity of the structure of interest within the samples, together with the amount of material required to obtain representative data from the samples.

Required material for both acrosyringium-positive and acrosyringium-negative sample pools was isolated from a single sample of skin, i.e. FFPEtissue (Table 4.1). From each block, multiple sequential sections were generated and mounted on laser capture microscopy (LCM)-appropriate slides, with single hematoxylin and eosin (H&E)-stained sections at set intervals of 10 µm (Figure 4.1 A). The H&E-stained sections were then used to identify regions with and without acrosyringia (as well as other secretory structures). This allowed targeted isolation by LCM on subsequent sections as indicated in Figure 4.1 to be used for quantitative proteomics analysis.

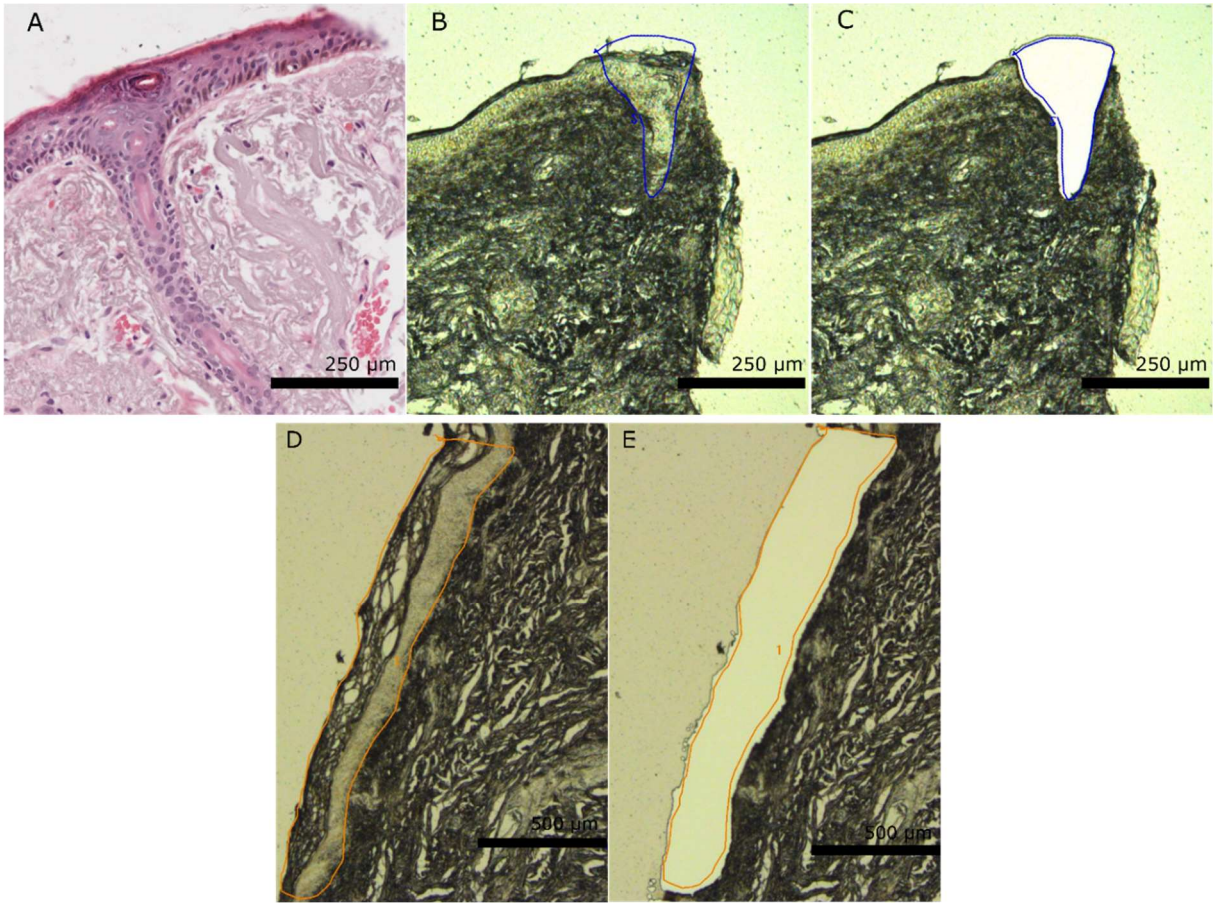

Figure 4.1 Pre and post microdissection of acrosyringium +ve and – ve FFPE skin sections.

A) H&E staining section of FFPE skin section with acrosyringia. B) Adjacent section to A), unstained and prior to microdissection, with the area to be microdissected outlined in blue. C) The same section as B) post microdissection. D) FFPE skin tissue section without acrosyringia present, prior to microdissection with the area to be microdissected outlined in orange. D) FFPE skin tissue section without acrosyringia present post microdissection.

Table 4.1 FFPE tissue isolation

Tissue sample	Tissue source
Sample 1	Foot
Sample 2	Axilla tissue block 1
Sample 3	Axilla tissue block 1
Sample 4	Axilla tissue block 2

Each LCM isolated microdissections was isolated as described in methods section 2.2.2 and were pooled to made up to a total volume of $1*10^7$ μm^3 (0.01 mm^3, < 0.01 mg) of FFPE tissue. Three biological replicates were prepared for each sample. For each experiments all the pooled LCM isolated microdissections were taken from a single FFPE tissue sample (block). All samples were processed using the method developed in Chapter 3 and depicted in Figure 2.1. Prior to analysis, equal proportions of each sample were pooled to allow for the generation of a reference sample to aid in label-free quantification. Repeated MS analysis was performed on each bioreplicate, each time integrating previously generated exclusion lists into the MS method. Following MS acquisition, the data were processed using Progenesis QI V2.4 and Mascot V1.2.

The initial comparison showed a lower number of common proteins than expected based on the preliminary investigations as described in Chapter 3, as indicated in Figure 4.2. In the case of both the acrosyringium-positive and acrosyringium-negative samples, the majority of proteins (64% to 78%) were identified in at least two of the biological replicates, consistent with replicate DDA studies reported in the literature from other types of biological samples.

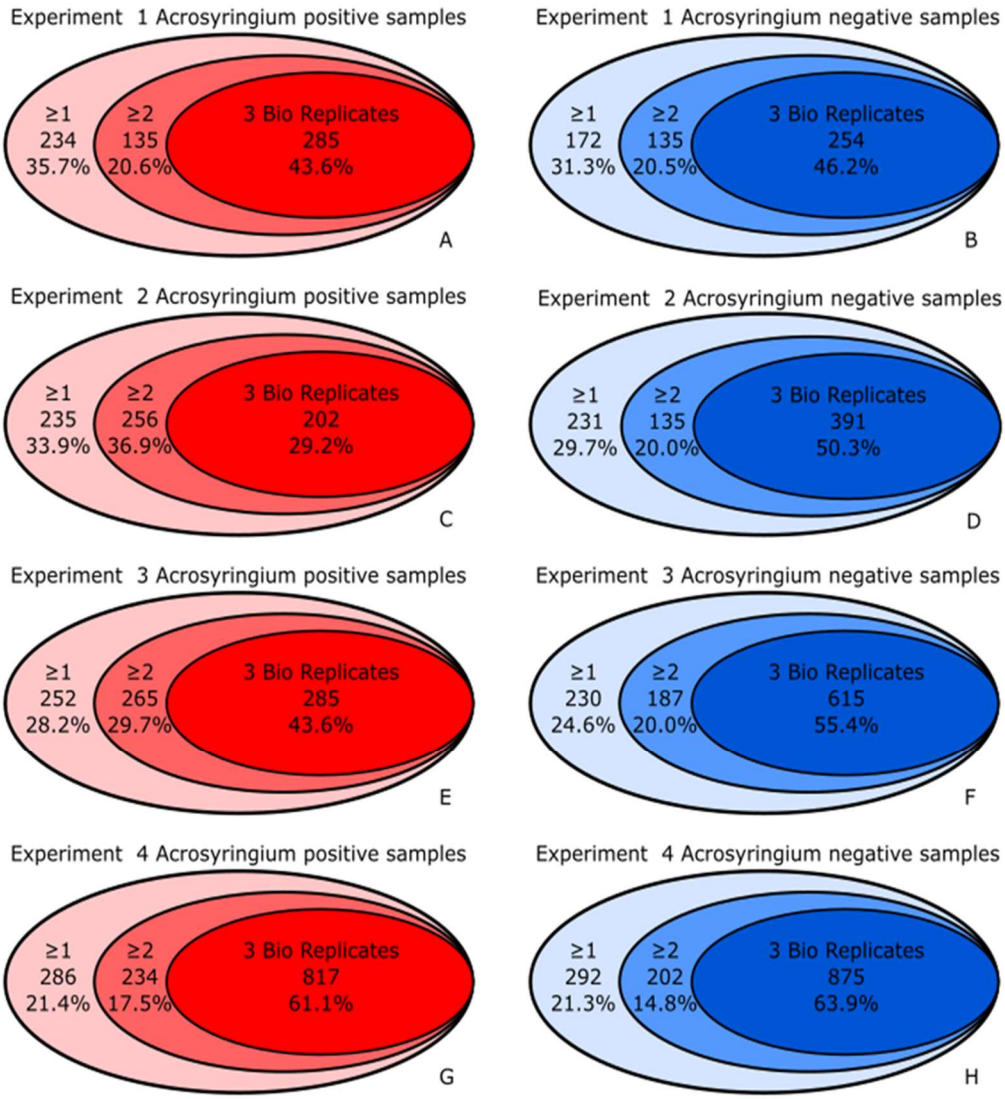

Figure 4.2 Overlap comparison of biological replicates

The overlap identifies the number of common proteins between each of the biological replicates for each of the different samples with an FDR of 1% and a P value of less than 0.01. Overlaps A, C, E and G represent ASC-positive samples and B, D, F and H represent ASC-negative samples.

Direct comparison of the acrosyringium-positive and acrosyringium-negative samples did not reveal any proteins that were consistently unique to either group, indicating either that there were no specific proteins differentiating the two groups in this analysis, or that unique proteins were not discernible via this technique. However, differences were observed in the relative abundance of many of these proteins (see below).

Across the four experiments using acrosyringium-positive samples and acrosyringium-negative samples with the search parameters of 1% FDR, P-value 0.01, 1,700 proteins were identified, with over 1,200 present in at least two replicates as shown in Figure 4.3 A. As indicated in Figure 4.4, gene ontology (GO) term analysis of proteins identified showed a strong association to structural composition as well as protein modification aspects, extracellular exosome, acetylation, extracellular matrix, RNA binding and focal adhesion.

In order to confirm whether the findings were representative of the tissue under investigation (or not), identifications were directly compared to two related proteomes as depicted in Figure 4.3 B. The first proteome was the Pax.DB (http://pax-db.org/dataset/9606/2395425797/) and includes data from 2021 human skin proteome entries, which investigate the skin proteome as a whole. The second was the eccrine sweat gland proteome generated by Chan Hyun Na (Na et al. 2019) where they did extensive LC-MS/MS analysis of ~250 eccrine sweat glands dissected from human abdominal tissue.

Of the 1700 proteins identified in this study, 91.3% (1,643) were identified in one or other of these datasets, with 68.8% (1,170 proteins) being found in both (Figure 4.3 B). This supports the conclusion that the proteins identified in the work presented are representative of the tissue from which they were isolated. A point to note is that the proteomic data generated by Chan Hyun Na (Na et al. 2019) were generated by analysis of the eccrine sweat gland as a whole. No segmentation of the regions was performed prior to analysis. Furthermore, the acrosyringium is significantly smaller than the other two regions of the gland. Thus, despite the large amount of information that can be obtained from this dataset, it is not possible to discern what components specifically relate to the acrosyringium.

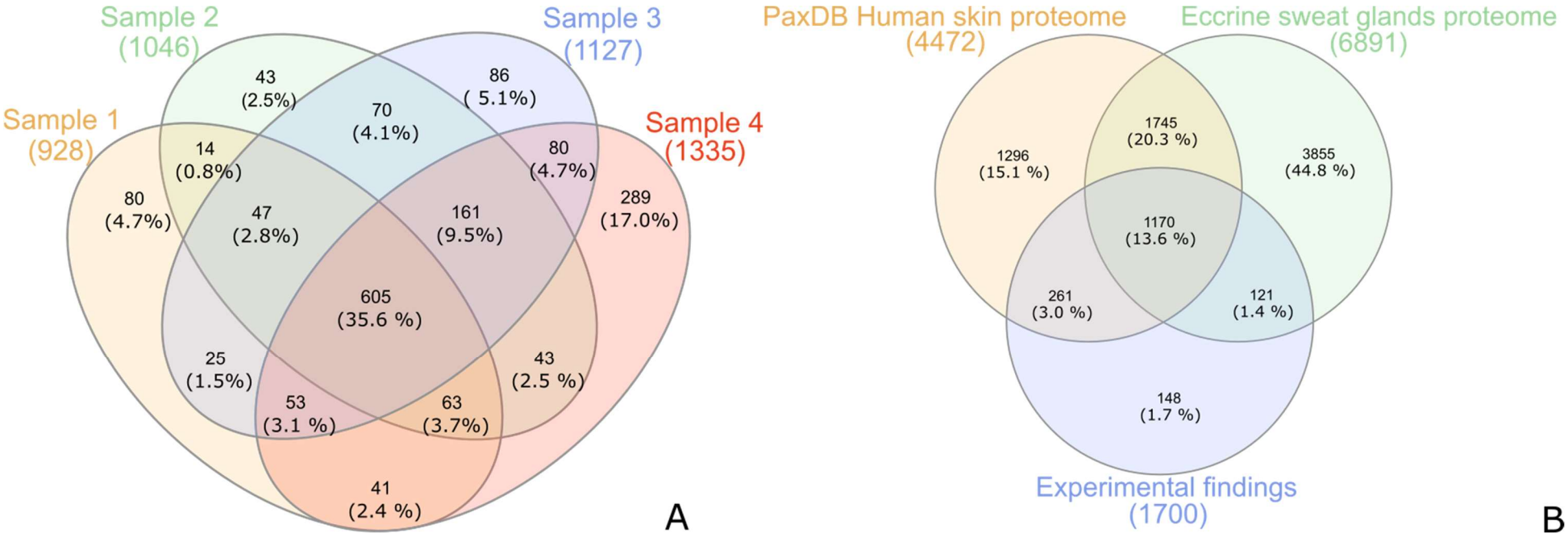

Figure 4.3 Comparison of protein identifications across multiple FFPE skin samples with an FDR of 1% at the peptide level and the identification of at least one unique peptide.

A) Overlap of the 1,700 protein identifications across all four replicates identifying the proteins common to each of the samples. B) Overlap of proteins identified with the results of targeted proteomic studies of the eccrine sweat gland and skin.

.

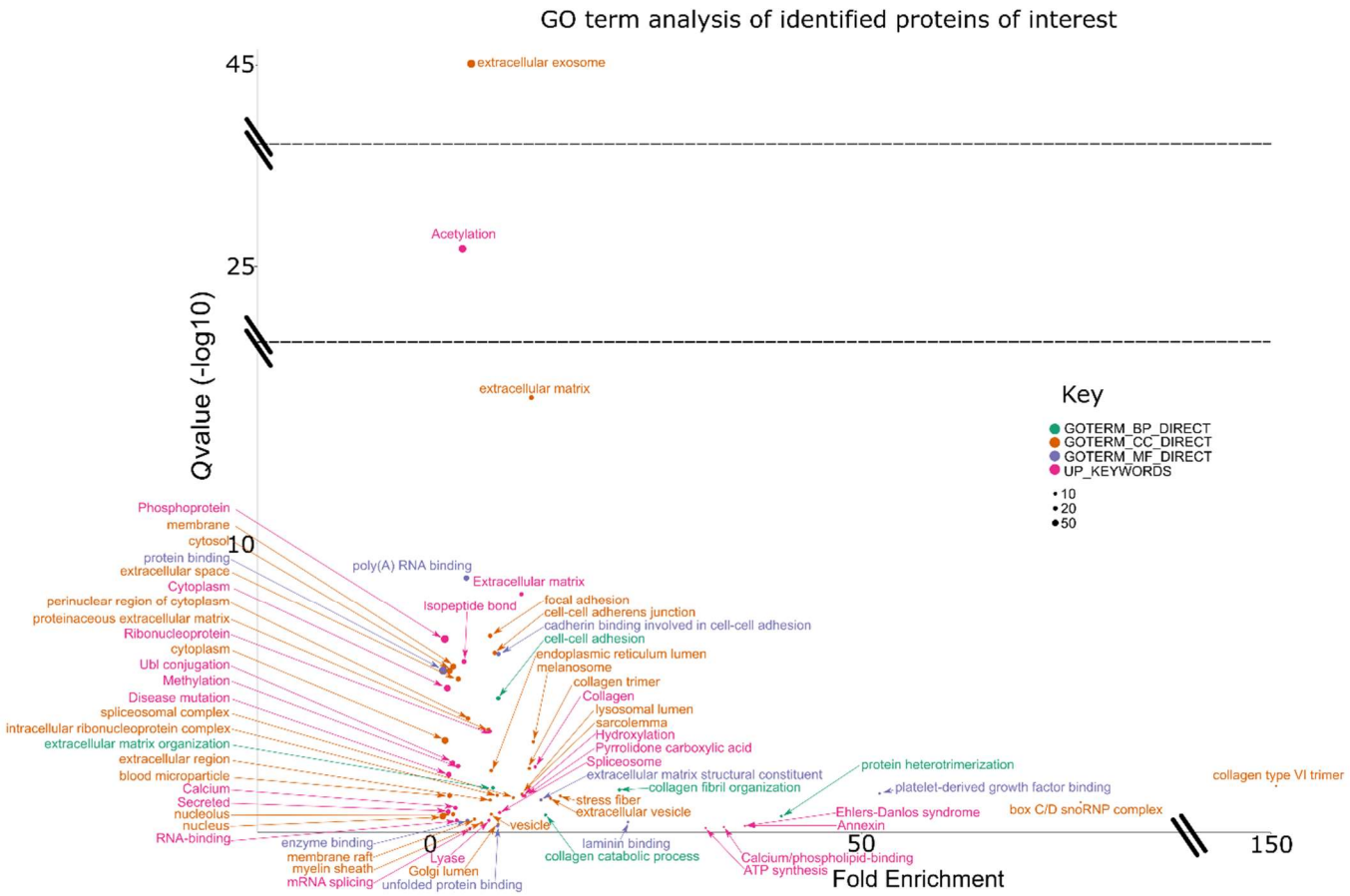

Figure 4.4 GO term analysis of all identified proteins.

All identified proteins were processed to an FDR of 1% and GO terms were identified using the Database for Annotation, Visualisation and Integrated Discovery (DAVID_V 6.8). Results were then filtered to a P-value < 0.05 (using the Benjamini-Hochberg procedure). BP = biological processes; CC = cellular compartment; MF = molecular function.

4.4.1 Acrosyringium-positive Protein Profile.

Label-free quantification was used to compare acrosyringium-positive and -negative samples to identify proteins that were significantly more or less prevalent in the acrosyringium-positive sample. Identified proteins were screened to an FDR of 1% at the peptide level, then further filtered to identification at a P-value less than 0.05. Out of the approximately 500 proteins shown in Figure 4.5 A and B, six proteins (Figure 4.5 B, highlighted in orange) were identified as being consistently significantly more prevalent across all four acrosyringium-positive sample sections compared with their AS-ve controls. An additional 18 proteins (Figure 4.5 B, highlighted in purple) were identified as more prevalent in at least three sample types. These 24 proteins warranted additional investigation and are listed in Table 4.1.

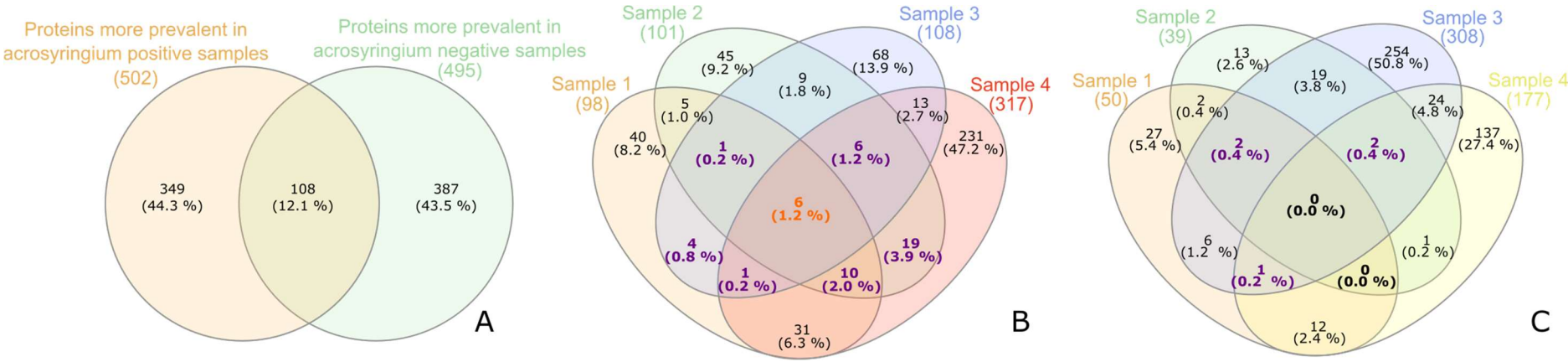

Figure 4.5 Comparison of protein identifications across multiple samples with significant differences in expression between acrosyringium-positive and -negative samples.

A) Total significant (P-value < 0.05) proteins identified by peaks comparing whether they were more prevalent in acrosyringium-positive samples or acrosyringium-negative samples. B) Overlap of proteins identified in each replicate shown to be significantly more prevalent (P-value < 0.05) within the acrosyringium-positive samples compared with acrosyringium-negative samples. C) Overlap of proteins identified in each replicate shown to be significantly less prevalent (P-value < 0.05) within the acrosyringium-positive samples compared with acrosyringium-negative samples.

Table 4.2 Summary of proteins of interest

Proteins that are significantly more prevalent in acrosyringium-positive samples identified in three or more of the experiments										
			Sample 1		**Sample 2**		**Sample 3**		**Sample 4**	
			Isolated from sole of foot		**Isolated from sole of Axilla**		**Isolated from sole of Axilla**		**Isolated from sole of Axilla**	
UniProtKB	**Protein names**	**Gene names**	**P value**	**Fold change**	**P value**	**Fold change**	**P value**	**Fold change**	**P value**	**Fold change**
P04259	Keratin-6B	KRT6B	0.000	7.626	0.000	6.233	0.000	4.591	0.000	10.073
P08779	Keratin-16	KRT16	0.000	2.644	0.001	2.022	0.007	1.903	0.000	4.756
P29373	Cellular retinoic acid-binding protein 2	CRABP2	0.000	1.728	0.000	1.713	0.019	1.243	0.000	3.469
P04083	Annexin A1	ANXA1	0.004	1.176	0.003	1.389	0.001	1.288	0.000	1.467
Q96IU4	Abhydrolase domain-containing protein 14B	ABHD14B	0.021	1.299	0.000	1.690	0.005	1.404	0.000	1.601
Q9BZJ3	Tryptase delta	TPSD1	0.000	4.313	0.000	6.696	0.000	4.852	0.000	1.691
P00352	Aldehyde dehydrogenase 1A1	ALDH1A1	0.000	2.462	N/A	N/A	0.000	10.197	0.000	3.191
P02462	Collagen alpha-1(IV) chain	COL4A1	0.001	2.426	0.036	1.303	N/A	N/A	0.000	1.911
P02538	Keratin-6A	KRT6A	0.013	1.543	0.000	1.820	0.003	1.362	0.024	1.167
P04843	Ribophorin-1	RPN1	N/A	N/A	0.000	1.227	0.049	1.163	0.020	1.132
P05141	ADP/ATP translocase 2	SLC25A5	0.010	1.263	0.000	1.227	N/A	N/A	0.001	1.466
P09211	Glutathione S-transferase P (EC 2.5.1.18)	GSTP1	N/A	N/A	0.026	1.458	0.011	1.511	0.000	1.380
P11047	Laminin subunit gamma-1	LAMC1	0.005	1.807	0.019	2.791	N/A	N/A	0.000	2.351
P11216	Glycogen phosphorylase, brain form (EC 2.4.1.1)	PYGB	0.000	1.759	0.006	1.333	N/A	N/A	0.000	2.154
P29401	Transketolase (EC 2.2.1.1)	TKT	0.012	1.420	0.003	1.365	N/A	N/A	0.002	1.279
P29508	Serpin B3	SERPINB3	0.038	3.558	0.000	2.261	0.000	1.830	N/A	N/A
P30044	Peroxiredoxin-5, mitochondrial (EC 1.11.1.24)	PRDX5	0.014	1.400	0.005	1.193	N/A	N/A	0.000	1.497
P30101	Protein disulfide-isomerase A3 (EC 5.3.4.1)	PDIA3	N/A	N/A	0.039	1.431	0.022	1.387	0.008	1.384
P30740	Leukocyte elastase inhibitor (LEI)	SERPINB1	0.007	1.633	0.004	1.452	N/A	N/A	0.000	2.438
P31151	Protein S100-A7	S100A7	0.004	11.702	0.040	1.306	N/A	N/A	0.000	1.934
P32926	Desmoglein-3	DSG3	0.029	1.277	0.011	1.380	N/A	N/A	0.000	1.845

P54709	Sodium/potassium-transporting ATPase subunit beta-	ATP1B3	N/A	N/A	0.034	1.192	0.013	1.342	0.000	1.556
Q96TA1	Protein Niban 2	NIBAN2	N/A	N/A	0.037	1.359	0.002	1.688	0.001	1.455
Q9NZT1	Calmodulin-like protein 5	CALML5	N/A	N/A	0.000	1.634	0.000	1.423	0.000	1.578
Proteins that are significantly more prevalent in acrosyringium-negative samples identified in three of the experimental samples										
P42357	Histidine ammonia-lyase (histidase; EC 4.3.1.3)	HAL	0.000	1.894	0.000	1.392	0.003	1.503	N/A	N/A
Q9NSA3	Beta-catenin-interacting protein 1	CTNNBIP1	0.010	1.324	0.000	1.891	0.001	2.671	N/A	N/A
P15924	Desmoplakin (DP)	DSP	0.002	1.316	N/A	N/A	0.003	1.270	0.000	1.337
P04040	Catalase (EC 1.11.1.6)	CAT	N/A	N/A	0.001	1.276	0.000	1.376	0.008	1.331
P27482	Calmodulin-like protein 3	CALML3	N/A	N/A	0.028	1.185	0.001	1.465	0.001	1.272

Proteins that were shown to have a significantly increased prevalence (Q and P values of < 0.05 when performing label-free quantification between the two groups) in the acrosyringium-positive samples had a fold difference that was quite small. Figure 4.6 shows the relative fold change of these differentially expressed c proteins across all four sets of tissue samples.

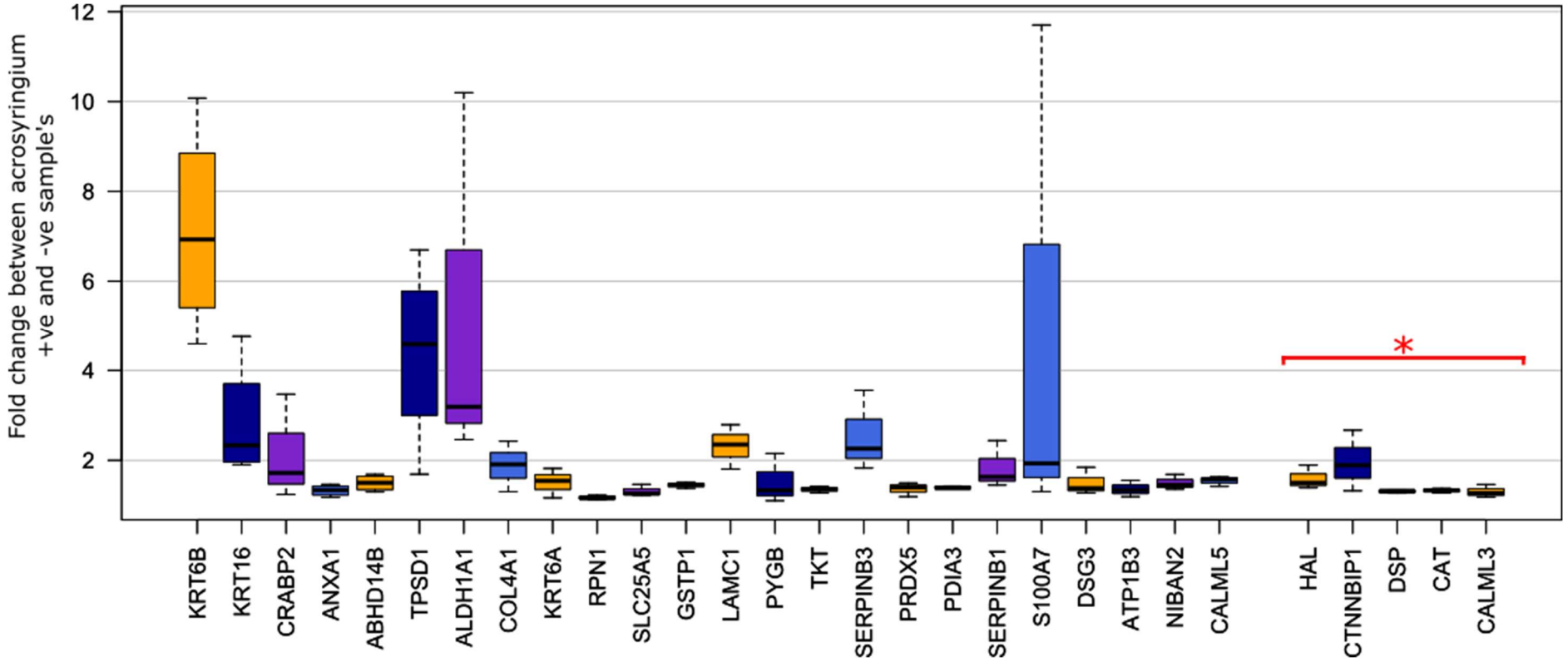

Figure 4.6 Comparison of fold change of significant proteins in acrosyringium-positive and -negative samples.

Significant proteins that are more prevalent in acrosyringium-positive samples identified in at least three of the tissues sets. Proteins highlighted with the red bracket are significant proteins that are more prevalent in acrosyringium-negative samples identified in three of the experiments.

The 24 proteins identified as significantly more prevalent in acrosyringium-positive samples were analysed using STRING to identify any interactions between them. As shown in Figure 4.7, there is evidence that 14 of these 24 proteins interact based on prior knowledge. These are predominantly binary interactions, although in some instances, namely KRT16 and DGS3, they appear to act as hubs for multiple interactions.

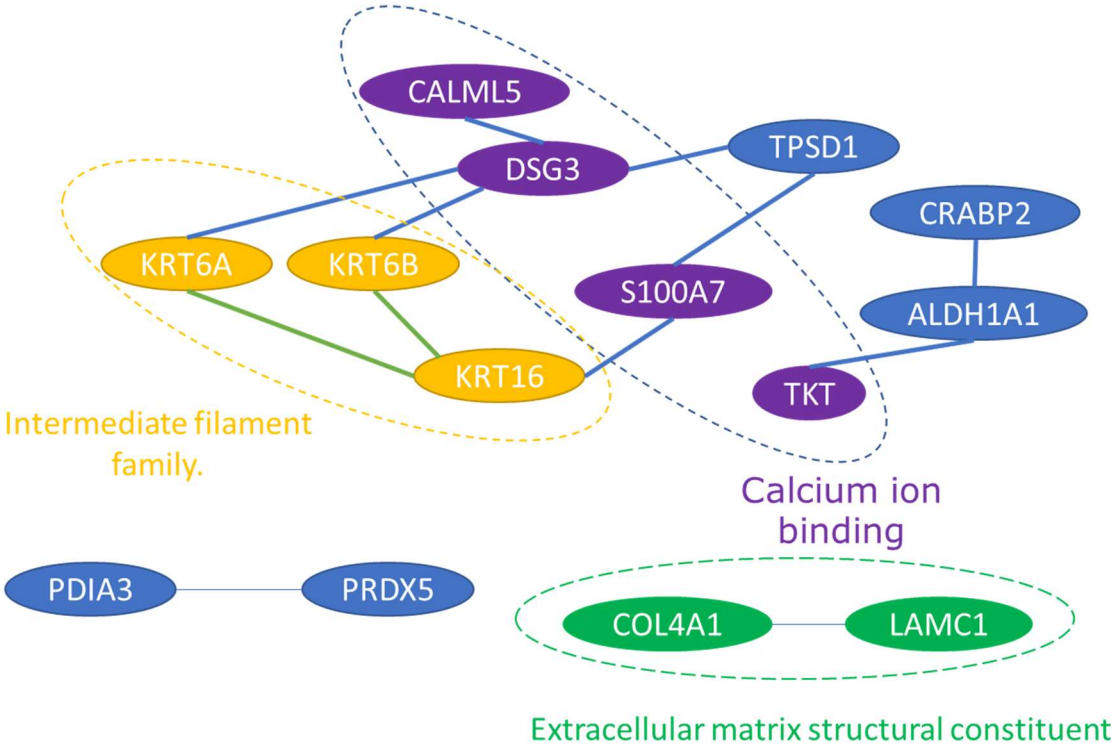

Figure 4.7 Network of proteins identified by string.org as significantly more prevalent in three or more comparisons of acrosyringium-positive and acrosyringium-negative samples.

The network highlights interactions based on experimental or database-derived evidence of medium confidence (interaction score > 0.4, light blue lines). The nodes that showed no connections of medium confidence were removed from the network. The interaction between KRT16, KRT6A and KRT6B (green lines) was absent from the original STRING database search but is well documented in the literature so was added manually

4.4.2 Acrosyringium-negative Protein Profile.

Approximately 400 of the proteins identified across these experiments were at lower levels in acrosyringium-positive samples (Fig 4.5A). The distribution of these proteins across the different tissue samples is presented in Figure 4.5C. Only five

proteins (Figure 4.5 C, highlighted in purple) were identified as less prevalent in the acrosyringium-positive samples across three of the four experiments as listed in Table 4.2. The fold difference in the prevalence of these five proteins ranged from approximately 1.1 to 2.6, indicating subtle differences between the two groups.

GO term analysis of these five proteins returned minimal results due to the small number of proteins identified, with CALML3, DSP and CAT associated with the cellular compartment, specifically the extracellular exosome, and DSP and CAT associated with the biological process of neutrophil degranulation.

QIAGEN Ingenuity Pathway Analysis (IPA) of the proteins identified as significantly more prevalent in acrosyringium positive samples as listed in table 4.2. IPA analysis associated multiple identified proteins to multiple pathways, of which only the "Wound Healing Signalling Pathway" had a significant (>1) positive Z scour allocated by IPA with proteins COL4A1, KRT16, KRT6B & LAMC1 (4/252 or ~1.6%)associated to the pathways.

4.5 Antibody-based Validation of quantitative proteomics differential expression analysis

In order to validate some of the differential protein expression findings in AS+ve versus AS-ve tissue observed using quantitative proteomics, immunohistochemical stating was used. In which FFPE was sections de-paraffined, rehydrated, HIAR traded, then treated with protein specific antibody's and dab stained as described in methods section 2.2.3. To stain regens of the tissue which contained the target protein (unique peptide of target protein) which the which the primary antibody was raised agents.

4.5.1 Keratin 6

Keratin 6 (KRT6A, UniProt accession number: P04259 and KRT6B, P02538) is a type 2 keratin cytoskeletal protein (larger keratins ranging from 50 to 70 kDa in size with a neutral or basic overall charge (Jacob et al. 2018)) involved in intercellular and intracellular matrices. KRT6 is known to be cytoplasmic, expressed in both the

epidermis and epithelial surfaces of tissues such as the skin, cervix, oral mucosa, bronchioles and tonsils. It is often associated with keratinocyte differentiation and wound healing. KRT6 has a number of isoforms derived from the genes KRT6A, KRT6B and KRT6C. One hypothesis for this number of isoforms is that each has the same overall effect of influencing cell migration and adhesion in wound healing but with a slightly different effect, allowing for a more refined influence on wound healing (Zhang, Yin, and Zhang 2019; Bowden 2010; Yoshida et al. 2020; Wang et al. 2018).

Keratins 6B and 6C were both identified as significantly more prevalent in acrosyringium-positive tissue. Keratin 6 is known to have a number of isoforms (Bowden 2010; Takahashi, Paladini, and Coulombe 1995; Wang et al. 2003) present in human skin. The main functional isoforms are KRT6A, KRT6B and KRT6C, which deviate in amino acid sequence by 2.1% as shown in Figure 4.8. KRT6B and KRT6C are the most similar, with only a 1.3% difference between the two amino acid sequences.

Further antibody validation was not performed as suitable antibodies to distinguish between keratin 6 isoforms with sufficient confidence could not be located. Even though the antibody manufacturer advertised their product as an isoform-specific antibody, the target sequence was ubiquitous in all keratin 6 isoforms. An example of this is shown in Figure 4.6, wherein the Abcam HPA045697 antibody advertised as a KRT6A-specific antibody utilises a target sequence ubiquitous in all three keratin 6 isoforms. This allows for the successful identification/staining of keratin 6 but does not distinguish between KRT6A and the other isoforms. Other manufacturers either did not provide information on the target region or sequences or did not provide any evidence that the antibodies were isoform-specific.

A set of antibodies targeting proteins were selected due to their association to the eccrine sweat gland with the aim of using them to identify the acrosyringium. These comprised keratin 77 (KRT77), keratin 17 (KRT17) and keratin 6 (KRT6) (Zhang, Yin, and Zhang 2019; Langbein et al. 2005). The proteome data confirmed the presence of these three proteins in the acrosyringium-positive samples.

Figure 4.9 depicts KRT6A antibody staining of skin. KRT6A showed cytoplasmic staining and no nuclear staining of the acrosyringium. In these examples, the luminal layer of cells belonging to the acrosyringium is distinct from the surrounding epidermal tissue, implying that the presence of KRT6 is higher within the acrosyringium than in the surrounding tissue and supporting the proteome results.

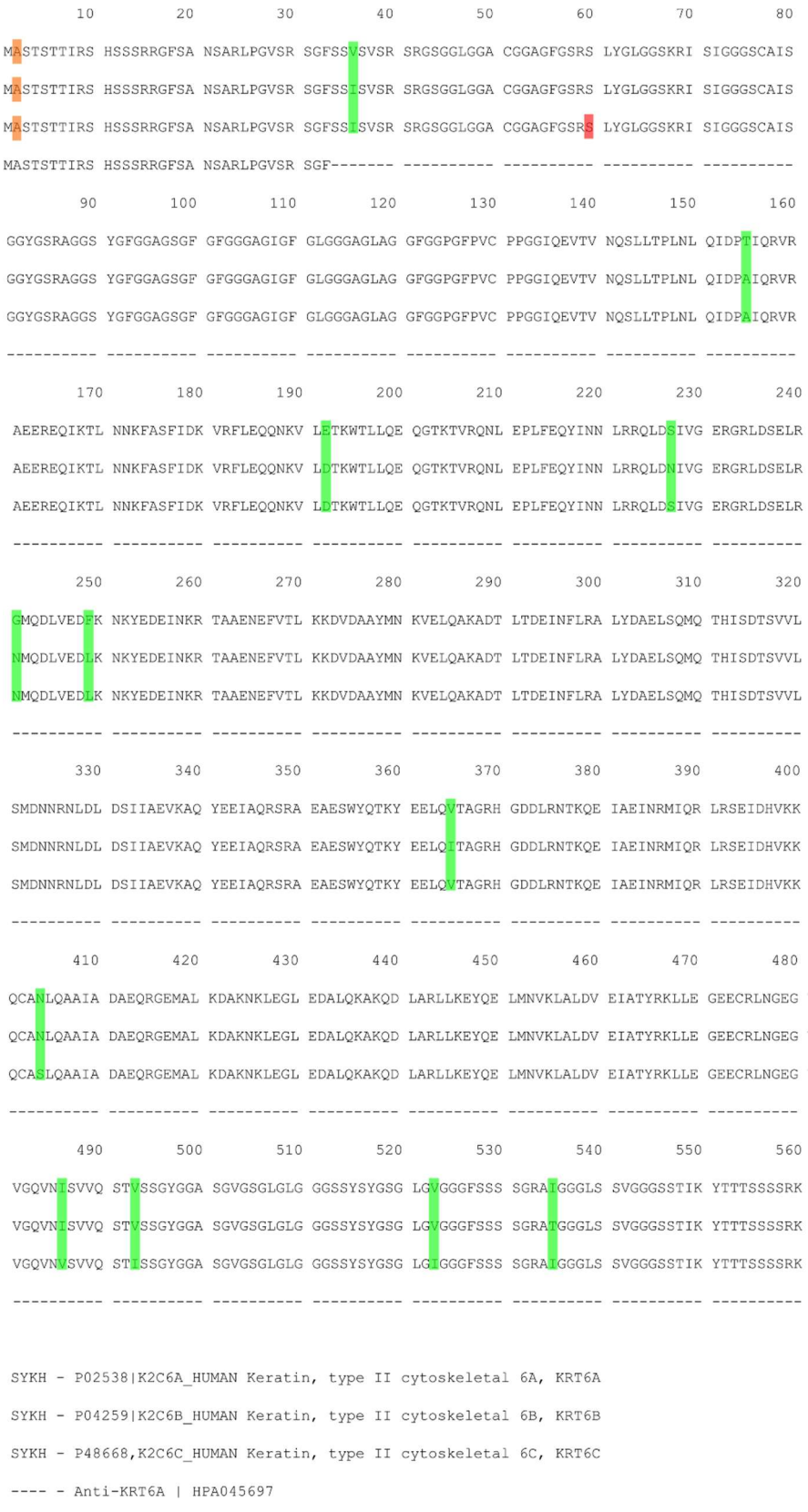

Figure 4.8 ***Protein sequence comparison of KRT6A, KRT6B and KRT6C.***

Orange indicates N-acetylalanine modification sites, red indicates phosphoserine modification sites and green indicates differences in the protein sequences.

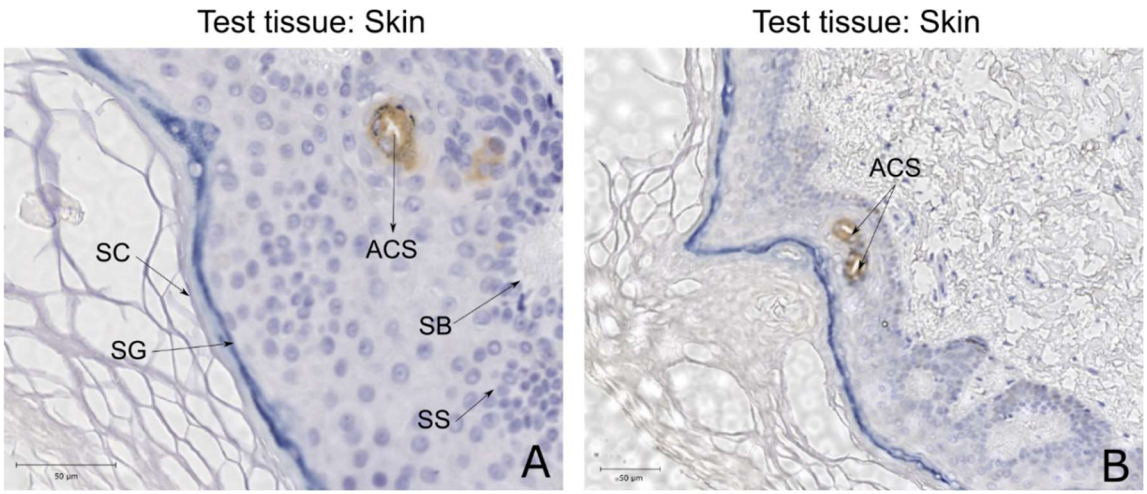

Figure 4.9 KRT6A antibody staining panel.

A-B) Human skin (epidermis and dermis) section stained with KRT6A antibody. acrosyringium(ACS), Stratum corneum (SC), Stratum granulosum (SG), Stratum spinosum (SS), Stratum basale (SB).

4.5.2 Keratin 16

Keratin 16 (KRT16, P08779) is a type 1 keratin cytoskeletal protein (smaller keratins ranging from 40 to 56.5 kDa in size with an acidic overall charge (Jacob et al. 2018)) involved in intracellular matrices. KRT16 is often associated with the innate immune response in skin. KRT16 has cytoplasmic expression in both the epidermis and epithelial surfaces of tissue such as the skin, oral mucosa, lungs and tonsils (Zhang, Yin, and Zhang 2019Bernot, 2002 #1366; Bhawan et al. 2010, 2005).

Anti-KRT16 antibody staining of a skin sample (Figure 4.10) showed significant staining throughout the epidermis and dermis. This degree of staining is expected as keratin 16 is a structural intermediate protein with strong cytoplasmic intracellular staining. The most prevalent staining seemed to be in the stratum basale, with expression waning slightly while proceeding through the epidermis. Antibody staining of KRT16 confirms the expression of the protein within the acrosyringium. In the examples generated (Figure 4.10 B-E), there is a distinction between the presence of KRT16 in the acrosyringium and the surrounding tissue. As the exact sensitivity of the antibody staining in these conditions is unknown, it is not possible to confirm differential KRT16 expression in the acrosyringium compared to the surrounding tissue from these results.

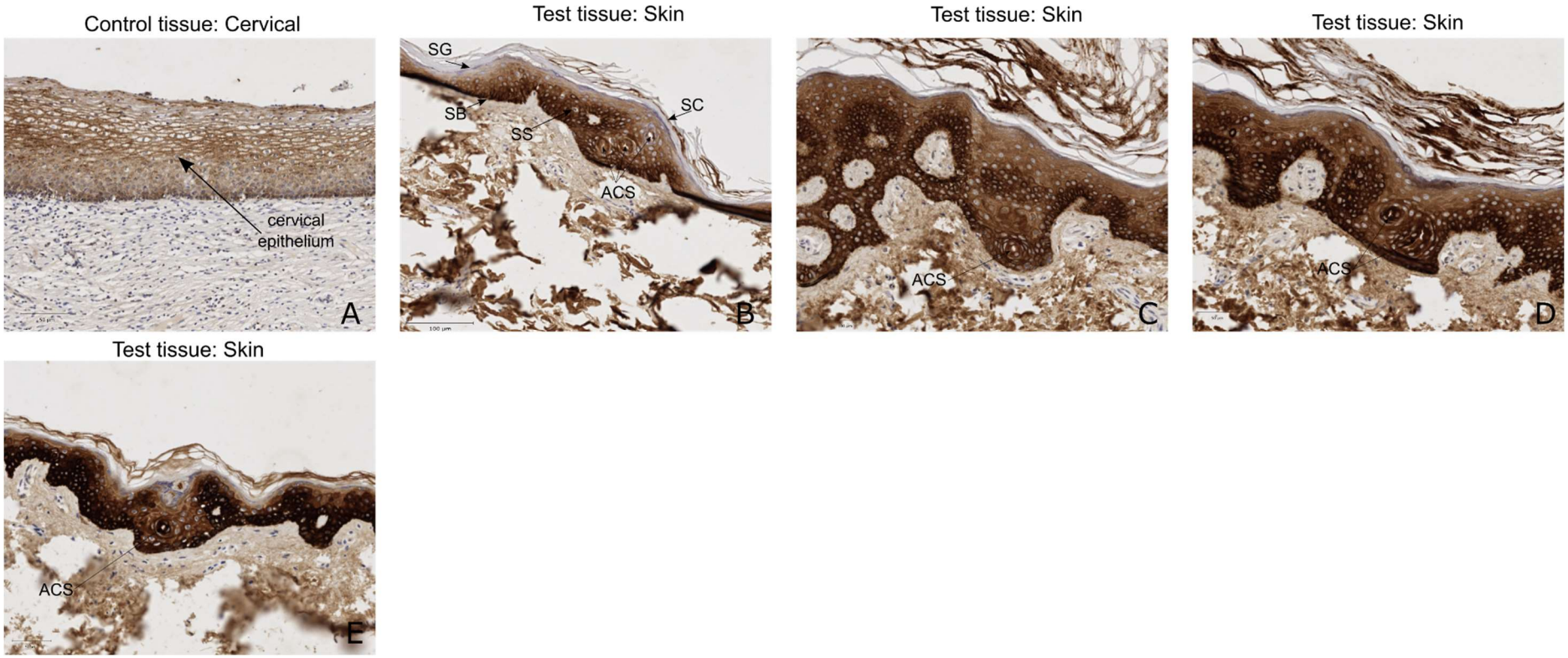

Figure 4.10 KRT16 antibody staining panel.

A) Human cervical section used as a positive tissue control for the KRT16 antibody. B-E) Human skin (epidermis and dermis) section stained with KRT16 antibody. acrosyringium(ACS), Stratum corneum (SC), Stratum granulosum (SG), Stratum spinosum (SS), Stratum basale (SB).

4.5.3 CRABP2

Cellular retinoic acid-binding protein 2 (CRABP2, P29373) is an intracellular protein belonging to the intracellular lipid-binding protein family. CRABP2 is responsible for the transport of retinoic acid from the cytoplasm to the retinoic acid receptor in the nucleus. It is involved in the regulation of cell proliferation, transcriptional coactivation, apoptosis, invasion and metastasis (Adamus et al. 2017; Collins and Watt 2008; Everts et al. 2007; Sugawara et al. 2012; Feng et al. 2019). Due to its function, CRABP2 expression is seen in both the cytoplasmic and nuclear regions of the cell. Furthermore, CRABP2 is found in a number of tissues, including the skin, oral mucosa, oesophagus and endometrium.

Antibody staining of CRABP2 (Figure 4.11) shows cytoplasmic and nuclear staining in the majority of cells within the epidermis. The only region where this is not consistently the case is the stratum basale. CRABP2 antibody staining of the skin confirms the presence of CRABP2 within the acrosyringium cells, but in several sections (Figure 4.11 D C, D, F, G and H), the luminal cells of the acrosyringium appear to be lighter in stain implying the lower presence of CRABP2 in comparison to the directly surrounding areas. If this is the case, this difference would not be defined in the proteomic data. As shown in Figure 4.1 C and D, the region around the acrosyringium was isolated for the acrosyringium-positive samples, including the stratum corneum, stratum lucidum, stratum granulosum, stratum spinosum and stratum basale. Therefore, if there was an increase in the prevalence of a specific protein in this region surrounding the acrosyringium as opposed to specifically in the acrosyringium itself in comparison to the acrosyringium-negative sample regions isolated, the protein would be processed and identified as being significantly more prevalent in the acrosyringium-positive sample. This is a limitation in specificity caused by the method used for tissue section isolation for quantitative proteomics analysis but was a necessary trade-off to allow for the collection of sufficient material to perform proteomic analysis of the acrosyringium from FFPE tissue.

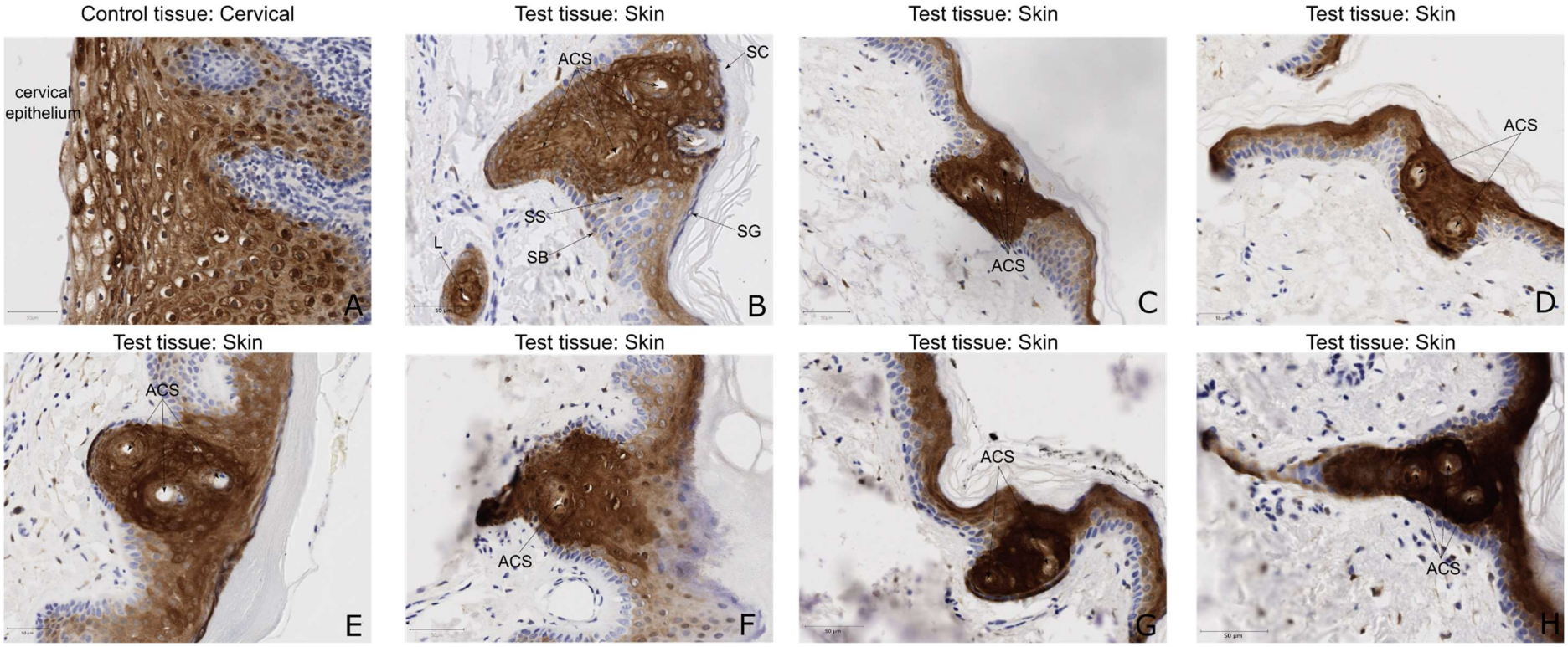

Figure 4.11 CRABP2 antibody staining panel

A) Human cervical section used as a positive tissue control for the CRABP2 antibody. B-H) Human skin (epidermis and dermis) section stained with CRABP2 antibody. acrosyringium(ACS), Stratum corneum (SC), Stratum granulosum (SG), Stratum spinosum (SS), Stratum basale (SB) and Lumen (L).

4.5.4 ABHD14B

Abhydrolase domain-containing protein 14B (ABHD14B, Q96IU4) belongs to the metabolic serine hydrolase family responsible for diverse hydrolytic reactions. ABHD14B is a component of the complex that forms the transcription initiation factor TFIID. Furthermore, studies show ABHD14B to be strongly associated with apoptosis. ABHD14B is reported to be localised to both cytoplasmic and nuclear regions of cells and is ubiquitous across human tissues due to its involvement with transcription (Padmanabhan et al. 2004; Rajendran et al. 2020; Sekiguchi, Miyata, and Nishimoto 1988).

Staining of ABHD14B (Figure 4.12) shows both cytoplasmic and nuclear expression of ABHD14B throughout the cells within the epidermis. Figure 4.12 confirms the expression of ABHD14B in acrosyringium luminal cells; furthermore, the images indicate a higher prevalence of ABHD14B in acrosyringium cells as indicated by the slightly darker staining of these structures in comparison to the surrounding tissue.

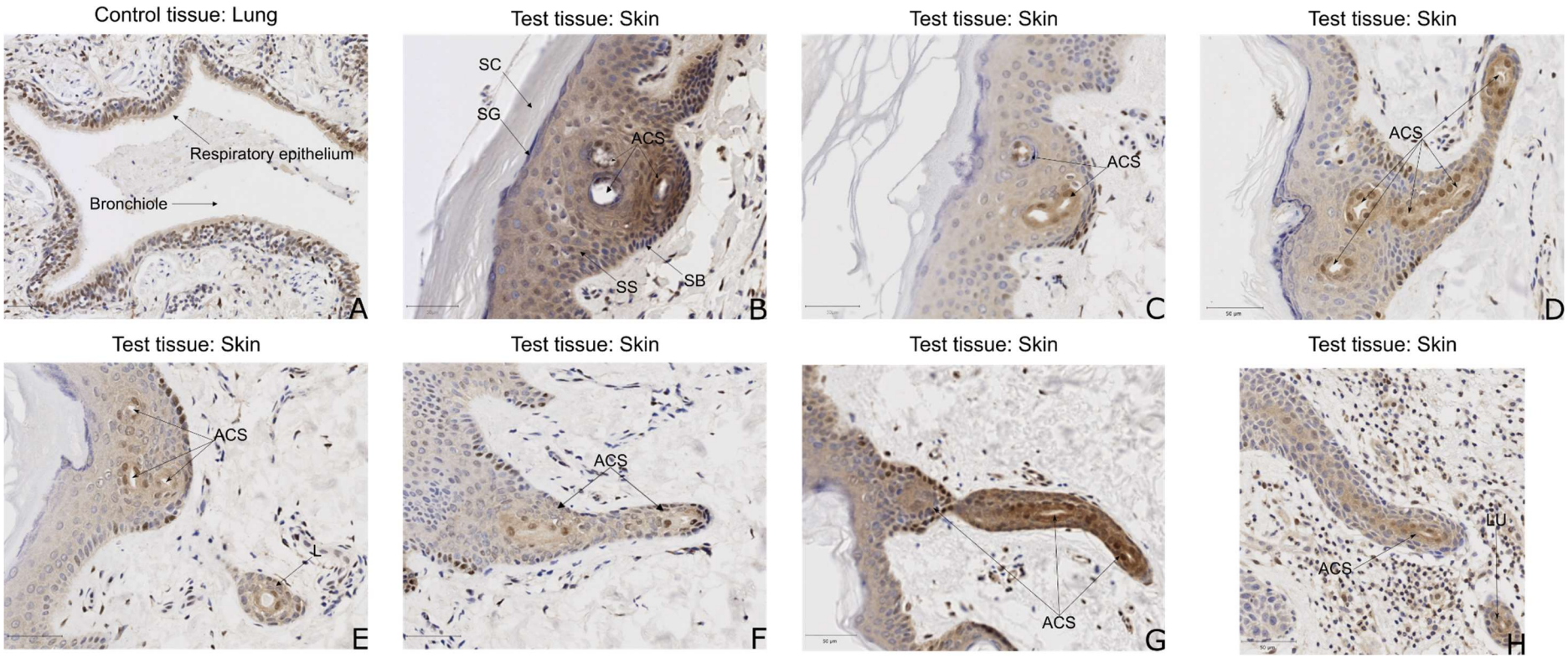

Figure 4.12 CRABP2 antibody staining panel

A) Human lung section used as a positive tissue control for the ABHD14B antibody. B-H) Human skin (epidermis and dermis) section stained with ABHD14B antibody. acrosyringium(ACS), Stratum corneum (SC), Stratum granulosum (SG), Stratum spinosum (SS), Stratum basale (SB).

4.5.5 TPSD1

Tryptase delta (TPSD1, Q9BZJ3-1) is a trypsin-like serine protease shown to cleave arginine and lysine as part of the innate immune response. It should be noted that TPSD1 has two isoforms differing by eight amino acids. Not much is known about the function of the second, truncated isoform (Q9BZJ3-2) and how it differs from Q9BZJ3-2. TPSD1 undergoes a number of PTMs such as truncation, glycosylation and orientation in order to become fully active before being utilised in response to foreign bodies. TPSD1 is typically expressed in mast cells due to their mobility as part of the innate immune system. TPSD1 is found in most tissues of the body (Trivedi and Caughey 2010; Payne and Kam 2004; Elst et al. 2022; Hernandez-Hernandez et al. 2012; Trivedi, Raymond, and Caughey 2008; Wang et al. 2002).

The results of the TPSD1 staining were unexpected. TPSD1 is a neutral protease associated with mast cells. This is exemplified by Figure 4.13 A and B, which depict staining in both the epidermis and epithelium. However, other samples containing acrosyringium showed no significant staining (Figure 4.13 C, D, E and F) despite the positive controls indicating successful staining.

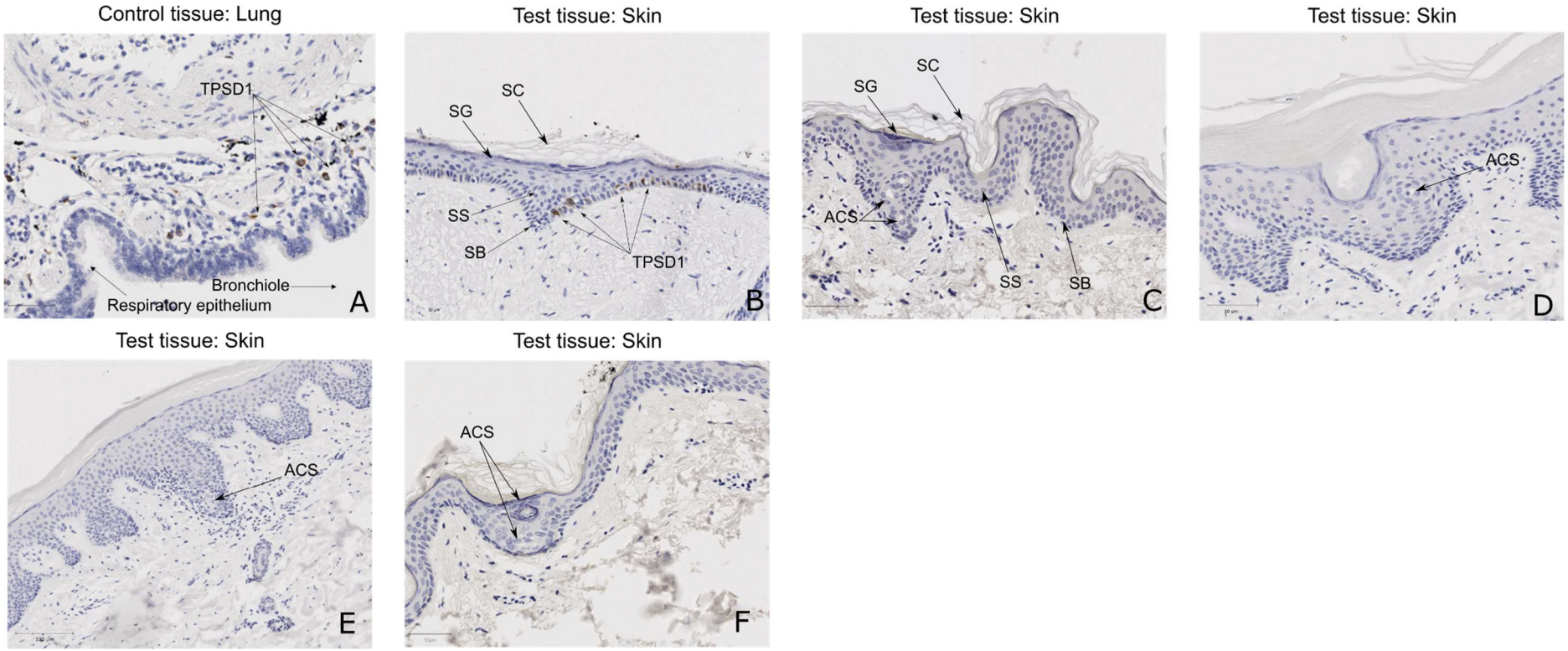

Figure 4.13 TPSD1 antibody staining panel.

A) Human lung section used as a positive tissue control for the TPSD1 antibody. B-F) Human skin (epidermis and dermis) section stained with TPSD1 antibody. acrosyringium(ACS), Stratum corneum (SC), Stratum granulosum (SG), Stratum spinosum (SS), Stratum basale (SB).

4.5.6 RPN1

Ribophorin-1 (RPN1, P04843) is one of the six subunits that make up the oligosaccharyl transferase enzyme responsible for N-glycosylation. As RPN1 is associated with the endoplasmic reticulum, the protein is seen in the cellular cytoplasm and is ubiquitously expressed in all tissues (Effantin et al. 2009; Ding et al. 2021; Boughton et al. 2021).

RPN1 antibody staining of a skin sample (Figure 4.14) shows staining of RPN1 within the epidermis. The stain is strongest within the cytoplasm and does not indicate a difference in expression between the acrosyringium and the surrounding tissue. Thus, the generated examples do not seem to distinguish between the presence of RPN1 in the acrosyringium and the surrounding tissue.

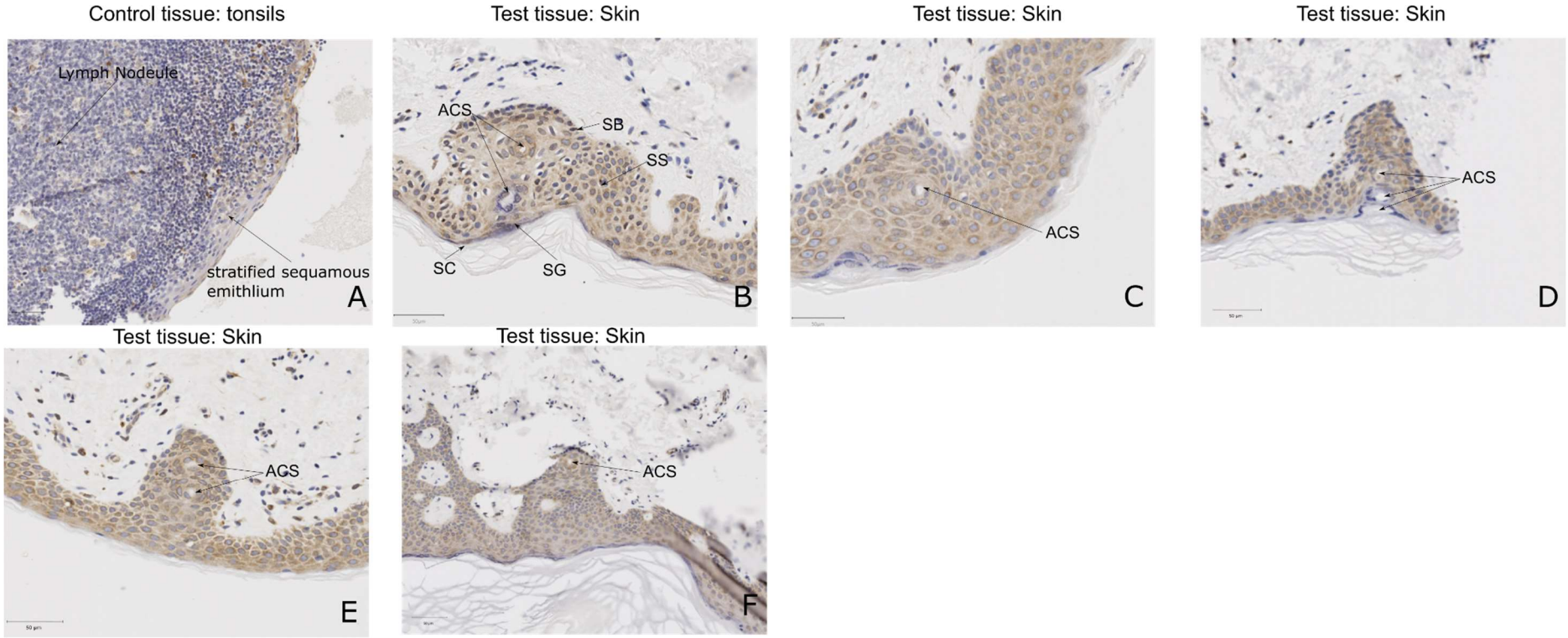

Figure 4.14 RPN1 antibody staining panel.

A) Human lung section used as a positive tissue control for the RPN1 antibody. B -F) Human skin (epidermis and dermis) section stained with RPN1 antibody. acrosyringium(ACS), Stratum corneum (SC), Stratum granulosum (SG), Stratum spinosum (SS), Stratum basale (SB).

4.5.7 GSTP1

Glutathione S-transferase P (GSTP1 or P09211) is derived from the gene GSTP1 and belongs to the GST family of isoenzymes. GSTP1 undergoes oligomerization to become active. In its active form, GSTP1 catalysis and deoxylation of electrophilic compounds reduce stress on the cell, increasing resistance to apoptosis and the metabolic toxicity of the cell. GSTP1 is found in the cytoplasm and is expressed in most human tissues (Cui et al. 2020; Gondalia et al. 2017).

Like RPN1, GSTP1 is ubiquitously expressed throughout the epidermis. Figure 4.15 depicts cytoplasmic staining of GSTP1, confirming that it is secreted in the acrosyringium and the surrounding epidermal tissue. In Figure 4.15, it is not possible to distinguish between the acrosyringium and surrounding epidermal tissue based on the staining of GSTP1.

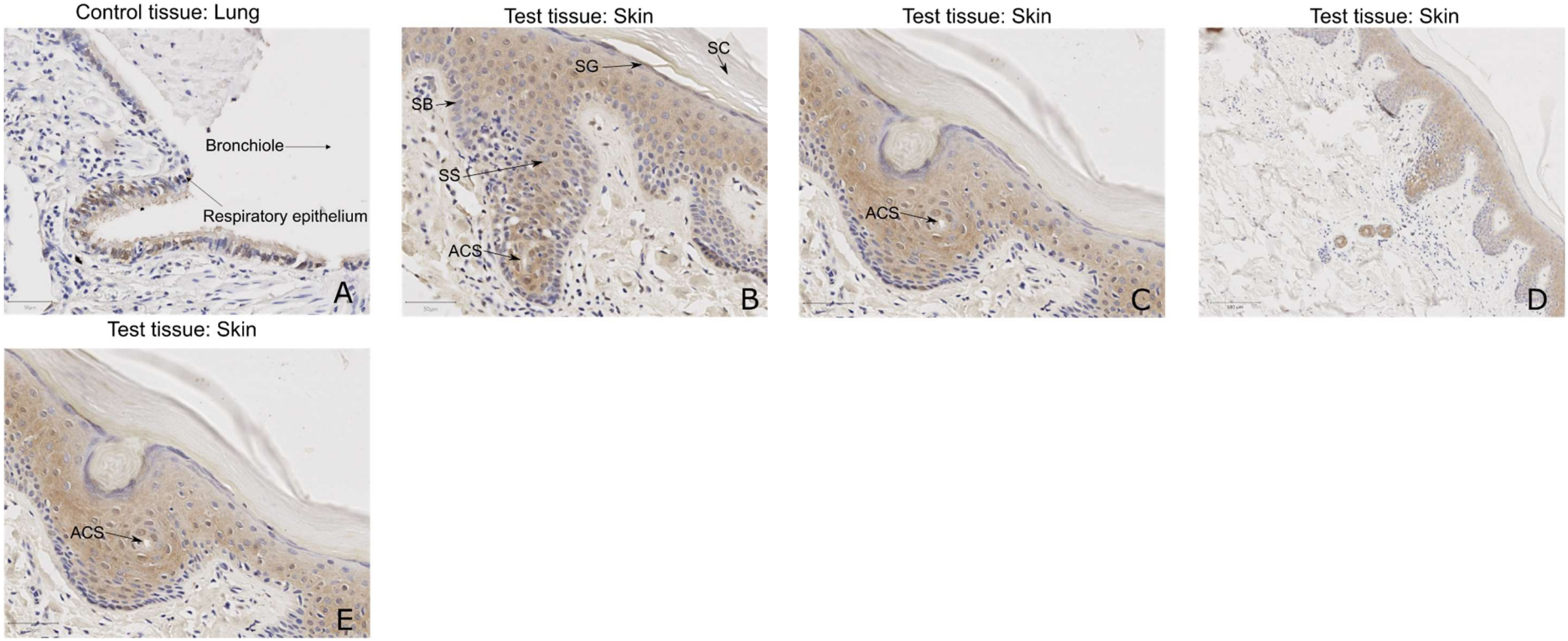

Figure 4.15 GSTP1 antibody staining panel.

A) Human lung section used as a positive tissue control for the GSTP1 antibody. B -E) Human skin (epidermis and dermis) section stained with GSTP1 antibody. acrosyringium(ACS), Stratum corneum (SC), Stratum granulosum (SG), Stratum spinosum (SS), Stratum basale (SB).

4.5.8 LAMC1

Laminin subunit gamma-1 (LAMC1, P11047) is an extracellular matrix glycoprotein that forms large complexes (chains) in combination with other laminin subunits (alpha, beta and gamma) to form laminin. Furthermore, laminin works in conjunction with collagen to form the fundamental architecture to which tissue adheres. Extracellular expression is observed in a variety of tissues including but not limited to the skin, lung, stomach, colon, smooth muscle, oesophagus and endometrium (Liu et al. 2019; Kunitomi et al. 2020).

LAMC1 is involved in cell adhesion and therefore, it is expected to have a strong presence throughout the epidermis. Figure 4.16 confirms the presence of LAMC1 within the acrosyringium, but as with RPN1 and GSTP1 staining, it does not distinguish the structure from the surrounding tissue.

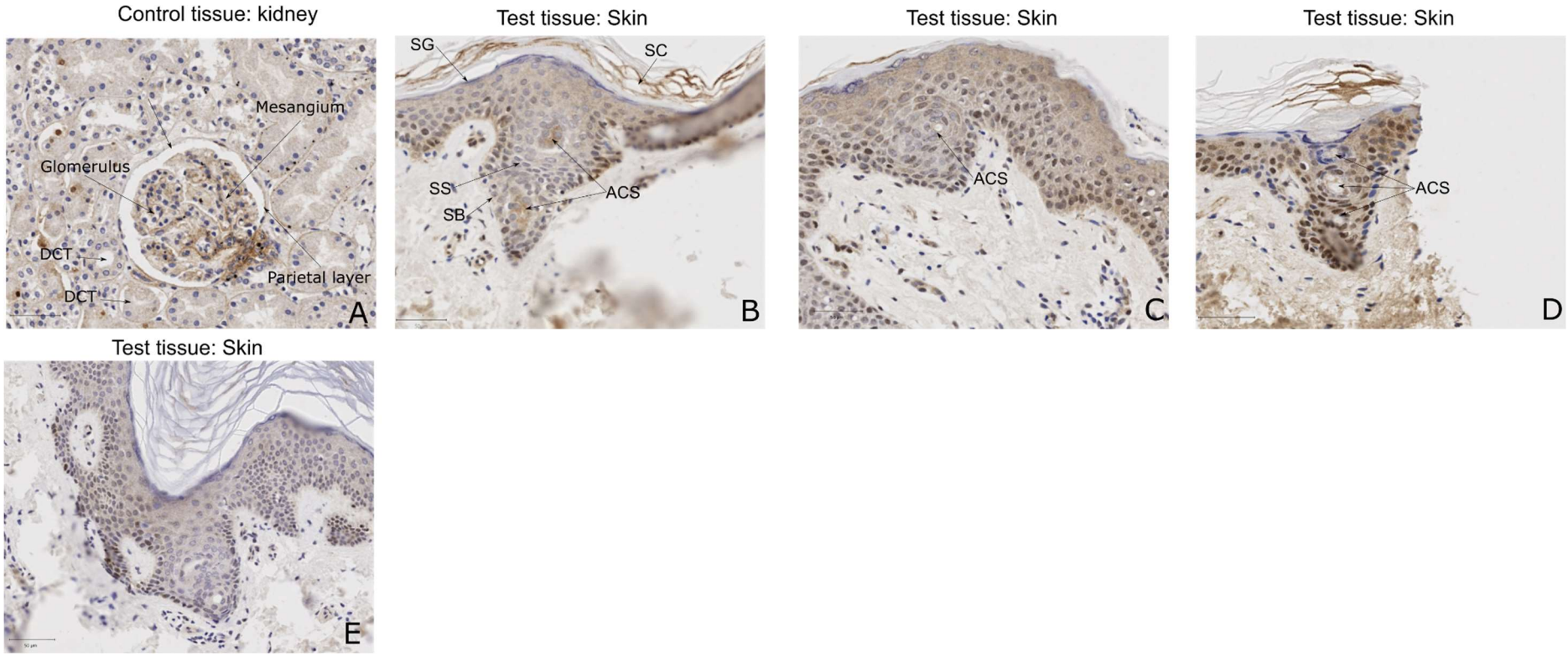

Figure 4.16 LAMC1 antibody staining panel.

A) Human kidney section used as a positive tissue control for the LAMC1 antibody. B -E) Human skin (epidermis and dermis) section stained with Lamc1 antibody. acrosyringium(ACS), Stratum corneum (SC), Stratum lucidum (Sl), Stratum granulosum (SG), Stratum spinosum (SS), Stratum basale (SB).

4.5.9 SERPINB3

Serine protease inhibitor (SERPINB3, P29508) belongs to the SERPIN family, which comprises 36 members. SERPINB3 mainly inhibits papain-like cysteine proteases, including cathepsins L, S and K and the papain proteolytic enzyme. Furthermore, SERPINB3 is associated with cell proliferation and anti-apoptotic function. Expression of SERPINB3 is seen in the cytoplasm of a number of tissues in the skin, bladder, oral mucosa, uterus, prostate, oesophagus, lung and testis (Pontisso 2014; Sun, Sheshadri, and Zong 2017; Quarta et al. 2010; Vidalino et al. 2009).

SERPINB3 was successfully stained and revealed a slightly different profile to previous examples (Figure 4.17). SERPINB3 was predominantly intracellularly expressed in the acrosyringium and, in some cases, in the epidermal tissue directly surrounding the structure. Additionally, significant staining of the stratum corneum of regions directly adjacent to the identified acrosyringium was observed. These are likely the outermost segments of the acrosyringium. Their distorted shape and size in comparison to the other regions of the acrosyringium could be due to the latter stages of keratinocyte differentiation as well as the influence of external factors such as the movement and stretching of the skin. Additionally, in the majority of the sections seen in Figure 4.17, the staining becomes more significant while moving through the epidermis, which may indicate an increase in expression as keratinocyte differentiation occurs.

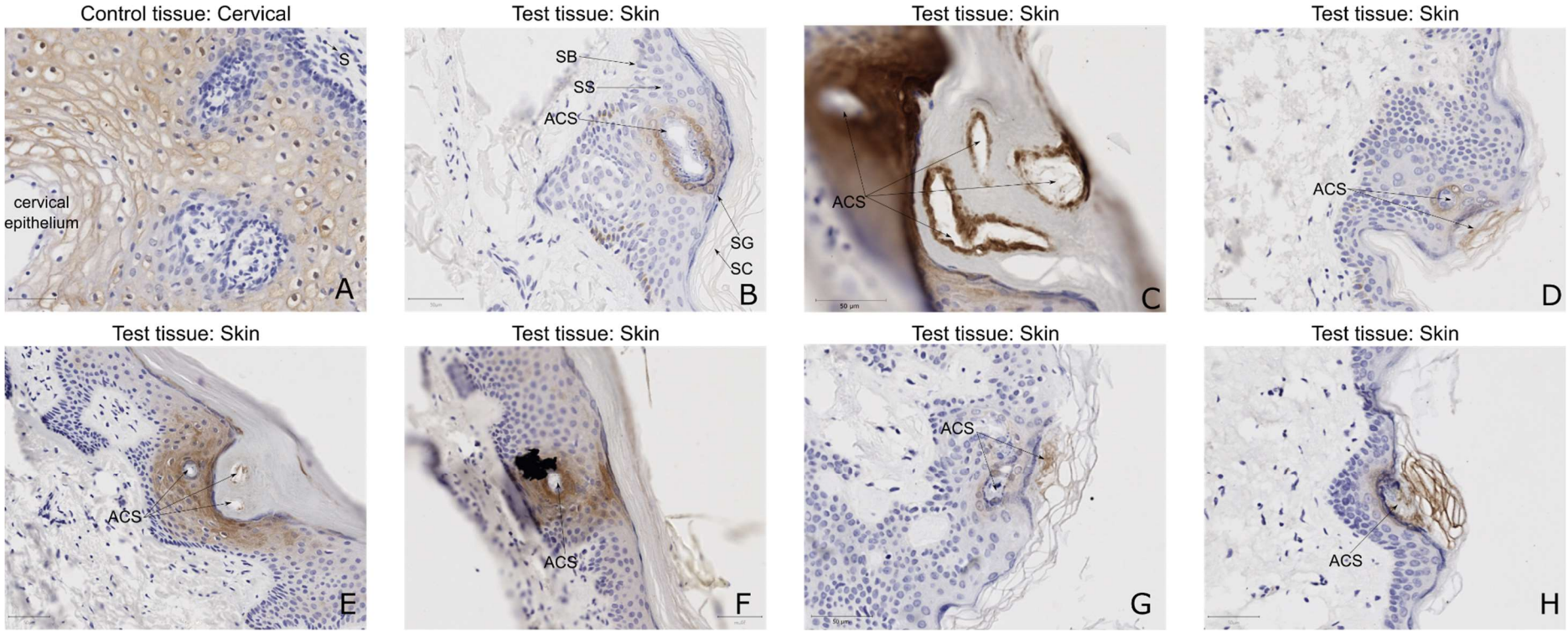

Figure 4.17 SERPINB3 antibody staining panel.

A) Human cervical section used as a positive tissue control for the SERPINB3 antibody. B -H) Human skin (epidermis and dermis) section stained with SERPINB3 antibody. acrosyringium(ACS), Stratum corneum (SC) Stratum granulosum (SG), Stratum spinosum (SS), Stratum basale (SB).

4.5.10 Annexin A1

Staining of annexin A1 in the skin (Figure 4.18) resulted in the most distinct staining of the acrosyringium in comparison to the surrounding tissue of all the proteins investigated. Staining occurred in both the cytoplasmic and nuclear regions of the luminal cells of the acrosyringium through the epidermis. In addition, similar to SERPINB3 (Figure 4.18 E, C and D), notable staining of the stratum corneum was observed (Figure 4.18 B-D and H), indicating the region of the acrosyringium that transects the stratum corneum.

One aspect to note is that the target sequence for the anti-annexin antibody is adjacent to the C-terminal of the protein, meaning that the protein being stained is the intact form of annexin A1 as opposed to the mimetic peptide form annexin A1 Ac2-26, which is typically also shown to be present (Dalli et al. 2012; Leoni et al. 2015; Girol et al. 2013; Euzger et al. 1999).

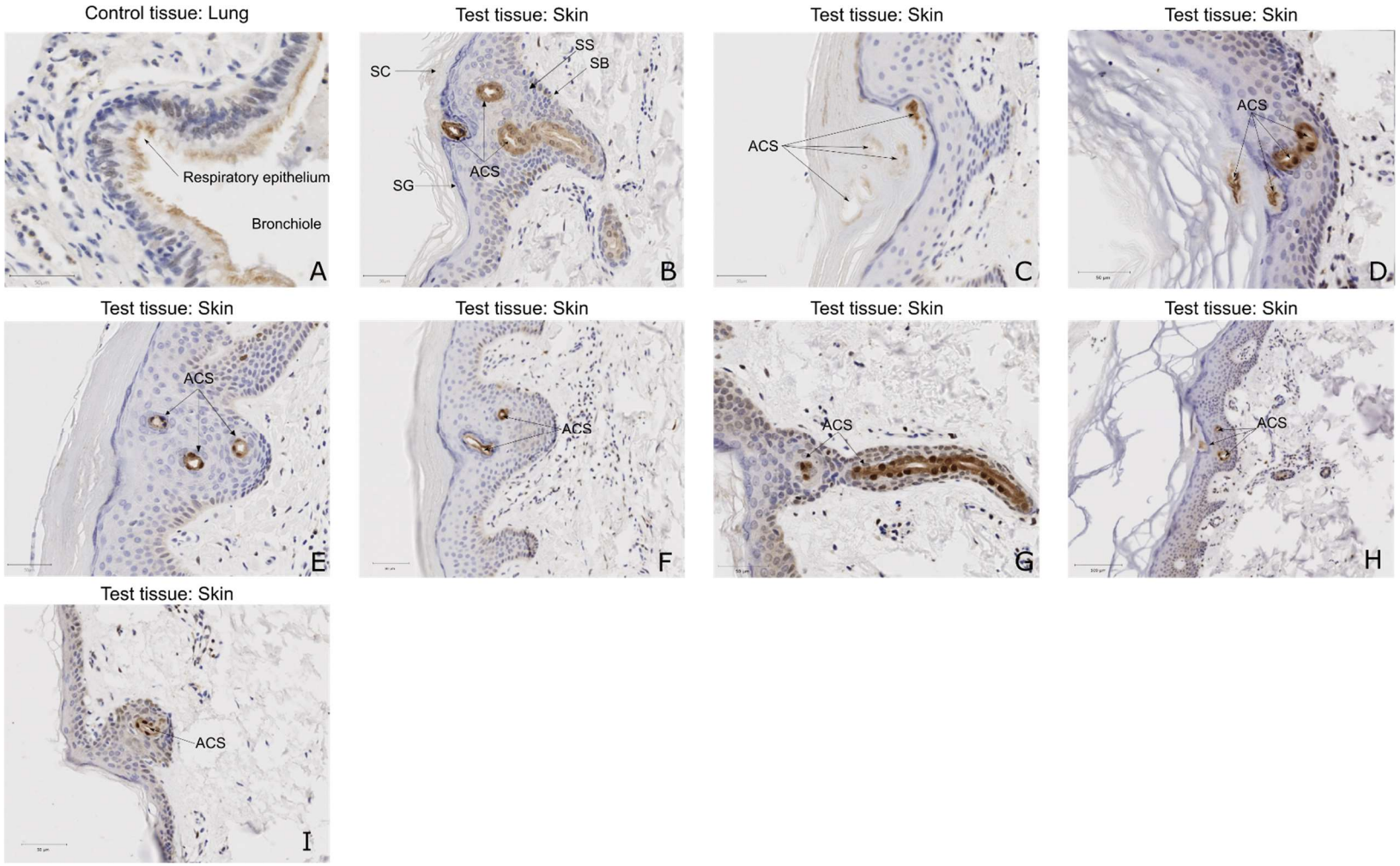

Figure 4.18 Annexin A1 antibody staining panel.

A) Human lung section used as a positive tissue control for the annexin A1 antibody. B-I) Human skin (epidermis and dermis) section stained with annexin A1 antibody acrosyringium(ACS), Stratum corneum (SC), Stratum lucidum (Sl), Stratum granulosum (SG), Stratum spinosum (SS), Stratum basale (SB).

4.5.11 CALML5

Anti-CALML5 antibody staining of skin samples generated a profile similar to those of SERPINB3 and annexin A1 (Figure 4.19). In the examples generated, both cytoplasmic and nuclear staining of the luminal cells of the acrosyringium was observed, along with some regions of the epidermis. As CALML5 is associated with keratinocyte differentiation, it is unsurprising that staining is prevalent towards the periphery of the epidermis. This supports the hypothesis that the acrosyringium is in a different stage of keratinocyte differentiation compared to the surrounding tissue. Like SERPINB3 and annexin A1, in Figure 4.19 D, the staining of regions of the stratum corneum implies that these are the porifera openings of the acrosyringium.

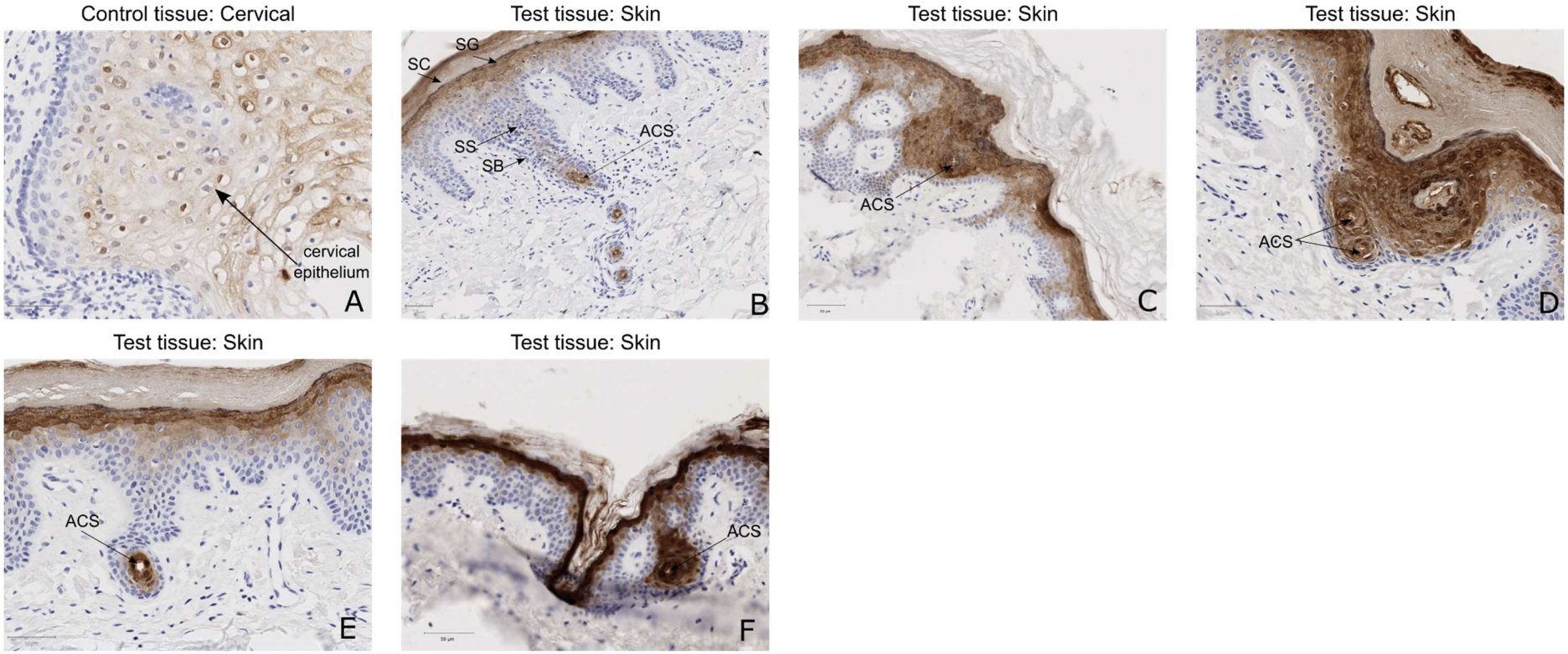

Figure 4.19 CALML5 antibody staining panel.

A) Human cervical section used as a positive tissue control for theCALML5 antibody. B -F) Human skin (epidermis and dermis) section stained with CALML5 antibody. acrosyringium(ACS), Stratum corneum (SC), Stratum granulosum (SG), Stratum spinosum (SS), Stratum basale (SB).

.

Table 4.3: Immunohistochemical staining summary table.

UniProtKB	Protein names	Gene names	Figuer	Acrosyringium	Stratum corneum	Stratum granulosum	Stratum spinosum	Stratum basale	Dermis
Q96IU4	Abhydrolase domain-containing protein 14B	ABHD14B	4.12	+		+	+	+	+
P04083	Annexin A1	ANXA1	4.18	+					
Q9NZT1	Calmodulin-like protein 5	CALML5	4.19	+	+	+	+		
P29373	Cellular retinoic acid-binding protein 2	CRABP2	4.11	+		+	+		
P09211	Glutathione S-transferase P (EC 2.5.1.18)	GSTP1	4.15	+	+	+	+		
P08779	Keratin-16	KRT16	4.1	+	+	+	+	+	+
P02538	Keratin-6A	KRT6A	4.09	+					
P04259	Keratin-6B	KRT6B	4.09	+					
P11047	Laminin subunit gamma-1	LAMC1	4.16	+	+	+	+	+	+
P04843	Ribophorin-1	RPN1	4.14	+	+	+	+	+	
P29508	Serpin B3	SERPINB3	4.17	+	+	+	+		
Q9BZJ3	Tryptase delta	TPSD1	4.13					+	

4.5.12 Other Proteins of Interest

Due to project limitations, it was not possible to generate antibody binding profiles for all 24 proteins. The 12 proteins described in the following sections were not further investigated with immunohistochemical methods. In some cases, searches were performed and either the antibody was inappropriate, or the protein distribution was well known. Findings on the antibody staining of skin with respect to these proteins were derived from online sources such as www.proteinatlas.org, www.atlasantibodies.com and www.abcam.com.

ADP/ATP translocase 2 (SLC25A5, P05141) is encoded by the gene SLC25A5 and belongs to the ANT gene family. SLC25A5 forms a homodimer that is membrane-bound to the inner mitochondrial membrane and involved in the transportation of ADP and ATP between the mitochondrial matrix and intermembrane space as part of the recycling of these molecules. SLC25A5 is present in the cellular cytoplasm and is expressed in most tissues of the body . (Lee et al. 2019) (Brenner et al. 2011). Investigation into the antibody staining of skin using the Protein Atlas indicated significant staining throughout the epidermis and structures within the dermis. Due to the ubiquitous nature of this protein, it is unlikely that any distinction could be seen between the acrosyringium and the surrounding tissue. Thus, it was considered one of the lower-priority targets.

Mitochondrial peroxiredoxin-5 (PRDX5, P30044) belongs to a family of antioxidant enzymes. PRDX5 is an antioxidant enzyme involved in the reduction of oxidative stress on the cell. Additionally, evidence shows that PRDX5 is involved in the regulation of intracellular Ca2+ concentrations. PRDX5 is highly expressed in the cytoplasm in most human tissues (De Simoni et al. 2013). Investigation of the staining profile of PRDX5 in skin samples revealed multiple examples in which staining was present throughout the epidermis, with a slight presence in the stratum basale. Furthermore, three examples were identified in which the acrosyringium was present in the PRDX5-stained skin samples. These examples confirm the expression/presence of PRDX5 within the acrosyringium. PRDX5 has

been well investigated and reported; thus, independent verification in this work was not required.

Protein Disulfidesomerase A3 (PDIA3, P30101) is derived from the gene PDIA3 and belongs to the disulfide isomerase family of multifunctional chaperones responsible for isomerization through the generation of disulphide bonds and regulation of other proteins via catalysis of oxidation, reduction and denitrosylation. PDIA3 specifically modulates the folding of glycoproteins via disulphide isomerase activity. PDIA3 is found in the cytoplasm and ubiquitously expressed in all human tissues (Kondo et al. 2019; Mahmood et al. 2021). Multiple examples of PDIA3 staining of skin were identified in which cytoplasmic staining was confluent throughout the epidermis. Furthermore, in the Protein Atlas database, an example was found in which the acrosyringium was present in the PDIA3-stained skin samples. This example confirmed the expression/presence of PDIA3 within the acrosyringium luminal cells. As this information was already available, independent validation of this target became a lower priority.

Protein S100-A7 (S100A7, P31151) is derived from a gene belonging to the S-100 family of highly conserved inhibitors of phosphorylation. S100A7 is a calcium-binding signalling molecule involved in keratinocyte morphology, proliferation and differentiation, in addition to acting as an antimicrobial peptide. S100-A7 is present in the cytoplasm and expressed in a number of tissues including the nasopharynx, oral mucosa, epididymis, vagina, cervix, skin and tonsils (Zhu et al. 2013; Son et al. 2016) (Fano et al. 1995) (Yamamoto et al. 2007). The S100-A7 staining profile of skin derived from the Protein Atlas comprised multiple stained sections in which both cytoplasmic and nuclear staining of the epidermal cells was visible, with staining intensity increasing while moving through the epidermis to the periphery of the skin. Due to the significant staining of the epidermis, it is unlikely that any distinction could be seen between the acrosyringium and the surrounding tissue and therefore, this protein was not chosen for further investigation.

Desmoglein-3 (DSG3, P32926) is a calcium-binding transmembrane glycoprotein and a component of desmosome cell adhesion. DSG3 also influences morphology and

has been associated with differentiation and cell migration. DSG3 secretion is highly localised to membranous regions of the cell and the protein is detected in the skin, oral mucosa, oesophagus, cervix and tonsils (Rehman et al. 2019). The DSG3 antibody staining profile of skin in the Protein Atlas showed consistent ubiquitous staining of the cell membrane throughout the epidermis. As a result, it is unlikely that any distinction could be seen between the acrosyringium and the surrounding tissue, eliminating this protein from further investigations.

Sodium/potassium-transporting ATPase subunit beta-3 (ATP1B3, P54709-1) is derived from the gene ATP1B3. Although ATP1B3 also has a truncated isoform (P54709-2), little information is available on how its function deviates from that of P54709-1. ATP1B3 is a glycoprotein subunit of the Na+/K+ ATPase complex responsible for maintaining the electrochemical osmotic gradients of Na and K ions across the plasma membrane. ATP1B3 is present within cytoplasmic and membranous regions of the cell and expressed in most human tissues (Clausen, Hilbers, and Poulsen 2017; Zhang et al. 2019; Pirahanchi, Jessu, and Aeddula 2022). Investigation of ATP1B3 antibody staining revealed ubiquitous staining of the cellular cytoplasm and membrane throughout the epidermis. Furthermore, staining was slightly prevalent in the stratum basale in comparison to the rest of the epidermis. As strong staining was visible throughout the epidermis, no distinction would likely be seen between the acrosyringium and the surrounding tissue; therefore, this protein was not chosen for further investigation.

Protein Niban 2 (NIBAN2, Q96TA1-1) has a function related to apoptosis. Furthermore, it has also been related to B-cell proliferation, density, development and malignancies. Additionally, it should be noted that NIBAN2 has a truncated isoform, Q96TA1-2, on which there is little to no information regarding its function and differences from Q96TA1-1. NIBAN2 is found in the cytoplasmic and membranous regions of the cell and expressed in most human tissues (Patel et al. 2017; Chen, Evans, and Evans 2011). Protein Atlas examples of NIBAN2 antibody staining show ubiquitous staining of the cell cytoplasm and membrane throughout the epidermis, which makes it unlikely that any distinction could be seen between

the acrosyringium and the surrounding tissue. Therefore, this protein was not further investigated in this work.

Collagen alpha-1 (IV) chain (COL4A1, P02462-1) is a fundamental component of the basement membrane scaffolding underlying the architecture of most tissues, forming long, interlocking chains of repeating subunits as part of the extracellular matrix. Additionally, although COL4A1 has a truncated isoform (P02462-2), it is unclear how it differs functionally from P02462-1. COL4A1 expression is associated with basement membranes and is seen in a variety of tissues, including the brain, thyroid, lung, gastrointestinal tract, , liver, spleen, kidney, urinary bladder, testis, ovary, endometrium, cervix, placenta, breast, heart muscle, smooth muscle, connective tissue, adipose tissue, and skin (Weng et al. 2012). Protein Atlas examples of COL4A1 antibody staining show ubiquitous intracellular staining of the dermis, with no staining in the epidermis except for the point of contact between the epidermis and dermis. Therefore, this protein was not chosen for further investigation.

Aldehyde dehydrogenase 1A1 (ALDH1A1, P00352) belongs to a family of aldehyde dehydrogenases and is responsible for the oxidation of aldehydes to carboxylic acids, such as retinoic acid. ALDH1A1 expression is cytoplasmic in a range of tissues including the cerebellum, hippocampus, caudate, thyroid gland, nasopharynx, bronchus, lung, stomach, small intestine, appendix, liver, gallbladder, pancreas, kidney, testis, epididymis, ovary, endometrium, soft tissue, adipose tissue, skin, , tonsil and bone marrow (Verma et al. 2021; Anderson et al. 2011). Protein Atlas examples of ALDH1A1-specific antibody staining of skin showed light cytoplasmic and membrane staining of cells within the stratum basale and stratum spinosum. Due to this very light, non-specific staining, this target was considered a low-priority example. However, when this target was revisited for thesis write-up, an example was found of a skin section with significant staining. In this example, significant staining of the epidermis (both cytoplasmic and nuclear staining) was observed between two dermal papillae in comparison to the surrounding tissue, where there was little to no staining. This was much like the example of SERPINB3 staining of the skin (Figure 4.17 D and E), in which staining of the cells was visible in the direct

vicinity of the acrosyringium but dissipated upon moving away from the luminal structure. No further structures were found in this example, so it is not possible to confirm whether this was an acrosyringium structure or another secretory gland. Further investigation is required, as without subsequent staining of sections to confirm the presence of the luminal structure, it is not possible to confirm the presence of this protein within the acrosyringium.

Leukocyte elastase inhibitor (SERPINB1, P30740-1) also belongs to the SERPIN family. SERPINB1 is a neutrophil serine protease inhibitor affecting neutrophil elastase and cathepsin G; it also regulates inflammatory caspases and B-cell proliferation. SERPINB1 also has a truncated isoform (P30740-2) which, to date, has no published material indicating differences in function from P30740-1. SERPINB1 is observed in the cytoplasm, and expressed in the rectum, spleen, skin, , tonsil and bone marrow (Choi et al. 2019b, 2019a; Baumann, Pham, and Benarafa 2013; El Ouaamari et al. 2016; Yoshida et al. 2020). Protein Atlas examples of investigations into the staining of skin using SERPINB1 antibody showed low staining of the cytoplasm of the stratum basale within the epidermis. Due to this low staining of tissues, this protein was not chosen for further investigation.

Glycogen phosphorylase, brain form (PYGB, P11216) is a key component in regulating and metabolising glycogen within the cell. PYGB is specifically responsible for the first stages of glycogenolysis, specifically adenosine triphosphate (ATP) production. PYGB is observed in the cytoplasm and is expressed in most human tissues (Migocka-Patrzalek and Elias 2021). Initial investigation into the staining of skin using an anti-PYGB antibody showed low staining of the cytoplasm of the stratum basale within the epidermis. Due to this low staining of tissues, PYGB was not chosen for further investigation.

Transketolase (TKT, P29401) is involved in the pentose phosphate pathway and glycolysis pathway contributing to the production of NADPH. TKT is observed ubiquitously in the nucleus of all human tissues (Gu et al. 2020; Kochetov and Solovjeva 2014). Protein Atlas examples of TKT antibody staining of skin sections show ubiquitous nuclear staining of the epidermis. Due to the ubiquitous nature of

the staining, it is unlikely that any distinction could be seen between the acrosyringium and the surrounding tissue; therefore, this protein was not chosen for further investigation.

4.6 Discussion

This chapter describes the successful isolation, identification and comparison of proteins from acrosyringium-positive and acrosyringium-negative FFPE epidermal samples utilising the optimised quantitative proteomics strategy developed in Chapter 3. Furthermore, the immunohistological staining of 12 proteins that were identified as significantly more prevalent within the acrosyringium-positive samples in the context of skin is described.

Figure 4.1 depicts the isolation of both acrosyringium-negative and -positive tissue. However, the use of this sample isolation method could contribute to some of the variation observed in later results. The method in question utilised very small amounts of tissue, consolidated to a total tissue volume of 0.01 mm^3. For the acrosyringium-negative samples, this material would have been relatively homogenous. However, with the acrosyringium-positive samples, although great care was taken to ensure sampling consistency, it was impossible to maintain the proportions of acrosyringium to the surrounding tissue. This variation in the proportion of acrosyringium to the surrounding tissue may account for some of the discrepancies seen at later stages in the immunohistochemical analysis, such as the fold difference in the content of the proteins of interest across the four repeats.

As shown in Figure 4.2, the overlap of 64% to 78% seen between biological replicates regarding the identified proteins was present in at least two of the biological replicates. The three main factors that most likely contributed to the variation within each of the biological replicates are as follows:

- The composition of each of the samples: The variation in individual isolates could contribute to differences in the prevalence of particular proteins when analysed.
- Sample size and complexity: One of the central dogmas of proteomics states that the greater the complexity of the sample, the more the material

needed in order to obtain a representative profile. As skin comprises thousands of proteins and additional modifications may be present due to the formalin fixation process, more material would be preferable. However, as one of the key goals of this research was the generation of a protein profile from much smaller samples, this trade-off was necessary.

- The stochastic nature of peptide ion selection for fragmentation in a DDA experiment: This, of course, will be somewhat influenced by sample size and complexity. Technical replicates of the same sample injected twice would only result in an overlap of 60%–80%.

When comparing the finding of this study to the other proteomic profile of the skin (Pax.DB (http://pax-db.org/dataset/9606/2395425797/)in general and specifically the eccrine sweet glad(Na et al. 2019) in Figure 4.3. Results are promising with the minority of identified proteins 96.6% (1643 /1700) corresponding to one or both of the other datasets. Implying that the extraction and proteomic analysis was successful and representative of the tissue analysed. The fact that there are a large number of proteins identified in the other detests in comparison to the one generated here was expected. As both the skin proteome and the eccrine sweet gland proteome contain structure that where not isolated and analysed as part of this study. For example in the case of the skin proteome other secretory glands such as the apocrine gland and structures such are hire follicles as shone in figure 1.1. In the case of the eccrine sweet gland proteome(Na et al. 2019) the other regens of the secretory col and lumen as illustrated in figure 1.3 and1.4. Both Which would undoubtedly result in addition identification due the additionally veered structure analysed. Additionally both case of other proteomic profile of the skin (Pax.DB (http://pax-db.org/dataset/9606/2395425797/)in general and specifically the eccrine sweet glad(Na et al. 2019). Much lager volume of tissue were analysed which as indicated by figure 3.4 results in a greater number of identifications more representative profile of the sample analysed. In the case of Chi Hyun Na(Na et al. 2019) analysis of the eccrine sweet gland proteome this further propagate by the use of multiple sample possessing methods to very the samples prier to LC-MS/MS analysis to perfume a more in-depth analysis of the tissue.

As indicated in Figure 4.3 B, 148 (8.7%) of the proteins identified from the human Uniprot database did not match either of the established protein databases (Pax.DB (http://pax-db.org/dataset/9606/2395425797/) and the eccrine sweat gland proteome (Na et al. 2019)) associated with the tissue being analysed. A contributing factor to these findings is the use of FFPE in this study. It is well documented that in the process of fixation and protein extraction for analysis, an alternative peptide profile is often generated, which is covered in Chapter 1. The majority of proteins in this group are known to be present within the skin, such as 40S ribosomal proteins, keratins, vibrant immunoglobulin gamma, interleukins and fibrillin. This confirms that the methodology and processing produced accurate results.

IPA findings identified "Wound Healing Signalling Pathway" as the only significant (P value <0.01 & Z scour >1) pathways according to that dataset analysed. Theses findings support the findings form the other analytical methods such as go analysis shown in figure 4.4 and string analysis in figure 4.7 associating the acrosyringium rich tissue cellular infrastructure and wound repair. The acrosyringium having a high association to wound repair is supported by both the findings here and other publications(Zhang, Yin, and Zhang 2019; Diao et al. 2019; Lobitz, Holyoke, and Montagna 1954; Lu and Fuchs 2014).

Twenty-four proteins were shown to have a significantly increased prevalence in acrosyringium-positive samples in comparison to acrosyringium-negative samples. Twelve of these proteins were selected for antibody staining. As indicated in Figure 4.6, the majority of the proteins of interest only exhibited a fold difference in content of between 1.1 and 2.5, the exceptions being KRT6, TPSD1, ALDH1A1 and S1007 A, which had higher fold differences. The low fold difference meant that the likelihood of being able to distinguish the acrosyringium from the surrounding tissue based on the staining of the specific proteins was quite low. Of the 12 proteins investigated with antibodies, 11 showed strong staining of the acrosyringium, confirming the presence of these target proteins within the structure.

Antibody staining of these targets in skin showed KRT6, annexin A1 and CALML5 to have more specific staining in the acrosyringium in comparison to other proteins as illustrated in Figures 4.9, 4.18 and 4.19. KRT6 had the most significant fold change between the two sample groups. However, the fold change difference for annexin A1 and CALML5 was much lower, suggesting that they may play a significant role within the acrosyringium and warrant additional investigation.

KRT6 showed the highest fold change between the acrosyringium-positive and -negative samples. However, validating this protein proved difficult as there are no isoform specific antibodies to permit differentiation. However, if time had allowed, it may have been interesting to distinguish between the isoforms and investigate their relation to the acrosyringium. Both keratin 6 and 16 were among the more significant proteins of interest, which were then identified as associated with each other in the STRING analysis. Fundamentally, both of these proteins are associated with cell-to-cell infrastructure and wound healing within the skin. An increase in KRT6 and KRT16 causes decreased cell migration, increasing cell-cell and cell-matrix connections, morphology and orientation. As seen in Figure 4.9, the expression of these proteins was highly localised to the acrosyringium, implying that these proteins and their pathways are continuously expressed and utilised in order to maintain acrosyringium structure in such a dynamic environment. This raises the question of whether this is a preventative feature to prevent the disruption of acrosyringium topography (whether cells are ready to react should damage occur) or a reactive feature that consistently induces the repair of these structures following exposure to environmental, chemical or bacterial stresses.

For the majority of the other samples screened using targeted antibodies, i.e. KRT16, CRABP2, ABHD14B, LAMC1, RPN1, SERPINB3 and GSTP1, staining of both the acrosyringium as well as the tissue directly surrounding it was observed to varying degrees. This validates the initial data confirming the presence of these proteins within the tissue with little distinction between the acrosyringium and the surrounding tissue as would be expected based on the low fold change difference in protein levels. However, CRABP2 and SERPINB3 staining (Figure 4.11 and 4.18) did show dark staining around the acrosyringium as opposed to areas further off, i.e.

outside the dermal papilla that the luminal structure transects. In combination with the online examples of PRDX5, this observation implies additional infrastructure to either maintain or support the acrosyringium in the dynamic environment of the epidermis.

The only outlier of the group screened using targeted antibodies was TPSD1 (Figure 4.13), which was not stained in any of the acrosyringium samples. As indicated in the introduction, this protease is predominantly associated with mast cells; however, it is also found in other environments, such as the testes.

Regarding the proteomic data, the main point of contention is that only one to two peptides of this protein were identified in each experimental analysis. Identification of such few peptides reduces protein identification confidence. However, in each of these cases, they were identified as unique peptides that passed all of the stringent criteria. Furthermore, TPSD1 is a small protein, with its intact form being only 242 amino acids in length and only a few of lysine and arginine present where cleavage by trypsin is possible. Thus, the pool of peptides that could be used to identify this protein could be very limited, especially when in competition for analysis in a complex sample such as a whole tissue lysate. Bearing this in mind, the likelihood of this protein being within the sample is high.

A number of physiological factors may have contributed to the observed results of the immunohistological TPSD1 staining.

The first of these is the presence of the second TPSD1 isoform, Q9BZJ3-2. As indicated in Figure 4.20, these two isoforms differ by eight amino acids. Even though this difference is not located within the target region of the antibody used, it is possible that the topography of this region was affected, preventing the antibody from binding to its target site.

Another factor likely contributing to this observation is the PTMs that influence TPSD1 protease activity. As indicated in Figure 4.20, which maps the PTMs of TPSD1 and the antigen sequence used, the antibody binding site for the anti-TPSD1 antibody is located within two regions that are affected by disulphide bonds that

affect enzyme activity. Thus, depending on the state of activity of the protein, it may not be possible to detect specific antibody binding.

TPSD1 also forms tetramers in which the protein is active. Depending on the orientation of the protein within the tetramer (Elst et al. 2022; Trivedi and Caughey 2010; Frungieri et al. 2002; Wang et al. 2002), the binding region of the antibody may or may not be exposed. As the manufacturer did not provide supplementary information, such as western blots with recombinant proteins or cell extracts as controls, it was not possible to determine what form of TPSD1 the antibody batch was binding/staining.

On a final note, as indicated in table 4.1 one of the tissue samples analysed was isolated from the sole of the foot (sample 1), whereas the other three tissue samples analysed were isolated for the axilla (samples 2-4). As these isolates were taken from different regions of the body it is possible that they could exhibit slightly different properties despite being part of the same structure. Morphologically the acrosyringium of the ESG from these two reges do differ in size due to the thickness of the epidermis of the two regions with the sole of the foot been thicker than the axilla is indicated in section 1.2 and figure 1.3. Comparison of the proteomic results between sample 1 and the accumulated samples 2,3 and 4 showed to be similar. Of the 1,700 proteins identified ~50% of the proteins were present in both groups as shone in figure 4.3 , with 4.7%(80) been unique to sample 1 and 45.4%(772) unique to samples 2,3 and 4. However as a basis of comparison this is very limited, due to the low sample number that is not evenly distributed between the two groups, the limited sample volume used to perform this analysis and the fact that the samples were taken from different individual could compound the variation seen. The purpose of this was not to investigate this particular potential variable however the results of this study could contribute to investigating this at a later time. In order to confirm if there are any difference in the acrosyringium obtained from different regions of the body additional testing would be required. Testing could include obtaining multiple samples from a single individual to allow for direct comparison. Or comparison of a much grater pool of individual to compensate for any variation seen between individual due to factors that could contribute to variation seen such as: age, ethnicity or sex. However at this point ether method is not feasible so could not be expanded upon concurrently.

Figure 4.20 TPSD1 protein sequence, PTM annotation and antibody target sequence.

Red, blue and green regions indicate amino acids with PTMs. The yellow region indicates the antigenic amino acids sequence targeted by the anti-TPSD1 antibody.

It is well documented that calcium ions play a significant role in cell function and signalling within the skin, contributing to processes such as homeostasis, immune responses, keratinocyte diversification, cell proliferation and adhesion, and wound healing. Four of the proteins of interest (CALML5, S100A7, DSG3 and ANXA1) were observed to form complexes with calcium ions or other heavy metals, resulting in the direct influence of these ions on protein activity. Furthermore, the majority of the other proteins of interest are indirectly influenced/regulated by other proteins that form complexes with calcium ions. Calcium ion concentration is known to play a significant role in differentiation within the epidermis, to the point where a calcium ion gradient is visible across the epidermis, thus resulting in the association of an approximate stage of keratinocyte differentiation with a calcium ion concentration range (Tsutsumi et al. 2009; 2018; Strudwick et al. 2015; Sutterlin et al. 2017; Ovaere et al. 2009). One hypothesis regarding acrosyringia is that they exist at a stage of differentiation different to that of the surrounding tissue. This could account for the very similar protein and peptide profiles generated by the two sample groups as indicated in Figure 4.3. Unfortunately, staining attempts using alizarin red to identify the presence of calcium within the sample were unsuccessful due to inconsistent staining. This is most likely due to alizarin red being insufficiently sensitive for the experiment.

In summary, the method developed in Chapter 3 was successfully implemented for the analysis of 0.01 mm^3 of FFPE human skin samples. Samples with and without the presence of acrosyringium were compared, and 24 proteins that were significantly more prevalent within the acrosyringium-positive samples were identified; the majority of these had associations with structural cellular components. A subset of these proteins was then selected for further investigation and validation using targeted antibodies, which confirmed the presence of these proteins within the acrosyringium structure. With the exception of the two KRT6 isoforms, the targets that displayed the most distinct staining of the acrosyringium in comparison to the surrounding tissue were CALML5 and ANXA1. Therefore, I proceeded to further investigate these two proteins, as discussed in the next chapter.

Chapter: 5 Investigation into acrosyringium-positive proteins of interest: Annexin A1 and Calmodulin-like protein

5.1 Introduction

Of the 25 proteins identified as more prevalent in acrosyringium-positive tissue than in acrosyringium-negative tissue, Annexin A1 and Calmoldulin-like protein 5 were selected for further study. Both exhibited strong contrast in staining in the acrosyringium compared to the surrounding tissue (Figs. 4.18, 4.19), validating the elevated levels observed in these different tissue regions by quantitative proteomics.

5.1.1 Annexin A1

Annexin A1 (AnxA1, UniProt accession number: P04083) belongs to the annexin family which comprises calcium-dependent phospholipid-binding proteins. First observed in the 1980's as a glucocorticoid regulated anti-inflammatory agent inhibiting prostaglandin E2 (PGE2) synthesis (Cloix et al. 1983; Cirino et al. 1987; Sheikh and Solito 2018), AnxA1 has been observed in a variety of forms. The full length form at 37 kDa has multiple Ca^{2+} ion binding sites and a N-terminal phosphorylation site, as well as a N-terminal derived peptides Ac2-26(Huang et al. 2020; Dalli et al. 2012). Understanding of its functionality has been expanded upon since the 1983, from being seen as an anti-inflammatory agent to influencing cytokine synthesis, the innate and adaptive immune systems, wound repair, tumour suppression, homeostasis, cell development, cell differentiation and cell migration (Zhang et al. 2021; Huang et al. 2020; Purvis, Solito, and Thiemermann 2019; Sheikh and Solito 2018; Kreft et al. 2016; Leoni et al. 2015; Cristante et al. 2013; Sakaguchi and Huh 2011; Parente and Solito 2004) (Parente and Solito 2004). Anxa1 is involved in a number of intercellular and intracellular functions and is reported to be localised across the nucleus, cytoplasm and cell membrane of most tissues to various degrees.

5.1.2 Calml5

Calmodulin-like protein 5 (Calml5, UniProt accession number: Q9NZT1) also referred to as Calmodulin-like skin protein (CLSP), was first discovered in 2000 (Mehul et al. 2000) due to its association to calmodulin and involvement in keratinocyte differentiation. Subsequent research has shown Calml5 to be involved in the regulation of keratinocyte differentiation but also keratinocyte proliferation and tumour suppression (Kitazawa et al. 2021; Abbreviations ; Takahara et al. 2019) Calml5 is involved in a number of intracellular functions and can be observed in the nucleus and cytoplasm of cells, and is most expressed in the epidermis of the skin, salivary gland, tonsils and epithelial surface of the oral mucosa and cervix.

5.1.3 ANXA1 and CALML5 expression and siRNA-mediated knockdown

To investigate the functional roles of ANXA1 and CALML5 an approach to alter the expression of these proteins and observe the effects in cells compared to original/wild type (WT) cells was taken. This had been intended to be a multistage approach starting with down-regulation of ANXA1 and CALML5 followed by an investigation into the effects this would have had on the model. Had there been sufficient time this would have been followed by investigating up-regulation of ANXA1 and CALML5 which more closely emulate what was observed in the acrosyringium in chapter 4. Of the established methods for adjusting protein expression, siRNA-mediated knockdown (KD) for both ANXA1 and CALML5 was selected as opposed to establishing knockout cell lines lacking the individual genes. The knockdown method was selected because it was deemed more feasible for the limited amount of time remaining for the project (Han 2018; Fire et al. 1998) particularly given the commercial availability of ANXA1- and CALML5-specific siRNA oligonucleotides and supporting kits.

5.1.4 Cell line

At the time of writing this thesis, there were no acrosyringium-specific cell lines available, nor was it feasible to culture a acrosyringium-specific primary cells (Diao et al. 2019) or generate an immortalised acrosyringium cell line. As indicated by the proteomic results in chapter 4.3 and supported by a number of previous publications (McGregor et al. 1991;

Shikiji et al. 2003; Christophers and Plewig 1973; Lu et al. 2012), there is little differentiate between the acrosyringium and surrounding keratinocytes. A hypothesis being that the acrosyringium may be comprised of keratinocytes at a different stage of differentiation than surroundings tissue (Diao et al. 2019; Langbein et al. 2008; Lu et al. 2012; Lu and Fuchs 2014) led to the selection of a keratinocyte cell line being the most appropriate model for this testing. Once again this was intended to be a multistage approach with initial investigation being performed on an immortalised keratinocyte cell line and then to be validated in a primary keratinocyte cell line, to ensure initial observations were not factors associated to the phenotypic properties due to immortalisation of the cell line.

For the initial stages of this investigation the spontaneously immortalised human keratinocyte cell line High sensitivity of human epidermal keratinocytes (HaCaT) was selected(Brosin et al. 1997). HaCaT cell line been derived from human souse being one of the key points of its selection. Hacat is considered as a reliable and well characterize keratinocytes in vitro model that emulates keratinocyte and how they differentiate through the different stratified layers of the skin in vivo(Brosin et al. 1997; Pessina et al. 2001; Yamazaki et al. 2004; Deyrieux and Wilson 2007). Investigation into the proteome of the HaCaT cell line confirmed it expressed both ANXA1 and CALML5(Rusanov et al. 2021). Additional key featurer that make the HaCaT cell line an ideal keratinocyte in vitro models, is its able to differentiated from and return to a basal cell form by adjustment of Ca2+ ion concentration within the culture media. As CALML5 function has been closely related to differentiation of keratinocytes(Sun et al. 2015; Kitazawa et al. 2021)and would allow of observation to be made at the different stages differentiation for CALML5 KD and ANXA1 KD. Furthermore, the HaCaT cell line dose not contain pathological condition such as human papillomavirus (HPV). As such condition could effect the inflammatory response which ANXA1 is in part associated to, as mentioned in 5.1.1. This is of importance as the inflammatory response (i.e. cytokine expression) can be used to monitor the effect of altered ANXA1 expiration in keratinocyte modal when exposing it to stresses, which the acrosyringium are exposed e.g. bacterial growth, changes in pH and osmolarity. These stresses can be simulated by use of bacterial lipopolysaccharides (LPS) to represent the presence and/or growth of bacteria in an in vitro models (Girol et al. 2013; Wang and Zhang 2018; He et al. 2019; Wu et al. 2020). If there had been sufficient time this would have been

followed by alteration to the culture media salt concentration (addition of synthetic sweat) to simulate the stress caused by sweating which caused changes in the pH and osmolarity. The availability and diverse way in which HaCaT cell line could be used as a keratinocyte model and monitored, was why it was selected for this stage of testing.

5.2 Aims

Based on observation of elevated expression of annexin A1 and CALML5 in acrosyringia rich tissue, this chapter aimed to investigate the contextual role of these two proteins using siRNA knockdown in keratinocytes.

5.3 Chapter 5 experimental overview

In this chapter experimentation focused on generation of siRNA knockdowns of ANXA1 and Calml5 in the HaCaT cell line. Following the successful generation of ANXA1 siRNA knockdowns a comparison between the ANXA1 knockdown and wild type call in both the basal and differentiated forms of the HaCaT cell, was performed. The comparison focused on the response of HaCaT cells to bacterial lipopolysaccharide by monitoring the cytokine IL6 and IL8 expression using Elisa assays. To determine if alteration of ANXA1 expression had effected HaCaT cells stress response resulting in variation of cytokine expression.

5.4 Results & Discussion

5.5 Anxa1 knockdown

Initial attempts to knockdown Anxa1 using siRNA HaCaT cells were unsuccessful, showing no distinguishable differences in the expression of pre- and post-treatment with siRNA. Subsequent attempts to knockdown Anxa1 KD were made, in which the following two variations of the method were used: 1) Double siRNA concentration from 25 nmol to 50 nmol per transfection; 2) Double transfection – the transfection was performed and then repeated 24 h later, as described in Chapter 2 (sections 2.3.3.2 and 2.3.3.3). Of the methods tested, the double transfection method was the only one shown to reduce the levels of Anxa1. The Anxa1 siRNA knockdown timeline is shown in Figure 5.1: in this Figure there are equivalent bands in the Anxa1 siRNA knockdown and the corresponding controls at 12 time

points, indicating an equal presence of Anxa1 in both siRNA treated Anxa1 knockdown and control samples. Figure 5.1 B illustrates the corresponding anti-alpha-tubulin-antibody western blots used as a loading control, indicating equivalent protein loading of samples from treated KD and control groups at this time point. All subsequent time points, with the exception of the 72 h time point, show a reduction in the prevalence of Anxa1 siRNA knockdown samples in comparison with corresponding controls.

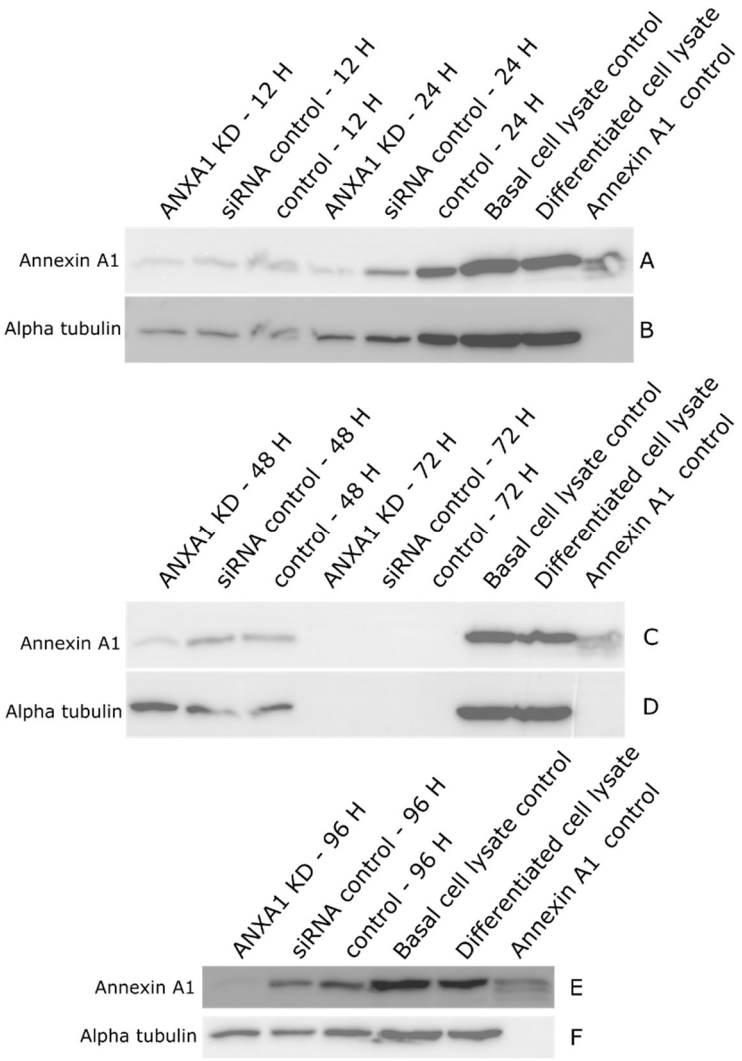

Figure 5.1 *Western blot of Anxa1 siRNA knockdown optimisation.*

HaCAT cells treated with targeted siRNA, siRNA control samples treated with non-specific siRNA, and control samples which were not treated with siRNA but went through the same processes as siRNA-treated samples. Alpha-tubulin was used as a loading control. From 24 hours onward, Anxa1 KD appeared to reduce in intensity in comparison with control samples, indicating a reduction in the presence of Anxa1; corresponding loading control bands remained constant.

In Figures 5.1 C and D, lanes for the Anxa1 knockdown, siRNA control and control groups in both the anti-Anxa1 and alpha-tubulin-treated Western blots are absent at the 72-h time point.

Western blots of the sample were repeated, but continued to show no presence of bands. This suggests that material was lost at some point during the processing of samples, leading to a missed time point. However, in the time points prior to- (Figure 5.1 C and D at 48 h) and after (Figure 5.1 E and F at 96 h) the 72 h time point, the Anxa1 KD bands appear reduced in intensity in comparison to control samples, indicating a reduction in the presence of Anxa1 in the Anxa1 KD samples, throughout the 48 h to 96 h time period. Coupled with the corresponding alpha-tubulin results, indicating equivalent loading of braces regarding band intensity, results show a drop in Anxa1 in the Anxa1 KD samples between 24 and 95 h time points. This demonstrates the successful generation of a partial Anxa1 KD, which could be used in subsequent investigation into keratinocytes stress response.

5.6 Anxa1 knockdown LPS treatment

The role of annexin A1 in mediating the response to inflammatory stimulus was investigated by treating HaCat cells with bacterial lipopolysaccharide (LPS), and measuring the production of proinflammatory cytokines Interleukin 6 (IL-6) and Interleukin 8 (IL-8), as a function of annexing A1 expression. Testing was performed on both the basal and differentiated forms of the HaCaT cell line with WT AnxA1 KD, in order to determine if differentiation impacted on the production of proinflammatory and neutrophil chemotactic factors. HaCaT cells were grown, treated with AnxA1 siRNA as previously described for 48 h before being exposed to LPS (0.0, 0.1, 1.0 and 10 mg/mL) for 24 h. IL-6 and IL-8 concentrations in the culture supernatants were then measured using commercial ELISA assays.

The effect of reduced annexin A1 levels on LPS-mediated release of IL-6 are shown in Figure 5.2.. As previously reported, with each incremental increase in LPS, an increase in IL-6 expression was observed (Wu et al. 2020). Interestingly, even in the absence of LPS, IL6

levels were significantly elevated in the media of both differentiated and undifferentiated HaCaT cells following annexin A1 knockdown ($p < 0.001$).

WIth the exception of undifferentiated cells treated with the maximal 10 mg/ml LPS, , expression of IL-6 in response to LPS was significantly greater following AnxA1 KD than in corresponding WT samples. (Figure 5.2 B).

Similar to IL-6 results, IL-8 expression (Figure 5.3) was significantly ($p<0.001$ to $p<0.05$) increased in AnxA1 KD samples compared to in WT samples in the majority of cases. In the absence of LPS, IL8 levels were significantly elevated in the media of both differentiated and undifferentiated HaCaT cells following annexin A1 knockdown ($p < 0.001$). The exceptions to increased IL-8 expression in AnxA1 KD samples compared to in WT samples included, basal cell WT and basal cell AnxA1 KD samples treated with 0.1 mg/ml of LPS (Figure 5.3 A), where IL-8 expression was relatively similar between the two samples. Additionally, in basal cell WT and basal cell AnxA1 KD samples treated with 1 mg/ml of LPS (Figure 5.3 B), significantly greater expression of IL-8 was observed in the WT samples compared to AnxA1 KD samples.

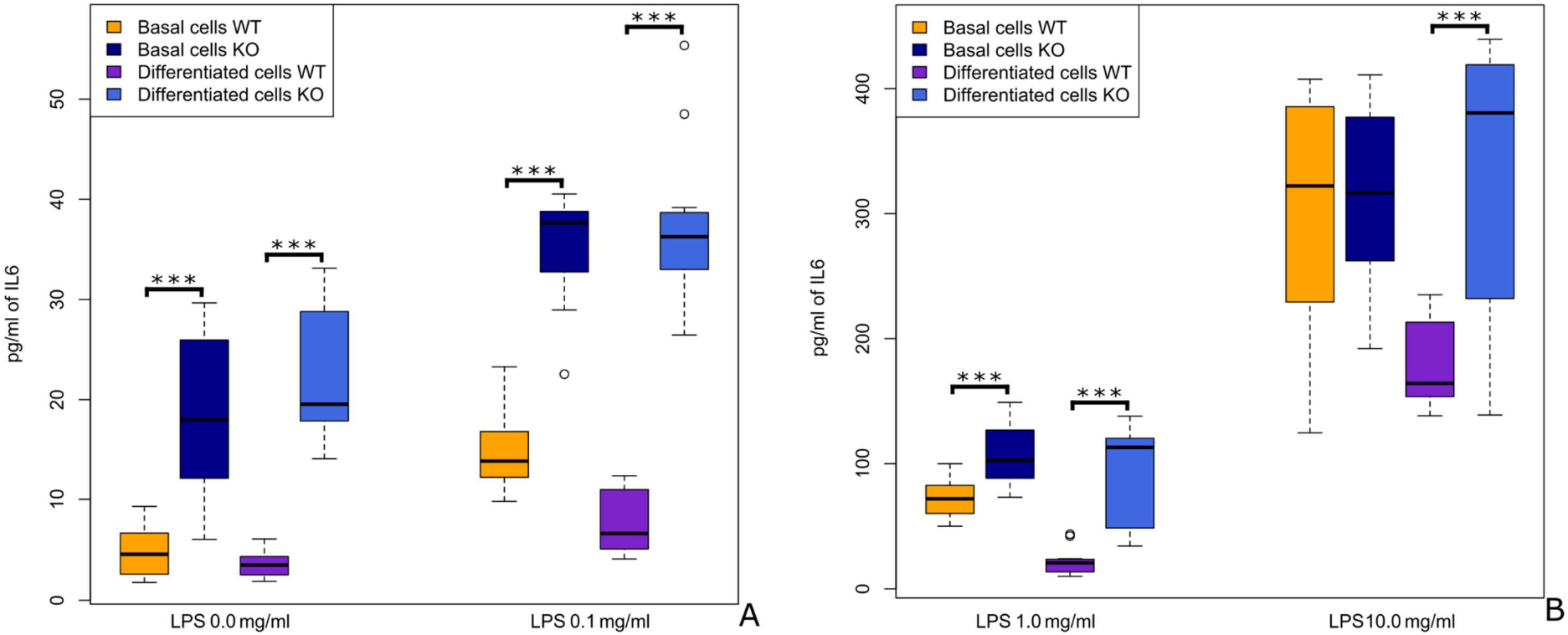

Figure 5.2 *IL6 response to LPS treatment of WT and Anxa1 KD HaCaT samples.*

*Statistical analysis of IL6 expression in WT and Anxa1 KD samples of basal and differentiated HaCaT cells when treated with LPS. A) illustrates LPS 0.0 mg/ml (untreated) and 0.1 mg/ml treated samples; B) illustrates LPS 1.0 mg/ml and 10 mg/ml treated samples. Values analysed using a two tail Test***P < 0.0001.*

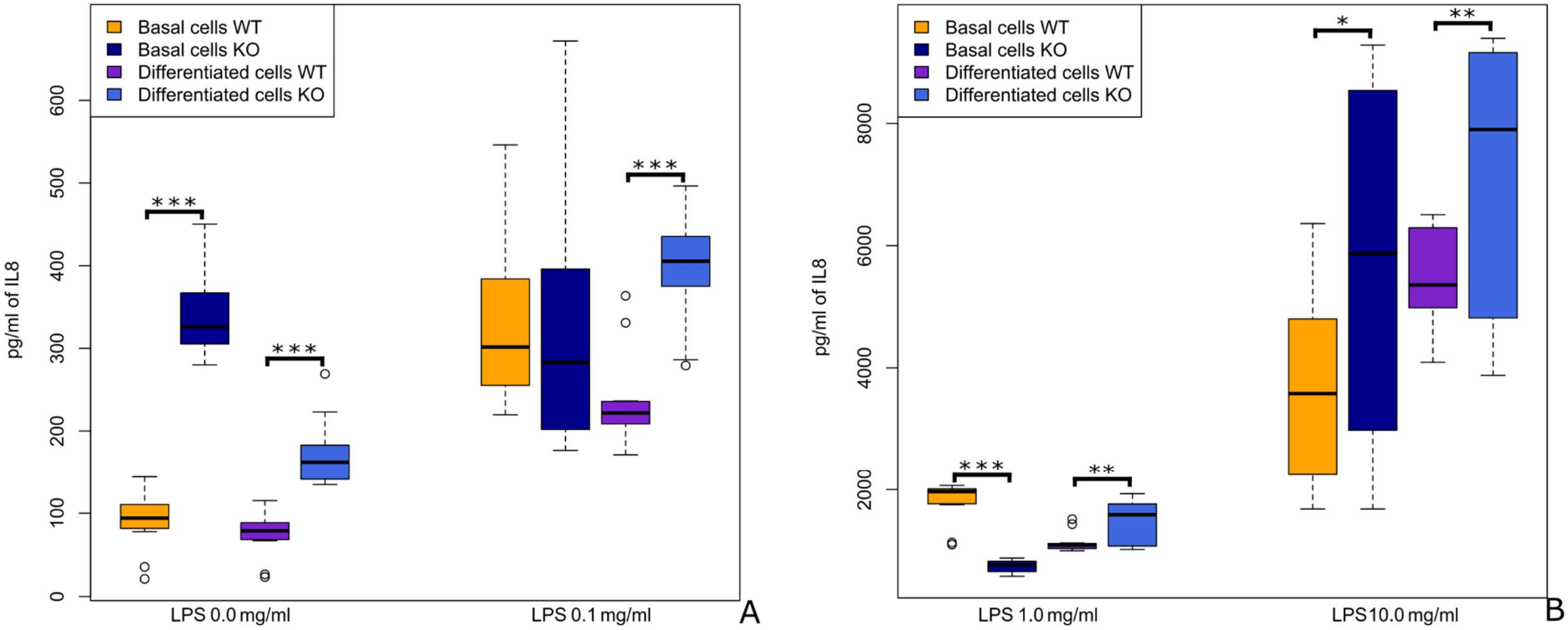

Figure 5.3 IL-8 response to LPS treatment in WT and Anxa1 KD HaCaT samples

*. WT and Anxa1 KD samples of basal and differentiated HaCaT cells were treated with a variety of LPS concentrations to determine if reduction in Anxa1 would affect cell stress inflammatory response. A) illustrates LPS 0.0 mg/ml and 0.1 mg/ml treated samples; B) illustrates LPS 1.0 mg/ml and 10 mg/ml treated samples. Values analysed using a two tail Test *P < 0.05, **P < 0.01 and ***P < 0.0001*

.

5.7 CalmL5 knockdown

Anti-CALML5 antibodies were used in the staining of FFPE tissue in Figure 4.19, but not of the antibodies evaluated were validated for use in Western blot analysis by the manufacturer. When used in a Western blot analysis of HaCaT cell lysate, no bands were observed (data not shown). Alternative antibodies were screened using the cell lysate from HaCaT cells, A-431 cells (ab7909, Abcam, (RRID:CVCL_0037)), a cuteanous squamous cell carcinoma cell line shown to express CALML5 (Kitazawa et al. 2021), and a recombinant form of human CALML5 protein as a positive control (Figure 5.2). Using this antibody (ab154631) a band at ~23 kDa was observed in all the cell lysates. With the exception being the recombinant protein, appearing at ~43 kDa which is in compliance with the manufactures specification. The CALML5 control bands appeared in a different location than the CALML5 lysate bands, as the recombinant protein contains an additional N-terminal polyhistidine (His) tag and Glutathione-S-transferase (GST) tag, making it significantly larger than the unmodified CALML5.

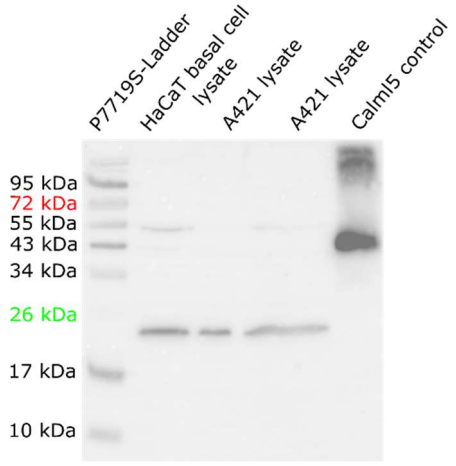

Figure 5.4 *Anti-CALML5 Western blot validation.*

Validation of ab154631 anti-CALML5 antibody in a Western blot. Forming a band at approximately 23 kDa for WT CALML5 and 43 kDa for the recombinant form of human CALML5 protein used as a positive control. This Western blot confirms that ab154631 anti-CALML5 antibodies can be used to detect the presence of CALML5 and can be detected in HaCaT cell lines.

Initial attempts to knockdown CALML5 in basal HaCaT cell lines using the CALML5-targeted siRNA pool, as per the manufacturer's recommended method, was unsuccessful, showing no discernible difference between CALML5 bands by immunoblotting in siRNA treated and untreated cells. After troubleshooting, a number of changes were made to the proposed methodology; Opti-MEM reduced serum media (Thermofisher 31985062) was incorporated during incubation of cells with siRNA, and the concentrations and intervals with which cells were incubated with siRNA was varied. Other changes included: single inoculation (SI) followed by a 12 h incubation (as recommended by the manufacturer), doubling the amount of siRNA (DS) from 25 nM to 50 nM followed by a 12 h incubation, and double inoculation (DI) by inoculating cells with siRNA, and then repeating after 12 h. A glyceraldehyde-3-phosphate dehydrogenase (GAPDH) knockdown was performed in tandem to determine whether failure to knockdown CALML5 was due to the method being used or specific to the siRNA. The results of the attempted CALML5 and GAPDH knockdowns are summarised in Figure 5.5.

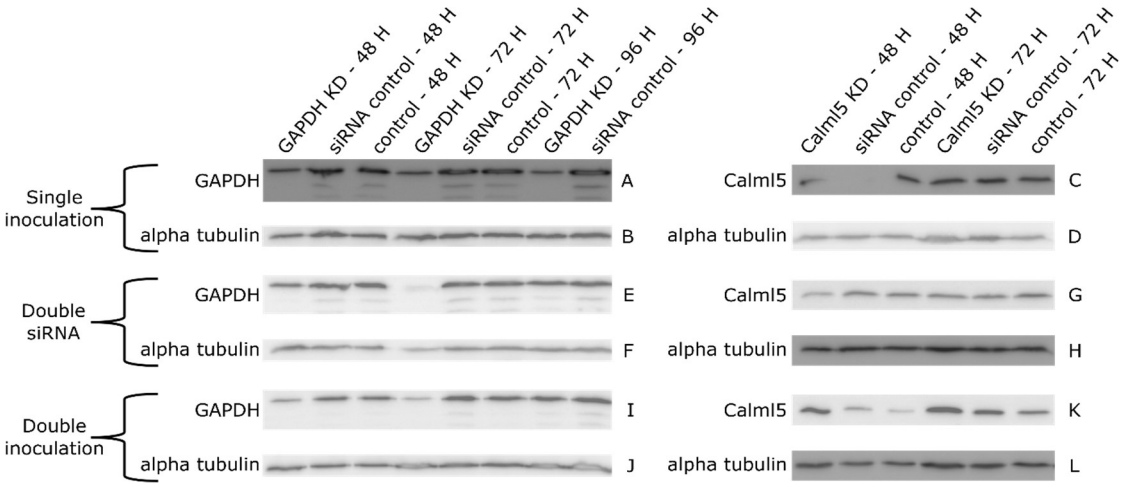

Figure 5.5 *Western blot summary of attempted CALML5 and GAPDH siRNA knockdowns*

. Three methods of generating CALML5 and GAPDH knockdown in HaCaT cells were attempted, including: single inoculation, double siRNA concentration and double inoculation. KD samples treated with targeted siRNA, siRNA control samples treated with non-specific siRNA, and control samples that were not treated with siRNA but went through the same processes as the siRNA treated samples. Alpha-tubulin was used as a loading control.

In panels C, G and K of Figure 5.3, the bands of CALML5 knockdown samples do not indicate any reduction in protein expression irrespective of conditions used (single siRNA inoculation, double siRNA concentration, or double inoculation) with reduction in CALML5 expression in comparison with the control lysates (Fig. 5.3, panels C, G, K). The corresponding lanes in panels D, H and L show equivalent levels of alpha-tubulin between CALML5 knockdown samples and corresponding control samples, implying loading of similar volumes of cell lysate between conditions. These results suggest that the CALML5 knockdown was unsuccessful.

However, in panels A, E and I of Figure 5.3, there is a notable difference between the bands of the GAPDH knockdown samples and corresponding controls. This is most prevalent in Figure 5.3 I, which indicates a notable reduction in GAPDH expression after 48 and 72 h treatment with GAPDH siRNA. This is further supported by the lack of significant difference in alpha-tubulin levels under the same conditions (Figure 5.3 J).

Successful generation of Anxa1 and GAPDH knockdowns indicates that the methods used for siRNA-mediated knockdown are suitable. However, the inability to alter the levels of CALML5 indicates that further method development, or alternative selection of SiRNA sequences, is required. Due to the limited timeline for this stage of the project, it was unfortunately not possible to perform additional methodological variations in order to generate CALML5 knockdowns.

5.8 Discussion

The initial aim of this study was to knockds both AnxA1 and CALML5 in the HaCaT cell line using siRNA and then investigate the phenotypic properties resulting from alteration of the expression of these proteins.TIme constraints, and issues with both knockdown of CalmL5 and antibody validation requirements, as well as lack of a suitable cell model meant that these investigations were constrained.

5.8.1 AnxA1 Knockdown

A successful AnxA1 KD in the HaCaT cell line was achieved and, to study the effects of triggering a stress response, the cells were treated with LPS. Specifically, the effects of cytokine expression in keratinocytes at varying doses of LPS were assessed.

Interestingly, control samples treated with no LPS (Figure 5.2 A and Figure 5.3 A) showed significant differences in IL-6 and IL-8 expression in both the basal and differentiated cells when comparing WT and AnxA1 KD samples. This suggests that Anxa1 inhibits cytokine expression, even in conditions where cells are not being stressed by foreign stimuli.

The same trend was observed in IL-6 and IL-8 expression when the LPS dose was increased. A significantly increased expression of IL-6 and IL-8 was observed in AnxA1 KD samples compared to WT samples in the majority of conditions tested. This supports the hypothesis that AnxA1 inhibits inflammatory response in both basal and differentiated keratinocytes. However, several anomalous results were observed in:

1) IL-6 basal cell WT and basal cell AnxA1 KD treated with 1 mg/ml of LPS (Figure 5.2 B).

2) IL-8 basal cell WT and basal cell AnxA1 KD treated with 0.1 mg/ml of LPS (Figure 5.2 A).

3) IL-8 basal cell WT and basal cell AnxA1 KD treated with 1 mg/ml of LPS (Figure 5.2 B).

In instance's 1 and 2, a similar distribution of values is seen in the WT and AnxA1 KD samples, resulting in no significant difference between the two groups. In instance 3, a significant difference is seen between the WT and AnxA1 KD samples, however, in the opposite manner as other significant results, with AnxA1 KD samples showing a significantly reduced response of IL-8 compared to the WT samples. According to previous literature, this is highly unlikely. This leads to the conclusion that this is a genuine anomalous result, which will be treated as such.

5.8.2 Future work on AnxA1

Had there been more time, further experimentation would have been focused on investigation of AnxA1 effects on keratinocytes when exposed to conditions indicative of ACS1. This would have included generation of HaCaT cells with up-regulated expression of AnxA1, in order to more closely match profiles exhibited by ASC1. The up-regulated AnxA1 HaCaT cells would have been used in conjunction with AnxA1 KD to investigate the effect of AnxA1 proliferation on wound healing, differentiation, stress response and cell viability when exposed to foreign material (LPS) or osmotic pressure (synthetic sweat). As well as investigating condition that could be associated AnxA1 in the context of keratinocytes such as Psoriasis (Wu et al. 2020).

5.8.3 CL5 CALML5 Knockdown

Despite several attempts to induce CALML5 knockdown, it was not achieved, as shown in Figure 5.5 C, G, K. Bands corresponding to CALML5-specific siRNA did not appear to be weaker than the corresponding untreated controls. It appears that the current methodology is not sufficient for producing CALML5 KD. Further investigation would be required to understand CALML5 in the HaCaT cell line.

5.8.4 CL5 Future work

Future work could also focus on generating CALML5 knockdown with alternative transfection reagents (examples here), varying concentrations, or increased transfection efficiency. Alternatively, increasing the concentration of CALML5-specific siRNA could be a line of further study, as previous attempts may not have

been sufficient to compensate for the turnover of CALML5 within the HaCaT cell line.

It is possible that the supply of CALML5 siRNA was not optimal; use of alternative suppliers or custom sets of CALML5-specific siRNA oligonucleotides would warrant investigations (Han 2018). Additional RT-PCR could be used to investigate and quantify whether the siRNA used were affecting the rate of CALML5 production, thereby helping to deduce whether the current results of the CALML5 knockdown were caused by the concentration of siRNA or the CALML5-specific siRNA.

Once conditions for succesful CALML5 KD had been optimised, they could be used to investigate its effects on keratinocytes. This could include the generation of a HaCaT cell line with up-regulated expression of CALML5. The CALML5 HaCaT cells could be used in conjunction with the CALML5 KD to investigate the effect of CALML5 on proliferation of wound healing and cell differentiation.

Chapter: 6 Discussion

6.1 Introduction

The work presented in this thesis generated an optimised method for isolation and protein analysis of small volumes (0.01 mm3) of FFPE tissue. Here, this enabled a proteomic analysis of the acrosyringium. The proteomic findings were validated using immunohistochemical methods, identifying several proteins that were significantly ($p > 0.05$) more prevalent within the acrosyringium than the surrounding tissue. These included AnxA1, KRT6 and CALML5. Further investigation into AnxA1 inflammatory inhibition in the context of keratinocytes, with the generation of an AnxA1 siRNA knockdown treated with LPS. This revealed significantly greater cytokine expression in AnxA1 knockdowns compared to wild-type. Inferring that increased expression of AnxA1 may be a response or preventative measure to prevent inflammation of the acrosyringium, and in turn, prevent the secretion of sweat.

Effective development of a mass spectrometry method was utilised to overcome the challenges of working with the acrosyringium of the eccrine sweat gland (ESG). The ESG are sparse within the skin even when in regions of high density; they vary from 50 to 650 ESG per cm2(Sonner et al. 2015; Wilke et al. 2007). The acrosyringium represents a small component of the ESG, and therefore, reduces the study target even further. Traditional and existing methods for processing FFPE for proteomics analysis are not suitable for such a small amount of sample material. In this study, the successful method for analysis linked heat-induced antigen retrieval (HIAR) with an in-solution trypsin digest, followed by analysis via LC-MS/MS. To further enhance the information from the digested sample, multiple analyses were performed. After each analysis, exclusion lists were generated for high confident peptide identifications, which were then incorporated into subsequent analytical runs, in order to optimise identification of the less intense peptide ions, and to delve as deeply as possible into the available proteome. The method developed for this work was performed on 25 times less material (<0.01 mm3) than was sampled

in other published studies, and yet it confidently identified approximately 1700 proteins per digest. This advantageous method has wide-reaching applications as FFPE tissue storage is widely used in pathology archives and relatively common amongst biobanks throughout the world, including rare and unusual samples. With such a small sample quantity now needed for analysis, this opens up the possibility of the method developed in this thesis being used in wide reaching areas of research, such as optimising the usage of rare and unusual samples and the accurate proteomic analysis of small features and discrepancies.

Even with the reduced volume of starting material that the optimised method now requires, in order to perform the analysis on specifically acrosyringium tissue, approximately 480 acrosyringa per analytical run would be required. Isolation of this quantity of material would not be feasible. Therefore, comparisons were made between samples of tissue with acrosyringium (acrosyringium-positive samples) to areas where there were no acrosyringium (acrosyringium-negative samples). Therefore deduce that any differences in the proteome is due to the acrosyringium.

1700 proteins were successfully identified from the four samples analysed. Furthermore, 24 proteins identified with a false discovery rate (FDR) of 1% were significantly more prevalent ($p > 0.05$) in the acrosyringium-positive samples compared to the acrosyringium-negative samples. The majority of the proteins of interest showed a one to two fold increase in expression, but this went as high as ten fold increase in the acrosyringium-positive samples. GO term analysis of these 24 proteins generally associated them with structural components of cells. Immunohistochemical staining of FFPE skin sections containing acrosyringium was performed on 11 of the 24 proteins of interest, enhancing the understanding of the spatial localisation of these proteins and to validate the proteomic results obtained. 10 proteins were in agreement with the proteomic observations and were shown to be expressed within the acrosyringium and surrounding tissue. Of these proteins, Keratin six (KRT6), Annexin A1 (AnxA1) and CALML5 (Figures 4.09, 4.19 and 4.20, respectively) showed the strongest staining of the acrosyringium compared to the surrounding tissue, proving a significant difference in the level of expression within

the acrosyringium compared to the surrounding tissue. Furthermore, CRABP2 and SERPINB3 staining (Figures 4.11 and 4.18, respectively) showed the strongest staining of the acrosyringium and the region directly around it, which then dissipated as you progressed further away. This could indicate that the tissue directly surrounding the acrosyringium has additional infrastructure to aid in its structure or function, despite showing no morphological differences from the surrounding tissue.

As AnxA1 and CALML5 showed the most significant difference between the acrosyringium and the surrounding tissue, further investigation into the effect of these proteins was performed in the context of keratinocytes. The HaCat cell line was chosen to act as a model system since it is well characterised keratinocyte and HaCat can differentiate. AnxA1 siRNA knockdown was successfully generated. One of the key functions of AnxA1 is to act as an inhibitor of inflammatory cytokines such as il6 and il8. A stress/inflammatory response was caused by introducing bacterial lipopolysaccharide (LPS, an antagonist exposed acrosyringium to imitate a bacterial invasion).

The results illustrate how AnxA1 expression affects the inflammatory response in response to LPS. The AnxA1 siRNA knockdown of IL6 and IL8 expression was significantly ($p > 0.001$ to > 0.05) greater than in the wild-type controls, both when treated with LPS and in samples not treated with LPS. This demonstrates that AnxA1 plays an active role in maintaining HaCat's steady state before the cells become stressed. CALML5 siRNA knockdown proved more difficult to achieve; a number of methods were investigated with no success. Further potential investigations into AnxA1, CALML5 and KRT6 could have included increasing the expression of the proteins in keratinocytes to more closely mimic what is seen in the acrosyringium. Based on the observations made and literature regarding these proteins of interest, a number of hypotheses could be made regarding their roles within the acrosyringium.

With AnxA1, elevated expression within the acrosyringium and not the surrounding tissue is observed. One of the key roles of AnxA1 is to inhibit inflammation. Changes of AnxA1 expression in keratinocytes has shown this is the case, indicating that within the acrosyringium, AnxA1 likely inhibits inflammation of the cells of the luminal surface. This could benefit the eccrine sweat gland and surrounding tissue by reducing the likelihood of the gland becoming blocked or overly stressed, resulting in cell death. The cells of the luminal surface are regularly exposed to inflammatory factors, but they have an anti-inflammatory response that enables a balance to be achieved. Preventing the failure to secrete generated sweat as is seen in cases of palmoplantar pustulosis (Hagforsen et al. 2010; Murakami et al. 2010; Hagforsen, Michaelsson, and Stridsberg 2011), where sweat is introduced directly into the tissue surrounding the gland, as opposed to on the surface of the skin. This leads to the question of whether this is a result of acrosyringium being consistently exposed to foreign material, which induces a stress/inflammatory response, e.g. sweat, metabolites, bacteria (LPS), etc. requiring inflammatory factor AnxA1 to be increased in that tissue ? Or is AnxA1 expression elevated as a preventative measure?

The proteomics and immunohistochemical analysis also showed increased expression of CALML5 in the acrosyringium in comparison to the surrounding tissue CALML5 is associated with differentiation in keratinocytes and is often used as a marker for this process(Sun et al. 2015). As the expression of CALML5 is elevated in the acrosyringium compared to the surrounding tissue, it could be hypothesised that CALML5 is involved in both the differentiation of keratinocytes and the more specific effects relating to the regulation of differentiation within the acrosyringium. Further work is required to confirm this hypothesis.

KRT6 is the 3rd protein that showed significantly greater expression in the acrosyringium in comparison to the surrounding tissue that is associated with wound repair within keratinocytes. From the elevated expression of KRT6 in the acrosyringium compared to the surrounding tissue, it is possible to surmise that these cells are either in a constant state of repair or in a state of readiness in

preparation for the required repair. This presents a particularly interesting avenue to investigate further.

6.2 Limitations of the study

The optimal approach to generating a proteomic profile of the acrosyringium would have been the analysis on solely acrosyringium specific tissue, or analyse in acrosyringium specific cells line which, as previously stated, was not feasible. The approach taken allowed for the proteomic analysis of acrosyringium as well as surrounding tissue providing an overview of the region. This identified a number of proteins that were present within and around acrosyringium and surrounding keratinocytes indicating meaningful similarities. This lends itself to the hypothesis that the acrosyringium may simply be a keratinocyte at a different stage of differentiation. This indicates the keratinocytes would be a feasible candidate for a carrier/bulk if a single cell analysis was performed on acrosyringium. With this direct comparison proteomic analysis method used, only the most obvious of differences are identified; some of the nuances to the proteome of the acrosyringium could have been lost or masked. This being a key point for further investigation.

Furthermore, to conduct a more robust study, it is necessary to include wide biological variation. Samples from only four donors were used in this study due to the limited number of suitable samples within the local biobank.

Lastly, One aspect that has not been discussed in this thesis so far is the apoeccrine sweat gland (AESG), the supposed intermediate between the apocrine and eccrine sweat glands. Published literature that supports the presence of the AESG notes that it is not always present within samples (Sato, Leidal, and Sato 1987; Sato and Sato 1987; Sato et al. 1989a; van der Putte 1994) and can only be distinguished by its morphology. Specifically, it occurs in secretory regions that have the appearance of the apocrine gland but a luminal stricture connecting them directly to the skin (like the larger eccrine sweat gland) when compared to the other sweat glands. To date, no publication has identified any immunohistochemical stains that could be used to distinguish between the AESG and the eccrine sweat gland (Bechara 2008;

Noel et al. 2013). In this work, care was taken during the isolation of acrosyringium-positive samples. None of the isolated acrosyringia appeared to be as unusually large as implied by the description of apoeccrine. This would suggest that no AESG-gland acrosyringium was collected.

6.3 Future investigations

Future research to expand on the work presented in this thesis could be separated into two lines of enquiry:

6.3.1 Advancement of proteomic analysis of FFPE tissue

FFPE tissue represents a vast resource thanks to the number and variety of samples and the time over which they have been curated, with FFPE stores still continually being added to. Furthermore, they require no special conditions for storage (refrigeration), and in some cases, they reduce some of the biological risks associated with handling samples. Unfortunately, the current methods for proteomic analysis of FFPE tissue can be inefficient and inaccurate. This is due to limitations with the tissue available, as well as the variety and number of modifications to the protein caused by the fixation process. This thesis has taken a step toward optimising that process. Yet, further improvements could be made to the methodology and automation of the proteomic workflow, to enable proteomics to be used in conjunction with pathological investigation of tissue biopsies to diagnose conditions, e.g. identification of multiple biomarkers within an isolated tumour sample.

There are a number of directions in which proteomic analysis of FFPE could be further optimised. These include the incorporation of single-cell proteomic techniques with isobaric labelling methods such as tandem mass tags (TMT). TMT have the added benefit of enabling researchers to analyse and compare multiple samples in a single analytical run with the use of complex kits. Alternatively, different techniques such as data-independent acquisition can also be used, which has been shown to improve data for label-free quantification(Davalieva et al. 2021; Kim et al. 2019; Muller et al. 2019; Quesada-Calvo et al. 2015; Strzelecka, Holman,

and Eyers 2015; Wang et al. 2022). Following data acquisition, the data processing can then be optimised, such as by creating a library of tissue-specific proteins in the skin (in this case), and in doing so, reducing the search space. This makes it more efficient to increase the number of potential protein modifications. As indicated in Chapter 3.6, the use of open PTM searches is a useful tool when comparing samples from different sources as it aids in identifying different PTM (caused by variations in the generation and storage of FFPE tissue) to be taken into consideration. Further research into these tools and techniques will hopefully allow for more efficient and confident use of FFPE tissue, which will make it more feasible to use and also provide us with access to a greater number of samples or alternative ways of storing future samples.

6.3.2 Proteomic profile of acrosyringium

As indicated in Chapter 6.2, the investigation performed does not provide a fully encompassing proteomic profile of the acrosyringium but constitutes more of an initial investigation. The information obtained furthers our understanding of what is present within the acrosyringium, but a number of lines of enquiry still remain.

Gaining a more representative proteomic profile of the acrosyringium with regards to the population, accounting for variables such as the location on the body from which samples are isolated, along with the sex, age and ethnicity of the donor, would provide a basis for determining potential effects on the development and functionality of the eccrine sweat gland. Having a greater understanding of a healthy proteomic profile of the acrosyringium would allow for investigation and understanding of conditions' associated structures, such as for palmoplantar pustulosis and hyperhidrosis, as well as their potential treatment. An increased number of samples may also provide additional insights into and lessen the controversy around the identification of the AESG gland, or confirm that it is some variant of either the apocrine or eccrine gland, as well as how and why such variance may occur.

A further point of investigation is the luminal surface of the acrosyringium. In order to gain a greater understanding of how this interacts with its local environment, such as degraded tissue, bacteria, foreign bodies or sweat. Future studies may determine whether it is directly interacting with sweat and altering its composition, a process seen for the rest of the eccrine sweat gland.

Chapter: 7 References

Abbreviations, Clsp. calmodulin-like skin protein.

Adamus, J., L. Feng, S. Hawkins, K. Kalleberg, and J. M. Lee. 2017. 'Climbazole boosts activity of retinoids in skin', Int J Cosmet Sci, 39: 411-18.

Addis, M. F., A. Tanca, D. Pagnozzi, S. Crobu, G. Fanciulli, P. Cossu-Rocca, and S. Uzzau. 2009. 'Generation of high-quality protein extracts from formalin-fixed, paraffin-embedded tissues', Proteomics, 9: 3815-23.

Alkhas, A., B. L. Hood, K. Oliver, P. N. Teng, J. Oliver, D. Mitchell, C. A. Hamilton, G. L. Maxwell, and T. P. Conrads. 2011. 'Standardization of a sample preparation and analytical workflow for proteomics of archival endometrial cancer tissue', J Proteome Res, 10: 5264-71.

Alzayady, K. J., L. Wang, R. Chandrasekhar, L. E. Wagner, 2nd, F. Van Petegem, and D. I. Yule. 2016. 'Defining the stoichiometry of inositol 1,4,5-trisphosphate binding required to initiate Ca2+ release', Sci Signal, 9: ra35.

Anderson, D. W., R. C. Schray, G. Duester, and J. S. Schneider. 2011. 'Functional significance of aldehyde dehydrogenase ALDH1A1 to the nigrostriatal dopamine system', Brain Res, 1408: 81-7.

Aneichyk, T., W. T. Hendriks, R. Yadav, D. Shin, D. Gao, C. A. Vaine, R. L. Collins, A. Domingo, B. Currall, A. Stortchevoi, T. Multhaupt-Buell, E. B. Penney, L. Cruz, J. Dhakal, H. Brand, C. Hanscom, C. Antolik, M. Dy, A. Ragavendran, J. Underwood, S. Cantsilieris, K. M. Munson, E. E. Eichler, P. Acuna, C. Go, R. D. G. Jamora, R. L. Rosales, D. M. Church, S. R. Williams, S. Garcia, C. Klein, U. Muller, K. C. Wilhelmsen, H. T. M. Timmers, Y. Sapir, B. J. Wainger, D. Henderson, N. Ito, N. Weisenfeld, D. Jaffe, N. Sharma, X. O. Breakefield, L. J. Ozelius, D. C. Bragg, and M. E. Talkowski. 2018. 'Dissecting the Causal Mechanism of X-Linked Dystonia-Parkinsonism by Integrating Genome and Transcriptome Assembly', Cell, 172: 897-909 e21.

Azimi, A., K. L. Kaufman, M. Ali, S. Kossard, and P. Fernandez-Penas. 2016. 'In Silico Analysis Validates Proteomic Findings of Formalin-fixed Paraffin Embedded Cutaneous Squamous Cell Carcinoma Tissue', Cancer Genomics Proteomics, 13: 453-65.

Azimzadeh, O., Z. Barjaktarovic, M. Aubele, J. Calzada-Wack, H. Sarioglu, M. J. Atkinson, and S. Tapio. 2010. 'Formalin-fixed paraffin-embedded (FFPE) proteome analysis using gel-free and gel-based proteomics', J Proteome Res, 9: 4710-20.

Baker, L. B. 2019. 'Physiology of sweat gland function: The roles of sweating and sweat composition in human health', Temperature (Austin), 6: 211-59.

Baker, L. B., P. J. D. De Chavez, C. T. Ungaro, B. C. Sopena, R. P. Nuccio, A. J. Reimel, and K. A. Barnes. 2019. 'Exercise intensity effects on total sweat electrolyte losses and regional vs. whole-body sweat [Na(+)], [Cl(-)], and [K(+)]', Eur J Appl Physiol, 119: 361-75.

Bantscheff, M., S. Lemeer, M. M. Savitski, and B. Kuster. 2012. 'Quantitative mass spectrometry in proteomics: critical review update from 2007 to the present', Anal Bioanal Chem, 404: 939-65.

Bastian, B. C., U. van der Piepen, J. Romisch, E. P. Paques, and E. B. Brocker. 1993. 'Localization of annexins in normal and diseased human skin', J Dermatol Sci, 6: 225-34.
Baumann, M., C. T. Pham, and C. Benarafa. 2013. 'SerpinB1 is critical for neutrophil survival through cell-autonomous inhibition of cathepsin G', Blood, 121: 3900-7, S1-6.
Bayer, M., L. Angenendt, C. Schliemann, W. Hartmann, and S. Konig. 2019. 'Are formalin-fixed and paraffin-embedded tissues fit for proteomic analysis?', J Mass Spectrom.
Bechara, F. G. 2008. 'Do we have apoeccrine sweat glands?', Int J Cosmet Sci, 30: 67-8; author reply 69-71.
Best, S., C. Caillaud, and M. Thompson. 2012. 'The effect of ageing and fitness on thermoregulatory response to high-intensity exercise', Scand J Med Sci Sports, 22: e29-37.
Bhawan, J., K. Whren, I. Panova, and M. Yaar. 2005. 'Keratin 16 expression in epidermal melanocytes of normal human skin', Am J Dermatopathol, 27: 476-81.
———. 2010. 'Keratin 16 expression in epidermal melanocytes', Br J Dermatol, 162: 218; author reply 18-9.
Biedermann, T., L. Pontiggia, S. Bottcher-Haberzeth, S. Tharakan, E. Braziulis, C. Schiestl, M. Meuli, and E. Reichmann. 2010. 'Human eccrine sweat gland cells can reconstitute a stratified epidermis', J Invest Dermatol, 130: 1996-2009.
Boughton, A. J., L. Liu, T. Lavy, O. Kleifeld, and D. Fushman. 2021. 'A novel recognition site for polyubiquitin and ubiquitin-like signals in an unexpected region of proteasomal subunit Rpn1', J Biol Chem, 297: 101052.
Bovell, Douglas. 2015. 'The human eccrine sweat gland: Structure, function and disorders', Journal of Local and Global Health Science, 2015.
Bowden, P. E. 2010. 'Mutations in a keratin 6 isomer (K6c) cause a type of focal palmoplantar keratoderma', J Invest Dermatol, 130: 336-8.
Brenner, C., K. Subramaniam, C. Pertuiset, and S. Pervaiz. 2011. 'Adenine nucleotide translocase family: four isoforms for apoptosis modulation in cancer', Oncogene, 30: 883-95.
Brosin, A., V. Wolf, A. Mattheus, and H. Heise. 1997. 'Use of XTT-assay to assess the cytotoxicity of different surfactants and metal salts in human keratinocytes (HaCaT). A feasible method for in vitro testing of skin irritants', Acta Derm Venereol, 77: 26-8.
Burat, B., A. Reynaerts, D. Baiwir, M. Fleron, G. Eppe, T. Leal, and G. Mazzucchelli. 2021. 'Characterization of the Human Eccrine Sweat Proteome-A Focus on the Biological Variability of Individual Sweat Protein Profiles', Int J Mol Sci, 22.
Chen, S., H. G. Evans, and D. R. Evans. 2011. 'FAM129B/MINERVA, a novel adherens junction-associated protein, suppresses apoptosis in HeLa cells', J Biol Chem, 286: 10201-9.
Chinese Human Liver Proteome Profiling, Consortium. 2010. 'First insight into the human liver proteome from PROTEOME(SKY)-LIVER(Hu) 1.0, a publicly available database', J Proteome Res, 9: 79-94.

Choi, Y. J., S. Kim, Y. Choi, T. B. Nielsen, J. Yan, A. Lu, J. Ruan, H. R. Lee, H. Wu, B. Spellberg, and J. U. Jung. 2019a. 'Publisher Correction: SERPINB1-mediated checkpoint of inflammatory caspase activation', Nat Immunol, 20: 664.
———. 2019b. 'SERPINB1-mediated checkpoint of inflammatory caspase activation', Nat Immunol, 20: 276-87.
Christophers, E., and G. Plewig. 1973. 'Formation of the acrosyringium', Arch Dermatol, 107: 378-82.
Cirino, G., R. J. Flower, J. L. Browning, L. K. Sinclair, and R. B. Pepinsky. 1987. 'Recombinant human lipocortin 1 inhibits thromboxane release from guinea-pig isolated perfused lung', Nature, 328: 270-2.
Clausen, M. V., F. Hilbers, and H. Poulsen. 2017. 'The Structure and Function of the Na,K-ATPase Isoforms in Health and Disease', Front Physiol, 8: 371.
Cloix, J. F., O. Colard, B. Rothhut, and F. Russo-Marie. 1983. 'Characterization and partial purification of 'renocortins': two polypeptides formed in renal cells causing the anti-phospholipase-like action of glucocorticoids', Br J Pharmacol, 79: 313-21.
Collins, C. A., and F. M. Watt. 2008. 'Dynamic regulation of retinoic acid-binding proteins in developing, adult and neoplastic skin reveals roles for beta-catenin and Notch signalling', Dev Biol, 324: 55-67.
Concepcion, A. R., M. Vaeth, L. E. Wagner, 2nd, M. Eckstein, L. Hecht, J. Yang, D. Crottes, M. Seidl, H. P. Shin, C. Weidinger, S. Cameron, S. E. Turvey, T. Issekutz, I. Meyts, R. S. Lacruz, M. Cuk, D. I. Yule, and S. Feske. 2016. 'Store-operated Ca2+ entry regulates Ca2+-activated chloride channels and eccrine sweat gland function', J Clin Invest, 126: 4303-18.
Cristante, E., S. McArthur, C. Mauro, E. Maggioli, I. A. Romero, M. Wylezinska-Arridge, P. O. Couraud, J. Lopez-Tremoleda, H. C. Christian, B. B. Weksler, A. Malaspina, and E. Solito. 2013. 'Identification of an essential endogenous regulator of blood-brain barrier integrity, and its pathological and therapeutic implications', Proc Natl Acad Sci U S A, 110: 832-41.
Cui, C. Y., and D. Schlessinger. 2015. 'Eccrine sweat gland development and sweat secretion', Exp Dermatol, 24: 644-50.
Cui, C. Y., J. Sima, M. Yin, M. Michel, M. Kunisada, and D. Schlessinger. 2016. 'Identification of potassium and chloride channels in eccrine sweat glands', J Dermatol Sci, 81: 129-31.
Cui, J., G. Li, J. Yin, L. Li, Y. Tan, H. Wei, B. Liu, L. Deng, J. Tang, Y. Chen, and L. Yi. 2020. 'GSTP1 and cancer: Expression, methylation, polymorphisms and signaling (Review)', Int J Oncol, 56: 867-78.
Dalli, J., T. Montero-Melendez, S. McArthur, and M. Perretti. 2012. 'Annexin A1 N-terminal derived Peptide ac2-26 exerts chemokinetic effects on human neutrophils', Front Pharmacol, 3: 28.
Davalieva, K., S. Kiprijanovska, A. Dimovski, G. Rosoklija, and A. J. Dwork. 2021. 'Comparative evaluation of two methods for LC-MS/MS proteomic analysis of formalin fixed and paraffin embedded tissues', J Proteomics, 235: 104117.
De Simoni, S., D. Linard, E. Hermans, B. Knoops, and J. Goemaere. 2013. 'Mitochondrial peroxiredoxin-5 as potential modulator of mitochondria-ER crosstalk in MPP+-induced cell death', J Neurochem, 125: 473-85.

Dennis, S. C., and T. D. Noakes. 1999. 'Advantages of a smaller bodymass in humans when distance-running in warm, humid conditions', Eur J Appl Physiol Occup Physiol, 79: 280-4.
Deyrieux, A. F., and V. G. Wilson. 2007. 'In vitro culture conditions to study keratinocyte differentiation using the HaCaT cell line', Cytotechnology, 54: 77-83.
Diao, J., J. Liu, S. Wang, M. Chang, X. Wang, B. Guo, Q. Yu, F. Yan, Y. Su, and Y. Wang. 2019. 'Sweat gland organoids contribute to cutaneous wound healing and sweat gland regeneration', Cell Death Dis, 10: 238.
Ding, J., J. Xu, Q. Deng, W. Ma, R. Zhang, X. He, S. Liu, and L. Zhang. 2021. 'Knockdown of Oligosaccharyltransferase Subunit Ribophorin 1 Induces Endoplasmic-Reticulum-Stress-Dependent Cell Apoptosis in Breast Cancer', Front Oncol, 11: 722624.
Effantin, G., R. Rosenzweig, M. H. Glickman, and A. C. Steven. 2009. 'Electron microscopic evidence in support of alpha-solenoid models of proteasomal subunits Rpn1 and Rpn2', J Mol Biol, 386: 1204-11.
El Ouaamari, A., E. Dirice, N. Gedeon, J. Hu, J. Y. Zhou, J. Shirakawa, L. Hou, J. Goodman, C. Karampelias, G. Qiang, J. Boucher, R. Martinez, M. A. Gritsenko, D. F. De Jesus, S. Kahraman, S. Bhatt, R. D. Smith, H. D. Beer, P. Jungtrakoon, Y. Gong, A. B. Goldfine, C. W. Liew, A. Doria, O. Andersson, W. J. Qian, E. Remold-O'Donnell, and R. N. Kulkarni. 2016. 'SerpinB1 Promotes Pancreatic beta Cell Proliferation', Cell Metab, 23: 194-205.
Elst, J., M. M. van der Poorten, A. L. Van Gasse, C. Mertens, M. M. Hagendorens, D. G. Ebo, and V. Sabato. 2022. 'Tryptase release does not discriminate between IgE- and MRGPRX2-mediated activation in human mast cells', Clin Exp Allergy.
Ersch, J., and T. Stallmach. 1999. 'Assessing gestational age from histology of fetal skin: an autopsy study of 379 fetuses', Obstet Gynecol, 94: 753-7.
Euzger, H. S., R. J. Flower, N. J. Goulding, and M. Perretti. 1999. 'Differential modulation of annexin I binding sites on monocytes and neutrophils', Mediators Inflamm, 8: 53-62.
Everts, H. B., J. P. Sundberg, L. E. King, Jr., and D. E. Ong. 2007. 'Immunolocalization of enzymes, binding proteins, and receptors sufficient for retinoic acid synthesis and signaling during the hair cycle', J Invest Dermatol, 127: 1593-604.
Fano, G., S. Biocca, S. Fulle, M. A. Mariggio, S. Belia, and P. Calissano. 1995. 'The S-100: a protein family in search of a function', Prog Neurobiol, 46: 71-82.
Feldman, Y., A. Puzenko, P. Ben Ishai, A. Caduff, I. Davidovich, F. Sakran, and A. J. Agranat. 2009. 'The electromagnetic response of human skin in the millimetre and submillimetre wave range', Phys Med Biol, 54: 3341-63.
Feng, X., M. Zhang, B. Wang, C. Zhou, Y. Mu, J. Li, X. Liu, Y. Wang, Z. Song, and P. Liu. 2019. 'CRABP2 regulates invasion and metastasis of breast cancer through hippo pathway dependent on ER status', J Exp Clin Cancer Res, 38: 361.
Fenn, J. B., M. Mann, C. K. Meng, S. F. Wong, and C. M. Whitehouse. 1989. 'Electrospray ionization for mass spectrometry of large biomolecules', Science, 246: 64-71.

Foll, M. C., M. Fahrner, V. O. Oria, M. Kuhs, M. L. Biniossek, M. Werner, P. Bronsert, and O. Schilling. 2018. 'Reproducible proteomics sample preparation for single FFPE tissue slices using acid-labile surfactant and direct trypsinization', Clin Proteomics, 15: 11.

Fox, C. H., F. B. Johnson, J. Whiting, and P. P. Roller. 1985. 'Formaldehyde fixation', J Histochem Cytochem, 33: 845-53.

Frungieri, M. B., S. Weidinger, V. Meineke, F. M. Kohn, and A. Mayerhofer. 2002. 'Proliferative action of mast-cell tryptase is mediated by PAR2, COX2, prostaglandins, and PPARgamma : Possible relevance to human fibrotic disorders', Proc Natl Acad Sci U S A, 99: 15072-7.

Gagnon, D., and C. G. Crandall. 2018. 'Sweating as a heat loss thermoeffector', Handb Clin Neurol, 156: 211-32.

Gagnon, D., and G. P. Kenny. 2012. 'Sex differences in thermoeffector responses during exercise at fixed requirements for heat loss', J Appl Physiol (1985), 113: 746-57.

Gibbons, C. H., B. M. Illigens, N. Wang, and R. Freeman. 2009. 'Quantification of sweat gland innervation: a clinical-pathologic correlation', Neurology, 72: 1479-86.

Girol, A. P., K. K. Mimura, C. C. Drewes, S. M. Bolonheis, E. Solito, S. H. Farsky, C. D. Gil, and S. M. Oliani. 2013. 'Anti-inflammatory mechanisms of the annexin A1 protein and its mimetic peptide Ac2-26 in models of ocular inflammation in vivo and in vitro', J Immunol, 190: 5689-701.

Giusti, L., and A. Lucacchini. 2013. 'Proteomic studies of formalin-fixed paraffin-embedded tissues', Expert Rev Proteomics, 10: 165-77.

Gondalia, R., C. L. Avery, M. D. Napier, R. Mendez-Giraldez, J. D. Stewart, C. M. Sitlani, Y. Li, K. C. Wilhelmsen, Q. Duan, J. Roach, K. E. North, A. P. Reiner, Z. M. Zhang, L. F. Tinker, J. D. Yanosky, D. Liao, and E. A. Whitsel. 2017. 'Genome-wide Association Study of Susceptibility to Particulate Matter-Associated QT Prolongation', Environ Health Perspect, 125: 067002.

Greenwell, A., J. F. Foley, and R. R. Maronpot. 1991. 'An enhancement method for immunohistochemical staining of proliferating cell nuclear antigen in archival rodent tissues', Cancer Lett, 59: 251-6.

Gu, N., W. Dai, H. Liu, J. Ge, S. Luo, E. Cho, C. I. Amos, J. E. Lee, X. Li, H. Nan, H. Yuan, and Q. Wei. 2020. 'Genetic variants in TKT and DERA in the nicotinamide adenine dinucleotide phosphate pathway predict melanoma survival', Eur J Cancer, 136: 84-94.

Gustafsson, O. J., G. Arentz, and P. Hoffmann. 2015. 'Proteomic developments in the analysis of formalin-fixed tissue', Biochim Biophys Acta, 1854: 559-80.

Hagforsen, E., H. Hedstrand, F. Nyberg, and G. Michaelsson. 2010. 'Novel findings of Langerhans cells and interleukin-17 expression in relation to the acrosyringium and pustule in palmoplantar pustulosis', Br J Dermatol, 163: 572-9.

Hagforsen, E., G. Michaelsson, and M. Stridsberg. 2011. 'Somatostatin receptors are strongly expressed in palmoplantar sweat glands and ducts: studies of normal and palmoplantar pustulosis skin', Clin Exp Dermatol, 36: 521-7.

Han, H. 2018. 'RNA Interference to Knock Down Gene Expression', Methods Mol Biol, 1706: 293-302.

Hayut, I., P. Ben Ishai, A. J. Agranat, and Y. Feldman. 2014. 'Circular polarization induced by the three-dimensional chiral structure of human sweat ducts', Phys Rev E Stat Nonlin Soft Matter Phys, 89: 042715.
He, Y., B. G. Kim, H. E. Kim, Q. Sun, S. Shi, G. Ma, Y. Kim, O. S. Kim, and O. J. Kim. 2019. 'The Protective Role of Feruloylserotonin in LPS-Induced HaCaT Cells', Molecules, 24.
Hernandez-Hernandez, L., C. Sanz, V. Garcia-Solaesa, J. Padron, A. Garcia-Sanchez, I. Davila, M. Isidoro-Garcia, and F. Lorente. 2012. 'Tryptase: genetic and functional considerations', Allergol Immunopathol (Madr), 40: 385-9.
Hibbert, S. A., M. Ozols, C. E. M. Griffiths, R. E. B. Watson, M. Bell, and M. J. Sherratt. 2018. 'Defining tissue proteomes by systematic literature review', Sci Rep, 8: 546.
Hibbs, R. G. 1958. 'The fine structure of human eccrine sweat glands', Am J Anat, 103: 201-17.
———. 1962. 'Electron microscopy of human apocrine sweat glands', J Invest Dermatol, 38: 77-84.
Hodge, K., S. T. Have, L. Hutton, and A. I. Lamond. 2013. 'Cleaning up the masses: exclusion lists to reduce contamination with HPLC-MS/MS', J Proteomics, 88: 92-103.
Horie, N., H. Yokozeki, and K. Sato. 1986. 'Proteolytic enzymes in human eccrine sweat: a screening study', Am J Physiol, 250: R691-8.
Hu, Y., C. Converse, M. C. Lyons, and W. H. Hsu. 2018. 'Neural control of sweat secretion: a review', Br J Dermatol, 178: 1246-56.
Huang, J. J., C. J. Xia, Y. Wei, Y. Yao, M. W. Dong, K. Z. Lin, L. S. Yu, Y. Gao, and Y. Y. Fan. 2020. 'Annexin A1-derived peptide Ac2-26 facilitates wound healing in diabetic mice', Wound Repair Regen, 28: 772-79.
Hussain, J. N., N. Mantri, and M. M. Cohen. 2017. 'Working Up a Good Sweat - The Challenges of Standardising Sweat Collection for Metabolomics Analysis', Clin Biochem Rev, 38: 13-34.
Ikeda, K., T. Monden, T. Kanoh, M. Tsujie, H. Izawa, A. Haba, T. Ohnishi, M. Sekimoto, N. Tomita, H. Shiozaki, and M. Monden. 1998. 'Extraction and analysis of diagnostically useful proteins from formalin-fixed, paraffin-embedded tissue sections', J Histochem Cytochem, 46: 397-403.
Jacob, J. T., P. A. Coulombe, R. Kwan, and M. B. Omary. 2018. 'Types I and II Keratin Intermediate Filaments', Cold Spring Harb Perspect Biol, 10.
Judd, A. M., D. B. Gutierrez, J. L. Moore, N. H. Patterson, J. Yang, C. E. Romer, J. L. Norris, and R. M. Caprioli. 2019. 'A recommended and verified procedure for in situ tryptic digestion of formalin-fixed paraffin-embedded tissues for analysis by matrix-assisted laser desorption/ionization imaging mass spectrometry', J Mass Spectrom, 54: 716-27.
Kahle, K. T., J. Rinehart, and R. P. Lifton. 2010. 'Phosphoregulation of the Na-K-2Cl and K-Cl cotransporters by the WNK kinases', Biochim Biophys Acta, 1802: 1150-8.
Kenney, W. L. 1997. 'Thermoregulation at rest and during exercise in healthy older adults', Exerc Sport Sci Rev, 25: 41-76.
Kim, Y. J., S. M. M. Sweet, J. D. Egertson, A. J. Sedgewick, S. Woo, W. L. Liao, G. E. Merrihew, B. C. Searle, C. Vaske, R. Heaton, M. J. MacCoss, and T.

Hembrough. 2019. 'Data-Independent Acquisition Mass Spectrometry To Quantify Protein Levels in FFPE Tumor Biopsies for Molecular Diagnostics', J Proteome Res, 18: 426-35.
Kitazawa, S., Y. Takaoka, Y. Ueda, and R. Kitazawa. 2021. 'Identification of calmodulin-like protein 5 as tumor-suppressor gene silenced during early stage of carcinogenesis in squamous cell carcinoma of uterine cervix', Int J Cancer, 149: 1358-68.
Kochetov, G. A., and O. N. Solovjeva. 2014. 'Structure and functioning mechanism of transketolase', Biochim Biophys Acta, 1844: 1608-18.
Kondo, R., K. Ishino, R. Wada, H. Takata, W. X. Peng, M. Kudo, S. Kure, Y. Kaneya, N. Taniai, H. Yoshida, and Z. Naito. 2019. 'Downregulation of protein disulfideisomerase A3 expression inhibits cell proliferation and induces apoptosis through STAT3 signaling in hepatocellular carcinoma', Int J Oncol, 54: 1409-21.
Kreft, S., A. R. Klatt, J. Strassburger, E. Poschl, R. J. Flower, S. Eming, C. Reutelingsperger, A. Brisson, and B. Brachvogel. 2016. 'Skin Wound Repair Is Not Altered in the Absence of Endogenous AnxA1 or AnxA5, but Pharmacological Concentrations of AnxA4 and AnxA5 Inhibit Wound Hemostasis', Cells Tissues Organs, 201: 287-98.
Kudlak, M., and P. Tadi. 2021. 'Physiology, Muscarinic Receptor.' in, StatPearls (Treasure Island (FL)).
Kunitomi, H., Y. Kobayashi, R. C. Wu, T. Takeda, E. Tominaga, K. Banno, and D. Aoki. 2020. 'LAMC1 is a prognostic factor and a potential therapeutic target in endometrial cancer', J Gynecol Oncol, 31: e11.
Langbein, L., M. A. Rogers, S. Praetzel, B. Cribier, B. Peltre, N. Gassler, and J. Schweizer. 2005. 'Characterization of a novel human type II epithelial keratin K1b, specifically expressed in eccrine sweat glands', J Invest Dermatol, 125: 428-44.
Lee, C. H., M. J. Kim, H. H. Lee, J. C. Paeng, Y. J. Park, S. W. Oh, Y. J. Chai, Y. A. Kim, G. J. Cheon, K. W. Kang, H. Youn, and J. K. Chung. 2019. 'Adenine Nucleotide Translocase 2 as an Enzyme Related to [(18)F] FDG Accumulation in Various Cancers', Mol Imaging Biol, 21: 722-30.
Leoni, G., P. A. Neumann, N. Kamaly, M. Quiros, H. Nishio, H. R. Jones, R. Sumagin, R. S. Hilgarth, A. Alam, G. Fredman, I. Argyris, E. Rijcken, D. Kusters, C. Reutelingsperger, M. Perretti, C. A. Parkos, O. C. Farokhzad, A. S. Neish, and A. Nusrat. 2015. 'Annexin A1-containing extracellular vesicles and polymeric nanoparticles promote epithelial wound repair', J Clin Invest, 125: 1215-27.
Li, H. H., G. Zhou, X. B. Fu, and L. Zhang. 2009. 'Antigen expression of human eccrine sweat glands', J Cutan Pathol, 36: 318-24.
Li, J., G. Z. Yang, H. Jin, and H. Y. Ding. 2012. '[Pathologic diagnosis and differential diagnosis of low-grade adenosquamous carcinoma of breast and syringomatous adenoma of nipple]', Zhonghua Bing Li Xue Za Zhi, 41: 301-4.
Liu, J., D. Liu, Z. Yang, and Z. Yang. 2019. 'High LAMC1 expression in glioma is associated with poor prognosis', Onco Targets Ther, 12: 4253-60.
Lobitz, W. C., Jr., J. B. Holyoke, and W. Montagna. 1954. 'Responses of the human eccrine sweat duct to controlled injury: growth center of the epidermal sweat duct unit', J Invest Dermatol, 23: 329-44.

Longuespee, R., D. Alberts, C. Pottier, N. Smargiasso, G. Mazzucchelli, D. Baiwir, M. Kriegsmann, M. Herfs, J. Kriegsmann, P. Delvenne, and E. De Pauw. 2016. 'A laser microdissection-based workflow for FFPE tissue microproteomics: Important considerations for small sample processing', Methods, 104: 154-62.

Lu, C., and E. Fuchs. 2014. 'Sweat gland progenitors in development, homeostasis, and wound repair', Cold Spring Harb Perspect Med, 4.

Lu, C. P., L. Polak, A. S. Rocha, H. A. Pasolli, S. C. Chen, N. Sharma, C. Blanpain, and E. Fuchs. 2012. 'Identification of stem cell populations in sweat glands and ducts reveals roles in homeostasis and wound repair', Cell, 150: 136-50.

Luebker, S. A., and S. A. Koepsell. 2016. 'Optimization of Urea Based Protein Extraction from Formalin-Fixed Paraffin-Embedded Tissue for Shotgun Proteomics', Int J Proteomics, 2016: 4324987.

Mahmood, F., R. Xu, M. U. N. Awan, Y. Song, Q. Han, X. Xia, and J. Zhang. 2021. 'PDIA3: Structure, functions and its potential role in viral infections', Biomed Pharmacother, 143: 112110.

Makarov, A. 2000. 'Electrostatic axially harmonic orbital trapping: a high-performance technique of mass analysis', Anal Chem, 72: 1156-62.

Marchione, D. M., I. Ilieva, K. Devins, D. Sharpe, D. J. Pappin, B. A. Garcia, J. P. Wilson, and J. B. Wojcik. 2020. 'HYPERsol: High-Quality Data from Archival FFPE Tissue for Clinical Proteomics', J Proteome Res, 19: 973-83.

Marino, F. E., Z. Mbambo, E. Kortekaas, G. Wilson, M. I. Lambert, T. D. Noakes, and S. C. Dennis. 2000. 'Advantages of smaller body mass during distance running in warm, humid environments', Pflugers Arch, 441: 359-67.

McGregor, J. M., J. N. Barker, M. H. Allen, and D. M. MacDonald. 1991. 'Antigenic profile of human acrosyringium', Br J Dermatol, 125: 413-8.

Mehul, B., D. Bernard, L. Simonetti, M. A. Bernard, and R. Schmidt. 2000. 'Identification and cloning of a new calmodulin-like protein from human epidermis', J Biol Chem, 275: 12841-7.

Metz, B., G. F. Kersten, P. Hoogerhout, H. F. Brugghe, H. A. Timmermans, A. de Jong, H. Meiring, J. ten Hove, W. E. Hennink, D. J. Crommelin, and W. Jiskoot. 2004. 'Identification of formaldehyde-induced modifications in proteins: reactions with model peptides', J Biol Chem, 279: 6235-43.

Metzler-Wilson, K., and T. E. Wilson. 2016. 'Impact of calcium regulation on eccrine sweating and sweating disorders: the view from cells to glands to intact human skin', Exp Physiol, 101: 345-6.

Migocka-Patrzalek, M., and M. Elias. 2021. 'Muscle Glycogen Phosphorylase and Its Functional Partners in Health and Disease', Cells, 10.

Moll, I., and R. Moll. 1992. 'Changes of expression of intermediate filament proteins during ontogenesis of eccrine sweat glands', J Invest Dermatol, 98: 777-85.

Montagna W, Parakkal PF. 1974. 'The structure and function of skin.' in Parakkal PF (ed.), The structure and function of skin (Academic Press, Inc: New York (NY)).

Montain, S. J., S. N. Cheuvront, and H. C. Lukaski. 2007. 'Sweat mineral-element responses during 7 h of exercise-heat stress', Int J Sport Nutr Exerc Metab, 17: 574-82.

Montgomery, I., D. M. Jenkinson, H. Y. Elder, D. Czarnecki, and R. M. MacKie. 1985. 'The effects of thermal stimulation on the ultrastructure of the human atrichial sweat gland. II. The duct', Br J Dermatol, 112: 165-77.
Morgan, R. O., D. W. Bell, J. R. Testa, and M. P. Fernandez. 1999. 'Human annexin 31 genetic mapping and origin', Gene, 227: 33-8.
Muller, F., L. Kolbowski, O. M. Bernhardt, L. Reiter, and J. Rappsilber. 2019. 'Data-independent Acquisition Improves Quantitative Cross-linking Mass Spectrometry', Mol Cell Proteomics, 18: 786-95.
Murakami, M., T. Ohtake, R. A. Dorschner, B. Schittek, C. Garbe, and R. L. Gallo. 2002. 'Cathelicidin anti-microbial peptide expression in sweat, an innate defense system for the skin', J Invest Dermatol, 119: 1090-5.
Murakami, M., T. Ohtake, Y. Horibe, A. Ishida-Yamamoto, V. B. Morhenn, R. L. Gallo, and H. Iizuka. 2010. 'Acrosyringium is the main site of the vesicle/pustule formation in palmoplantar pustulosis', J Invest Dermatol, 130: 2010-6.
Murphrey, M. B., A. O. Safadi, and T. Vaidya. 2020. 'Histology, Apocrine Gland.' in, StatPearls (Treasure Island (FL)).
Na, C. H., N. Sharma, A. K. Madugundu, R. Chen, M. Atalar Aksit, G. D. Rosson, G. R. Cutting, and A. Pandey. 2019. 'Integrated transcriptomic and proteomic analysis of human eccrine sweat glands identifies missing and novel proteins', Mol Cell Proteomics.
Niedecken, H. W., E. Biwer, R. Bauer, and H. W. Kreysel. 1990. '[Acrosyringium and follicular infundibulum: immunomorphologic aspects]', Z Hautkr, 65: 578-81.
Nirmalan, N. J., C. Hughes, J. Peng, T. McKenna, J. Langridge, D. A. Cairns, P. Harnden, P. J. Selby, and R. E. Banks. 2011. 'Initial development and validation of a novel extraction method for quantitative mining of the formalin-fixed, paraffin-embedded tissue proteome for biomarker investigations', J Proteome Res, 10: 896-906.
Noel, F., G. E. Pierard, P. Delvenne, P. Quatresooz, P. Humbert, and C. Pierard-Franchimont. 2013. 'Immunohistochemical sweat gland profiles', J Cosmet Dermatol, 12: 179-86.
O'Rourke, M. B., and M. P. Padula. 2016. 'Analysis of formalin-fixed, paraffin-embedded (FFPE) tissue via proteomic techniques and misconceptions of antigen retrieval', Biotechniques, 60: 229-38.
Olsen, J. V., B. Macek, O. Lange, A. Makarov, S. Horning, and M. Mann. 2007. 'Higher-energy C-trap dissociation for peptide modification analysis', Nat Methods, 4: 709-12.
Ostasiewicz, P., and J. R. Wisniewski. 2017. 'A Protocol for Large-Scale Proteomic Analysis of Microdissected Formalin Fixed and Paraffin Embedded Tissue', Methods Enzymol, 585: 159-76.
Ostasiewicz, P., D. F. Zielinska, M. Mann, and J. R. Wisniewski. 2010. 'Proteome, phosphoproteome, and N-glycoproteome are quantitatively preserved in formalin-fixed paraffin-embedded tissue and analyzable by high-resolution mass spectrometry', J Proteome Res, 9: 3688-700.
Ovaere, P., S. Lippens, P. Vandenabeele, and W. Declercq. 2009. 'The emerging roles of serine protease cascades in the epidermis', Trends Biochem Sci, 34: 453-63.

Padmanabhan, B., T. Kuzuhara, N. Adachi, and M. Horikoshi. 2004. 'The crystal structure of CCG1/TAF(II)250-interacting factor B (CIB)', J Biol Chem, 279: 9615-24.
Parente, L., and E. Solito. 2004. 'Annexin 1: more than an anti-phospholipase protein', Inflamm Res, 53: 125-32.
Park, J. H., G. T. Park, I. H. Cho, S. M. Sim, J. M. Yang, and D. Y. Lee. 2011. 'An antimicrobial protein, lactoferrin exists in the sweat: proteomic analysis of sweat', Exp Dermatol, 20: 369-71.
Patel, S. J., G. L. Trivedi, C. C. Darie, and B. D. Clarkson. 2017. 'The possible roles of B-cell novel protein-1 (BCNP1) in cellular signalling pathways and in cancer', J Cell Mol Med, 21: 456-66.
Payne, V., and P. C. Kam. 2004. 'Mast cell tryptase: a review of its physiology and clinical significance', Anaesthesia, 59: 695-703.
Perkins, D. N., D. J. Pappin, D. M. Creasy, and J. S. Cottrell. 1999. 'Probability-based protein identification by searching sequence databases using mass spectrometry data', Electrophoresis, 20: 3551-67.
Pessina, A., A. Raimondi, A. Cerri, M. Piccirillo, M. G. Neri, C. Croera, P. Foti, and E. Berti. 2001. 'High sensitivity of human epidermal keratinocytes (HaCaT) to topoisomerase inhibitors', Cell Prolif, 34: 243-52.
Pirahanchi, Y., R. Jessu, and N. R. Aeddula. 2022. 'Physiology, Sodium Potassium Pump.' in, StatPearls (Treasure Island (FL)).
Pontisso, P. 2014. 'Role of SERPINB3 in hepatocellular carcinoma', Ann Hepatol, 13: 722-7.
Prakriya, M., and R. S. Lewis. 2015. 'Store-Operated Calcium Channels', Physiol Rev, 95: 1383-436.
Prost-Squarcioni, C. 2006. '[Histology of skin and hair follicle]', Med Sci (Paris), 22: 131-7.
Puchtler, H., and S. N. Meloan. 1985. 'On the chemistry of formaldehyde fixation and its effects on immunohistochemical reactions', Histochemistry, 82: 201-4.
Purvis, G. S. D., E. Solito, and C. Thiemermann. 2019. 'Annexin-A1: Therapeutic Potential in Microvascular Disease', Front Immunol, 10: 938.
Quarta, S., L. Vidalino, C. Turato, M. Ruvoletto, F. Calabrese, M. Valente, S. Cannito, G. Fassina, M. Parola, A. Gatta, and P. Pontisso. 2010. 'SERPINB3 induces epithelial-mesenchymal transition', J Pathol, 221: 343-56.
Quesada-Calvo, F., V. Bertrand, R. Longuespee, A. Delga, G. Mazzucchelli, N. Smargiasso, D. Baiwir, P. Delvenne, M. Malaise, M. C. De Pauw-Gillet, E. De Pauw, E. Louis, and M. A. Meuwis. 2015. 'Comparison of two FFPE preparation methods using label-free shotgun proteomics: Application to tissues of diverticulitis patients', J Proteomics, 112: 250-61.
Raiszadeh, M. M., M. M. Ross, P. S. Russo, M. A. Schaepper, W. Zhou, J. Deng, D. Ng, A. Dickson, C. Dickson, M. Strom, C. Osorio, T. Soeprono, J. D. Wulfkuhle, E. F. Petricoin, L. A. Liotta, and W. M. Kirsch. 2012. 'Proteomic analysis of eccrine sweat: implications for the discovery of schizophrenia biomarker proteins', J Proteome Res, 11: 2127-39.

Rajendran, A., K. Vaidya, J. Mendoza, J. Bridwell-Rabb, and S. S. Kamat. 2020. 'Functional Annotation of ABHD14B, an Orphan Serine Hydrolase Enzyme', Biochemistry, 59: 183-96.
Reddy, M. M., and P. M. Quinton. 1994. 'Rapid regulation of electrolyte absorption in sweat duct', J Membr Biol, 140: 57-67.
Rehman, A., Y. Cai, C. Hunefeld, H. Jedlickova, Y. Huang, M. Teck Teh, U. Sharif Ahmad, J. Uttagomol, Y. Wang, A. Kang, G. Warnes, C. Harwood, D. Bergamaschi, E. Kenneth Parkinson, M. Rocken, and H. Wan. 2019. 'The desmosomal cadherin desmoglein-3 acts as a keratinocyte anti-stress protein via suppression of p53', Cell Death Dis, 10: 750.
Reichel, F. F., D. L. Dauletbekov, R. Klein, T. Peters, G. A. Ochakovski, I. P. Seitz, B. Wilhelm, M. Ueffing, M. Biel, B. Wissinger, S. Michalakis, K. U. Bartz-Schmidt, M. D. Fischer, and Rd-Cure Consortium. 2017. 'AAV8 Can Induce Innate and Adaptive Immune Response in the Primate Eye', Mol Ther, 25: 2648-60.
Rittie, L., D. L. Sachs, J. S. Orringer, J. J. Voorhees, and G. J. Fisher. 2013. 'Eccrine sweat glands are major contributors to reepithelialization of human wounds', Am J Pathol, 182: 163-71.
Robinson, S., S. D. Gerking, E. S. Turrell, and R. K. Kincaid. 1950. 'Effect of skin temperature on salt concentration of sweat', J Appl Physiol, 2: 654-62.
Rusanov, A. L., D. D. Romashin, V. G. Zgoda, T. V. Butkova, and N. G. Luzgina. 2021. 'Protein dataset of immortalized keratinocyte HaCaT cells and normal human keratinocytes', Data Brief, 35: 106871.
Saga, K. 2001. 'Histochemical and immunohistochemical markers for human eccrine and apocrine sweat glands: an aid for histopathologic differentiation of sweat gland tumors', J Investig Dermatol Symp Proc, 6: 49-53.
Sakaguchi, M., and N. H. Huh. 2011. 'S100A11, a dual growth regulator of epidermal keratinocytes', Amino Acids, 41: 797-807.
Sato, K. 1977. 'The physiology, pharmacology, and biochemistry of the eccrine sweat gland', Rev Physiol Biochem Pharmacol, 79: 51-131.
Sato, K., W. H. Kang, K. Saga, and K. T. Sato. 1989a. 'Biology of sweat glands and their disorders. I. Normal sweat gland function', J Am Acad Dermatol, 20: 537-63.
———. 1989b. 'Biology of sweat glands and their disorders. II. Disorders of sweat gland function', J Am Acad Dermatol, 20: 713-26.
Sato, K., R. Leidal, and F. Sato. 1987. 'Morphology and development of an apoeccrine sweat gland in human axillae', Am J Physiol, 252: R166-80.
Sato, K., and F. Sato. 1987. 'Sweat secretion by human axillary apoeccrine sweat gland in vitro', Am J Physiol, 252: R181-7.
Scheltema, R. A., J. P. Hauschild, O. Lange, D. Hornburg, E. Denisov, E. Damoc, A. Kuehn, A. Makarov, and M. Mann. 2014. 'The Q Exactive HF, a Benchtop mass spectrometer with a pre-filter, high-performance quadrupole and an ultra-high-field Orbitrap analyzer', Mol Cell Proteomics, 13: 3698-708.
Schwartz, A., R. J. Adams, W. J. Ball, Jr., J. H. Collins, S. S. Gupte, L. K. Lane, A. S. Reeves, and E. T. Wallick. 1980. 'Structure, function and regulation of Na-K-ATPase', Int J Biochem, 12: 287-93.
Scicchitano, M. S., D. A. Dalmas, R. W. Boyce, H. C. Thomas, and K. S. Frazier. 2009. 'Protein extraction of formalin-fixed, paraffin-embedded tissue enables

robust proteomic profiles by mass spectrometry', J Histochem Cytochem, 57: 849-60.
Sekiguchi, T., T. Miyata, and T. Nishimoto. 1988. 'Molecular cloning of the cDNA of human X chromosomal gene (CCG1) which complements the temperature-sensitive G1 mutants, tsBN462 and ts13, of the BHK cell line', EMBO J, 7: 1683-7.
Semkova, K., M. Gergovska, J. Kazandjieva, and N. Tsankov. 2015. 'Hyperhidrosis, bromhidrosis, and chromhidrosis: Fold (intertriginous) dermatoses', Clin Dermatol, 33: 483-91.
Shaw, P. J., B. Qu, M. Hoth, and S. Feske. 2013. 'Molecular regulation of CRAC channels and their role in lymphocyte function', Cell Mol Life Sci, 70: 2637-56.
Sheikh, M. H., and E. Solito. 2018. 'Annexin A1: Uncovering the Many Talents of an Old Protein', Int J Mol Sci, 19.
Shi, S. R., C. Cote, K. L. Kalra, C. R. Taylor, and A. K. Tandon. 1992. 'A technique for retrieving antigens in formalin-fixed, routinely acid-decalcified, celloidin-embedded human temporal bone sections for immunohistochemistry', J Histochem Cytochem, 40: 787-92.
Shi, S. R., R. J. Cote, and C. R. Taylor. 1997. 'Antigen retrieval immunohistochemistry: past, present, and future', J Histochem Cytochem, 45: 327-43.
Shi, S. R.. 1998. 'Antigen retrieval immunohistochemistry used for routinely processed celloidin-embedded human temporal bone sections: standardization and development', Auris Nasus Larynx, 25: 425-43.
Shi, S. R., S. A. Imam, L. Young, R. J. Cote, and C. R. Taylor. 1995. 'Antigen retrieval immunohistochemistry under the influence of pH using monoclonal antibodies', J Histochem Cytochem, 43: 193-201.
Shi, S. R., M. E. Key, and K. L. Kalra. 1991. 'Antigen retrieval in formalin-fixed, paraffin-embedded tissues: an enhancement method for immunohistochemical staining based on microwave oven heating of tissue sections', J Histochem Cytochem, 39: 741-8.
Shi, S. R., C. Liu, B. M. Balgley, C. Lee, and C. R. Taylor. 2006. 'Protein extraction from formalin-fixed, paraffin-embedded tissue sections: quality evaluation by mass spectrometry', J Histochem Cytochem, 54: 739-43.
Shi, S. R., C. Liu, and C. R. Taylor. 2007. 'Standardization of immunohistochemistry for formalin-fixed, paraffin-embedded tissue sections based on the antigen-retrieval technique: from experiments to hypothesis', J Histochem Cytochem, 55: 105-9.
Shi, S., P. Zhang, Q. Cheng, J. Wu, J. Cui, Y. Zheng, X. Y. Bai, and X. Chen. 2013. 'Immunohistochemistry of deparaffinised sections using antigen retrieval with microwave combined pressure cooking versus immunofluorescence in the assessment of human renal biopsies', J Clin Pathol, 66: 374-80.
Shi, V. Y., M. Leo, L. Hassoun, D. S. Chahal, H. I. Maibach, and R. K. Sivamani. 2015. 'Role of sebaceous glands in inflammatory dermatoses', J Am Acad Dermatol, 73: 856-63.

Shikiji, T., M. Minami, T. Inoue, K. Hirose, H. Oura, and S. Arase. 2003. 'Keratinocytes can differentiate into eccrine sweat ducts in vitro: involvement of epidermal growth factor and fetal bovine serum', J Dermatol Sci, 33: 141-50.
Son, E. D., H. J. Kim, K. H. Kim, B. H. Bin, I. H. Bae, K. M. Lim, S. J. Yu, E. G. Cho, and T. R. Lee. 2016. 'S100A7 (psoriasin) inhibits human epidermal differentiation by enhanced IL-6 secretion through IkappaB/NF-kappaB signalling', Exp Dermatol, 25: 636-41.
Sonner, Z., E. Wilder, J. Heikenfeld, G. Kasting, F. Beyette, D. Swaile, F. Sherman, J. Joyce, J. Hagen, N. Kelley-Loughnane, and R. Naik. 2015. 'The microfluidics of the eccrine sweat gland, including biomarker partitioning, transport, and biosensing implications', Biomicrofluidics, 9: 031301.
Steffen, M. M., S. P. Dearth, B. D. Dill, Z. Li, K. M. Larsen, S. R. Campagna, and S. W. Wilhelm. 2014. 'Nutrients drive transcriptional changes that maintain metabolic homeostasis but alter genome architecture in Microcystis', ISME J, 8: 2080-92.
Strauss, J. S. 2006. 'Human sebaceous glands: how studies of skin surface lipids have provided knowledge of their function and control', Dermatology, 213: 261.
Strudwick, X. L., D. L. Lang, L. E. Smith, and A. J. Cowin. 2015. 'Combination of low calcium with Y-27632 rock inhibitor increases the proliferative capacity, expansion potential and lifespan of primary human keratinocytes while retaining their capacity to differentiate into stratified epidermis in a 3D skin model', PLoS One, 10: e0123651.
Strzelecka, D., S. W. Holman, and C. E. Eyers. 2015. 'Evaluation of dimethyl sulfoxide (DMSO) as a mobile phase additive during top 3 label-free quantitative proteomics', Int J Mass Spectrom, 391: 157-60.
Sugawara, T., K. Nemoto, Y. Adachi, N. Yamano, N. Tokuda, M. Muto, R. Okuyama, S. Sakai, and Y. Owada. 2012. 'Reduced size of sebaceous gland and altered sebum lipid composition in mice lacking fatty acid binding protein 5 gene', Exp Dermatol, 21: 543-6.
Sun, B. K., L. D. Boxer, J. D. Ransohoff, Z. Siprashvili, K. Qu, V. Lopez-Pajares, S. T. Hollmig, and P. A. Khavari. 2015. 'CALML5 is a ZNF750- and TINCR-induced protein that binds stratifin to regulate epidermal differentiation', Genes Dev, 29: 2225-30.
Sun, Y., N. Sheshadri, and W. X. Zong. 2017. 'SERPINB3 and B4: From biochemistry to biology', Semin Cell Dev Biol, 62: 170-77.
Suttapitugsakul, S., H. Xiao, J. Smeekens, and R. Wu. 2017. 'Evaluation and optimization of reduction and alkylation methods to maximize peptide identification with MS-based proteomics', Mol Biosyst, 13: 2574-82.
Sutterlin, T., E. Tsingos, J. Bensaci, G. N. Stamatas, and N. Grabe. 2017. 'A 3D self-organizing multicellular epidermis model of barrier formation and hydration with realistic cell morphology based on EPISIM', Sci Rep, 7: 43472.
Takahara, Y., N. Miyachi, M. Nawa, and M. Matsuoka. 2019. 'Calmodulin-like skin protein suppresses the increase in senescence-associated beta-galactosidase induced by hydrogen peroxide or ultraviolet irradiation in keratinocytes', Cell Biol Int, 43: 835-43.

Takahashi, K., R. D. Paladini, and P. A. Coulombe. 1995. 'Cloning and characterization of multiple human genes and cDNAs encoding highly related type II keratin 6 isoforms', J Biol Chem, 270: 18581-92.
Tapper, R. 1990. 'Biology of the sweat glands', J Am Acad Dermatol, 22: 699-700.
Thavarajah, R., V. K. Mudimbaimannar, J. Elizabeth, U. K. Rao, and K. Ranganathan. 2012. 'Chemical and physical basics of routine formaldehyde fixation', J Oral Maxillofac Pathol, 16: 400-5.
Thompson, S. M., R. A. Craven, N. J. Nirmalan, P. Harnden, P. J. Selby, and R. E. Banks. 2013. 'Impact of pre-analytical factors on the proteomic analysis of formalin-fixed paraffin-embedded tissue', Proteomics Clin Appl, 7: 241-51.
Thomson, M. L. 1954. 'A comparison between the number and distribution of functioning eccrine sweat glands in Europeans and Africans', J Physiol, 123: 225-33.
Toyomoto, T., D. Knutsen, G. Soos, and K. Sato. 1997. 'Na-K-2Cl cotransporters are present and regulated in simian eccrine clear cells', Am J Physiol, 273: R270-7.
Tripathi, S. R., E. Miyata, P. B. Ishai, and K. Kawase. 2015. 'Morphology of human sweat ducts observed by optical coherence tomography and their frequency of resonance in the terahertz frequency region', Sci Rep, 5: 9071.
Trivedi, N. N., and G. H. Caughey. 2010. 'Mast cell peptidases: chameleons of innate immunity and host defense', Am J Respir Cell Mol Biol, 42: 257-67.
Trivedi, N. N., W. W. Raymond, and G. H. Caughey. 2008. 'Chimerism, point mutation, and truncation dramatically transformed mast cell delta-tryptases during primate evolution', J Allergy Clin Immunol, 121: 1262-8.
Tsutsumi, M., S. Denda, K. Inoue, K. Ikeyama, and M. Denda. 2009. 'Calcium ion gradients and dynamics in cultured skin slices of rat hindpaw in response to stimulation with ATP', J Invest Dermatol, 129: 584-9.
Tyers, M., and M. Mann. 2003. 'From genomics to proteomics', Nature, 422: 193-7.
Usuda, N., H. Arai, H. Sasaki, T. Hanai, T. Nagata, T. Muramatsu, R. L. Kincaid, and S. Higuchi. 1996. 'Differential subcellular localization of neural isoforms of the catalytic subunit of calmodulin-dependent protein phosphatase (calcineurin) in central nervous system neurons: immunohistochemistry on formalin-fixed paraffin sections employing antigen retrieval by microwave irradiation', J Histochem Cytochem, 44: 13-8.
van der Putte, S. C. 1994. 'Apoeccrine glands in nevus sebaceus', Am J Dermatopathol, 16: 23-30.
Verde, T., R. J. Shephard, P. Corey, and R. Moore. 1982. 'Sweat composition in exercise and in heat', J Appl Physiol Respir Environ Exerc Physiol, 53: 1540-5.
Verma, M., M. I. K. Khan, R. V. Kadumuri, B. Chakrapani, S. Awasthi, A. Mahesh, G. Govindaraju, P. L. Chavali, A. Rajavelu, S. Chavali, and A. Dhayalan. 2021. 'PRMT3 interacts with ALDH1A1 and regulates gene-expression by inhibiting retinoic acid signaling', Commun Biol, 4: 109.
Vidalino, L., A. Doria, S. Quarta, M. Zen, A. Gatta, and P. Pontisso. 2009. 'SERPINB3, apoptosis and autoimmunity', Autoimmun Rev, 9: 108-12.
Wang, F., S. Chen, H. B. Liu, C. A. Parent, and P. A. Coulombe. 2018. 'Keratin 6 regulates collective keratinocyte migration by altering cell-cell and cell-matrix adhesion', J Cell Biol, 217: 4314-30.

Wang, H. W., H. P. McNeil, A. Husain, K. Liu, N. Tedla, P. S. Thomas, M. Raftery, G. C. King, Z. Y. Cai, and J. E. Hunt. 2002. 'Delta tryptase is expressed in multiple human tissues, and a recombinant form has proteolytic activity', J Immunol, 169: 5145-52.
Wang, X., and Y. Zhang. 2018. 'Resveratrol alleviates LPS-induced injury in human keratinocyte cell line HaCaT by up-regulation of miR-17', Biochem Biophys Res Commun, 501: 106-12.
Wang, Y., T. M. Lih, L. Chen, Y. Xu, M. D. Kuczler, L. Cao, K. J. Pienta, S. R. Amend, and H. Zhang. 2022. 'Optimized data-independent acquisition approach for proteomic analysis at single-cell level', Clin Proteomics, 19: 24.
Wang, Z., P. Wong, L. Langbein, J. Schweizer, and P. A. Coulombe. 2003. 'Type II epithelial keratin 6hf (K6hf) is expressed in the companion layer, matrix, and medulla in anagen-stage hair follicles', J Invest Dermatol, 121: 1276-82.
Watabe, A., T. Sugawara, K. Kikuchi, K. Yamasaki, S. Sakai, and S. Aiba. 2013. 'Sweat constitutes several natural moisturizing factors, lactate, urea, sodium, and potassium', J Dermatol Sci, 72: 177-82.
Weng, Y. C., A. Sonni, C. Labelle-Dumais, M. de Leau, W. B. Kauffman, M. Jeanne, A. Biffi, S. M. Greenberg, J. Rosand, and D. B. Gould. 2012. 'COL4A1 mutations in patients with sporadic late-onset intracerebral hemorrhage', Ann Neurol, 71: 470-7.
Wilke, K., A. Martin, L. Terstegen, and S. S. Biel. 2007. 'A short history of sweat gland biology', Int J Cosmet Sci, 29: 169-79.
Wilkins, M. R., C. Pasquali, R. D. Appel, K. Ou, O. Golaz, J. C. Sanchez, J. X. Yan, A. A. Gooley, G. Hughes, I. Humphery-Smith, K. L. Williams, and D. F. Hochstrasser. 1996. 'From proteins to proteomes: large scale protein identification by two-dimensional electrophoresis and amino acid analysis', Biotechnology (N Y), 14: 61-5.
Wisniewski, J. R. 2013. 'Proteomic sample preparation from formalin fixed and paraffin embedded tissue', J Vis Exp.
Wisniewski, J. R., P. Ostasiewicz, and M. Mann. 2011. 'High recovery FASP applied to the proteomic analysis of microdissected formalin fixed paraffin embedded cancer tissues retrieves known colon cancer markers', J Proteome Res, 10: 3040-9.
Wisniewski, J. R., A. Zougman, N. Nagaraj, and M. Mann. 2009. 'Universal sample preparation method for proteome analysis', Nat Methods, 6: 359-62.
Wortsman, X., L. Carreno, C. Ferreira-Wortsman, R. Poniachik, K. Pizarro, C. Morales, P. Calderon, and A. Castro. 2019. 'Ultrasound Characteristics of the Hair Follicles and Tracts, Sebaceous Glands, Montgomery Glands, Apocrine Glands, and Arrector Pili Muscles', J Ultrasound Med, 38: 1995-2004.
Wu, S., M. Zhao, Y. Sun, M. Xie, K. Le, M. Xu, and C. Huang. 2020. 'The potential of Diosgenin in treating psoriasis: Studies from HaCaT keratinocytes and imiquimod-induced murine model', Life Sci, 241: 117115.
Xie, L., L. Jin, J. Feng, and J. Lv. 2017. 'The Expression of AQP5 and UTs in the Sweat Glands of Uremic Patients', Biomed Res Int, 2017: 8629783.
Yamamoto, Y., Y. Aoyama, E. Shu, K. Tsunoda, M. Amagai, and Y. Kitajima. 2007. 'Anti-desmoglein 3 (Dsg3) monoclonal antibodies deplete desmosomes of

Dsg3 and differ in their Dsg3-depleting activities related to pathogenicity', J Biol Chem, 282: 17866-76.
Yamashita, S., and O. Katsumata. 2017. 'Heat-Induced Antigen Retrieval in Immunohistochemistry: Mechanisms and Applications', Methods Mol Biol, 1560: 147-61.
Yamazaki, T., H. Nakano, M. Hayakari, M. Tanaka, J. Mayama, and S. Tsuchida. 2004. 'Differentiation induction of human keratinocytes by phosphatidylethanolamine-binding protein', J Biol Chem, 279: 32191-5.
Yoshida, A., K. Yamamoto, T. Ishida, T. Omura, T. Itoh, C. Nishigori, T. Sakane, and I. Yano. 2020. 'Sunitinib decreases the expression of KRT6A and SERPINB1 in 3D human epidermal models', Exp Dermatol.
Zhang, C. C., R. Li, H. Jiang, S. Lin, J. C. Rogalski, K. Liu, and J. Kast. 2015. 'Development and application of a quantitative multiplexed small GTPase activity assay using targeted proteomics', J Proteome Res, 14: 967-76.
Zhang, H., X. Fu, Y. Ao, M. Nan, Z. Qiu, X. Jia, Y. Xiao, D. Liu, and X. Guo. 2021. 'ANXA1 affects murine hair follicle growth through EGF signaling pathway', Gene, 771: 145343.
Zhang, J., L. Xin, B. Shan, W. Chen, M. Xie, D. Yuen, W. Zhang, Z. Zhang, G. A. Lajoie, and B. Ma. 2012. 'PEAKS DB: de novo sequencing assisted database search for sensitive and accurate peptide identification', Mol Cell Proteomics, 11: M111 010587.
Zhang, S. H., D. X. Liu, L. Wang, Y. H. Li, Y. H. Wang, H. Zhang, Z. K. Su, W. G. Fang, X. X. Qin, D. S. Shang, B. Li, X. N. Han, W. D. Zhao, and Y. H. Chen. 2019. 'A CASPR1-ATP1B3 protein interaction modulates plasma membrane localization of Na(+)/K(+)-ATPase in brain microvascular endothelial cells', J Biol Chem, 294: 6375-86.
Zhang, X., M. Yin, and L. J. Zhang. 2019. 'Keratin 6, 16 and 17-Critical Barrier Alarmin Molecules in Skin Wounds and Psoriasis', Cells, 8.
Zhang, Y., B. R. Fonslow, B. Shan, M. C. Baek, and J. R. Yates, 3rd. 2013. 'Protein analysis by shotgun/bottom-up proteomics', Chem Rev, 113: 2343-94.
Zhang, Y., M. Muller, B. Xu, Y. Yoshida, O. Horlacher, F. Nikitin, S. Garessus, S. Magdeldin, N. Kinoshita, H. Fujinaka, E. Yaoita, M. Hasegawa, F. Lisacek, and T. Yamamoto. 2015. 'Unrestricted modification search reveals lysine methylation as major modification induced by tissue formalin fixation and paraffin embedding', Proteomics, 15: 2568-79.
Zhu, L., S. Okano, M. Takahara, T. Chiba, Y. Tu, Y. Oda, and M. Furue. 2013. 'Expression of S100 protein family members in normal skin and sweat gland tumors', J Dermatol Sci, 70: 211-9.

Chapter: 8 Appendix

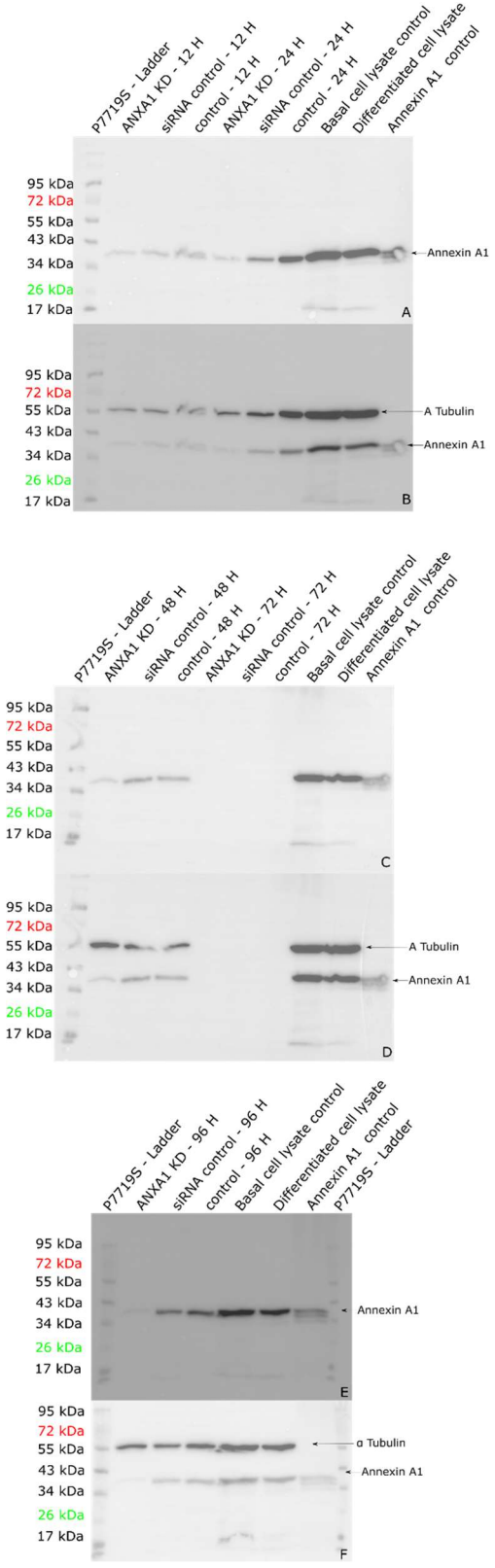

Figure 8.1 Full *Western blot of Anxa1 siRNA knockdown optimisation.(Figure 5.1)*

HaCAT cells treated with targeted siRNA, siRNA control samples treated with non-specific siRNA, and control samples which were not treated with siRNA but went through the same processes as siRNA-treated samples. Alpha-tubulin was used as a loading control. From 24 hours onward, Anxa1 KD appeared to reduce in intensity in comparison with control samples, indicating a reduction in the presence of Anxa1; corresponding loading control bands remained constant.

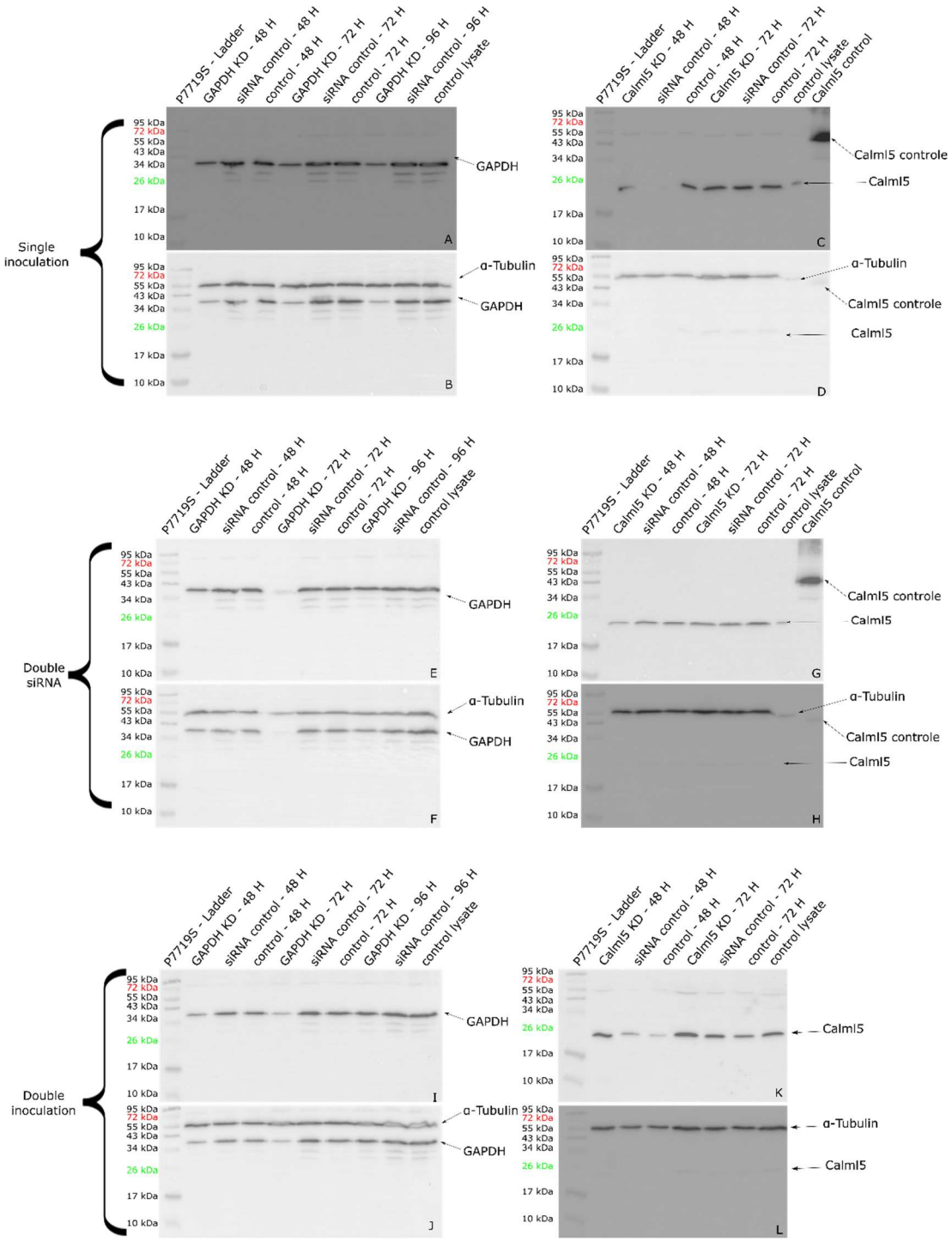

Figure 8.2 Full *Western blot summary of attempted CALML5 and GAPDH siRNA knockdowns (Figure5.5)*

. Three methods of generating CALML5 and GAPDH knockdown in HaCaT cells were attempted, including: single inoculation, double siRNA concentration and double inoculation. KD samples treated with targeted siRNA, siRNA control samples treated with non-specific siRNA, and control samples that were not treated with siRNA but went through the same processes as the siRNA treated samples. Alpha-tubulin was used as a loading control.